

**SIMULATION AND EXPERIMENTAL STUDIES
ON BELT CONVEYOR DRIVE SYSTEM FOR
ENERGY CONSERVATION IN
UNDERGROUND MINES**

Thesis

Submitted in partial fulfilment of the requirements for the degree of

DOCTOR OF PHILOSOPHY

by

N V SARATHBABU GORIPARTI



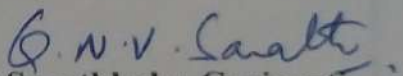
DEPARTMENT OF MINING ENGINEERING
NATIONAL INSTITUTE OF TECHNOLOGY KARNATAKA,
SURATHKAL, MANGALORE-575025

June, 2022

DECLARATION

by the Ph. D Scholar

I hereby declare that the Research Thesis entitled “**Simulation and Experimental Studies on Belt Conveyor Drive System for Energy Conservation in Underground Mines**” which is being submitted to the **National Institute of Technology Karnataka, Surathkal** in partial fulfillment of the requirements for the award of the Degree of **Doctor of Philosophy in Mining Engineering** is a bonafide report of the research work carried out by me. The material contained in this Research Thesis has not been submitted to any University or Institution for the award of any degree.


N V Sarathbabu Goriparti

(Reg. No.: 158005MN15F09)

Department of Mining Engineering

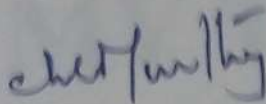
Place: NITK, Surathkal

Date: 09/06/22

CERTIFICATE

This is to certify that the Research Thesis entitled "Simulation and Experimental Studies on Belt Conveyor Drive System for Energy Conservation in Underground Mines" submitted by Mr. N V Sarathbabu Goriparti (Register Number: 158005MNI15F09) as the record of the research work carried out by him, is accepted as the Research Thesis submission in partial fulfillment of the requirements for the award of degree of **Doctor of Philosophy**.

Research Guides



Dr. Ch. S. N. Murthy
Professor – HAG
Department of Mining Engineering
National Institute of Technology Karnataka,
Surathkal



Dr. M. Aruna
Associate Professor
Department of Mining Engineering
National Institute of Technology Karnataka,
Surathkal



10/06/2022
Dr. M. Aruna
Associate Professor, Head and Chairman, DRPC
Department of Mining Engineering
National Institute of Technology Karnataka, Surathkal

Head
Department of Mining Engineering
National Institute of Technology Karnataka, Surathkal
P.O. SRINIVASNAGAR - 576 025
Karnataka State, India

**DEDICATED
TO
MY FAMILY,
MY TEACHERS AND
MY FRIENDS**

ACKNOWLEDGEMENT

I am indebted to my supervisor Dr. Ch. S. N. Murthy, Professor - HAG, Department of Mining Engineering, National Institute of Technology Karnataka (NITK), Surathkal, for his excellent guidance and support throughout the research work.

Further I am thankful to my co-supervisor Dr. M. Aruna, Associate Professor, Department of Mining Engineering, National Institute of Technology Karnataka (NITK), Surathkal, for his excellent guidance and moral support throughout the research work. His constant encouragement, help and review of the entire work during the course of the investigation are invaluable.

I wish to thank all the members of the Research Program Assessment Committee (RPAC) including Dr. M. Govinda Raj, Professor, Department of Mining Engineering, NITK, Surathkal and Dr. Dattatraya N Gaonkar, Associate Professor, Department of Electrical Engineering, NITK, Surathkal for their unbiased appreciation and criticism all through this research work.

I wish to express my sincere thanks to Dr. M. Aruna, Associate Professor, Head and DRPC Chairman, Department of Mining Engineering, NITK, Surathkal and former head Dr. K. Ram Chandar, Prof. M. Govinda Raj and Prof. V. R. Sastry for providing the departmental facilities, which ensured the satisfactory progress of my research work.

I express my sincere gratitude to Prof. Harsha Vardhan, Professor, Department of Mining Engineering, NITK, Surathkal, Dr. Anup Kumar Tripathi, Assistant Professor, Department of Mining Engineering, NITK, Surathkal, and Dr. B. M. Kunar, Assistant Professor, Department of Mining Engineering, NITK, Surathkal and Dr. Sandi Kumar Reddy, Assistant Professor, NITK Surathkal for their constant encouragement during my research work.

I express my heartfelt thanks to all the non-teaching staff of the Department of Mining Engineering, NITK, Surathkal who helped me in one way or the other during the course of my work. Also, I thank NITK, Surathkal, for providing financial assistance and all the necessary facilities to make this research peaceful.

I owe my deepest gratitude to The Singareni Collieries Company (SCCL), Telangana for giving permission to collect data for my research work.

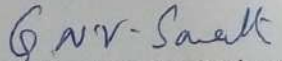
Also, I owe my deepest gratitude to Sri. S. V. S. S. Ramalingeswaradu, General Manager (HRD), SCCL, Telangana, Sri. Srinivasu, DGM, SCCL, Telangana, Sri. Subba Rao, PA to GM, SCCL, Telangana, for their help during collecting data in their Workshops and Mines.

I would like to thank my friends Mr. Harish Kumar N S, Mr. Balaji Rao K, Mr. Harish H, Mr. Vijay Kumar S, Mrs. Gayana B C, Mr., Mr. Balaraju Jakulla, Mr. Raghu Chandr Garimella, Ch. Vijay Kumar, Mr. Bharath Kumar S, and Mr. Tejeswaran K M, for their countless help during my research work.

Finally, I would like to share this moment of happiness with my father Mr. Ravisekhar Goriparti, my mother Mrs. G Maha Lakshmi my father in law Mr. V Durgarao, my mother in law Mrs. V Anantha Rama Lakshmi, my cousin Mr. Avinash Nagh, my wife Mrs. G Gnana Naga Sirisha, my son Mr. G. Purna Aravind and my daughter G. Naga Vaishnavi for all the sacrifices and compromises they have made during the tenure of my Ph. D work.

And above all, I am thankful to the Almighty Lord Ayyappa Swamy for his grace.

I am sure I have forgotten someone. I assure you that this is a shortcoming on my part and not on yours. I beg you to forgive me for my oversight.


N V Sarathbabu Goriparti

Place: NITK, Surathkal

Date: 09/06/22

ABSTRACT

Transportation of extruded material from the underground to the surface is a significant area concentrating underground mining technologies. With available technology, belt conveyors are mostly adopted for transporting extruded materials. The conveyor belt system's efficiency directly relates to underground mines' productivity, which is a significant area of research that is needed. A conveyor system's efficiency can be estimated in terms of energy consumption and the specific energy consumed.

In the present study, the belt conveyor system's efficiency is illustrated considering three different ways, i.e., field investigation, simulation, and experimentation. Under field investigations, data relevant to three different field belt conveyors (FBCs), namely Gantry (FBC1), 5L (FBC2), and Surface (FBC3) from the production department of GDK-1&3 incline, The Singareni Collieries Company limited, Ramagundam, Telangana, India was collected. Collected data includes energy consumption and a specific energy for each belt conveyor system. These systems possess different varying dimensions along length and height. The data was processed, energy calculations such as energy consumption and specific energy of all three belt conveyors were estimated. This study illustrates how the length of the belt, inclination, and drive motor affect the belt conveyor system's energy consumption.

To further improvise the energy losses, simulation studies on the field's data were carried out for predicting both energy consumption and specific energy. The simulation was carried out using MATLAB 2018b under two categories. These include a non VFD (variable frequency drive) and VFD-based simulation models. To develop a simulation model reference voltage vector was consider as input. Upon comparison of both models, it was observed that a VFD-based simulation model could significantly reduce both energy consumption and specific energy, i.e., incorporation of a VFD to the belt conveyor system reduces energy consumption, in turn, specific energy. The minimization in annual energy consumption and specific energy achieved on interfacing VFD were found to be 9.4% (2390kWh), 2.31% (2041kWh) and 7.3% (7797kWh) for energy consumption and 10.4% (0.20866 kW/ton-km), 2.55% (0.02166kW/ton-km) and 5.93% (0.12384 kW/ton-km) for specific energy with respect to FBC1, FBC2 and FBC3.

A simulation model was also developed for the laboratory belt conveyor (LBC) considering length and three different heights, namely, LBC1, LBC2, and LBC3), individually for both non VFD and VFD incorporations. To simulate a VFD, the principle of working of a proportional integral (PI) control was thoroughly studied, and the structural design was simulated. The study revealed similar observations as field data simulations. The minimization in annual energy consumption and specific energy achieved on interfacing VFD were found to be 9.9%, 9%, and 7.6% for energy consumption and 12.2%, 11.5%, and 10.2% for specific energy for LBC1, LBC2, and LBC3.

In order to validate the simulation study, an experiment on a LBC system was carried out. The experimentation was done for three different simulated elevations and variable loadings from 20% to 100% of the rated belt capacity. Readings for both non VFD and VFD unit incorporations were recorded. It was observed that the results of incorporating a VFD unit to the belt conveyor system reduce the energy consumption and specific energy. With the use of VFDs, the reduction in energy consumption for LBC1, LBC2, and LBC3 are 9.6%, 8.55%, and 7.2%, respectively. And, the reduction in specific energy for LBC1, LBC2, and LBC3 are 11.5%, 11.3%, and 9.89%, respectively.

Statistical analysis is also carried using Minitab V 18. Linear regression models are developed to predict the specific energy. Models are developed individually for both non VFD and VFD incorporations. Linear regression models are developed for laboratory belt conveyor system. A graph of actual vs. predicted specific energy are plotted for each of the said systems. The specific energy of the belt conveyor system depends on various factors; the speed of the belt, supply voltage to the motor, applied force, the mass of the material, and applied input and output powers. However, its significance on the specific energy of the belt conveyor has been varied with and without connecting the controller.

TABLE OF CONTENTS

	PAGE NO.
CONTENTS	
DECLARATION	i
CERTIFICATE	ii
ACKNOWLEDGEMENT	iv
ABSTRACT	vi
TABLE OF CONTENTS	ix
LIST OF FIGURES	xiii
LIST OF TABLES	xvii
NOMENCLATURE	xix
CHAPTER 1 INTRODUCTION	1
1.1 General	1
1.2 Thesis Outline	4
CHAPTER 2 LITERATURE REVIEW	5
2.1 Introduction	5
2.2 Modelling of Belt Conveyor	7
2.2.1 Motional resistance model	7
2.2.2 Energy conversion model	9
2.3 Specific Energy	11
2.4 Space Vector Modulated Direct Torque Control (SVM-DTC) of Induction Motor Drive	11
2.4.1 Induction motor model	11
2.4.2 Voltage source inverter	13
2.4.3 Concept of DTC	14
2.4.4 Space vector modulated DTC	17
2.4.5 Proportional-Integral-Derivative (PID) control	20
CHAPTER 3 ORIGIN, OBJECTIVES, JUSTIFICATION AND SCOPE OF THE RESEARCH WORK	21
3.1 Origin of the Research Work	21
3.2 Objectives of the Research Work	21

3.3 Purpose of the Research Work	22
3.4 Scope of Research Work	22
CHAPTER 4 RESEARCH METHODOLOGY	23
4.1 Field Visit	23
4.2 Simulation Studies	23
4.3 Laboratory Studies	24
4.4 Statistical Analysis	24
CHAPTER 5 FIELD INVESTIGATION	25
5.1 Study Area	25
5.2 About Belt Conveyor Systems in GDK 1&3 Incline	26
5.3 Technical Details and Rated Values	27
5.4 Results and Discussions	29
CHAPTER 6 SIMULATION STUDIES	35
6.1 Blocks used in the Construction of Simulink Models for FBC and LBC Systems	35
6.2 Simulink Models for FBC and LBC	40
6.3 Studies on FBC and LBC systems	56
6.4 Results and Discussions	57
6.4.1 Influence of feed rate on performance parameters of FBCs	57
6.4.1.1 Influence of feed rate on performance parameters of FBC1	57
6.4.1.2 Influence of feed rate on performance parameters of FBC2	61
6.4.1.3 Influence of feed rate on performance parameters of FBC3	66
6.4.1.4 Influence of feed rate on percentage variation in belt speed, annual energy consumption, efficiency and specific energy between non-VFD and VFD based FBCs	70
6.4.2 Influence of feed rate on performance parameters of LBCs	74
6.4.2.1 Influence of feed rate on performance parameters of LBC1, LBC2 and LBC3	74

6.4.2.2 Influence of feed rate on percentage variation in belt speed, annual energy consumption, efficiency and specific energy between non-VFD and VFD based FBCs	81
6.4.3 Dynamic response of field and laboratory drive motors – An analysis	84
6.4.3.1 Dynamic response of field drive motor at varied load	84
6.4.3.2 Dynamic response of laboratory drive motor at varied load	91
6.4.4 Comparison of non-VFD and VFD based FBCs and LBCs based on current	98
6.4.4.1 Dynamic response of current for non-VFD and VFD based FBCs-An analysis	98
6.4.4.2 Dynamic response of current for non-VFD and VFD based LBCs -An analysis	102
6.5 Overall Discussion and Findings of Simulation Studies	105
CHAPTER 7 LABORATORY STUDIES	107
7.1 Experimentation and Methodology	107
7.2 Specifications and Fabrication Details of LBCs	110
7.3 Results and Discussions	111
7.3.1 Influence of mass of the material on belt speed for non-VFD and VFD LBCs	112
7.3.2 Influence of mass of the material on annual energy consumption for non-VFD and VFD LBCs	114
7.3.3 Influence of mass of the material on efficiency consumption for non-VFD and VFD LBCs	117
7.3.4 Influence of mass of the material on specific energy consumption for non-VFD and VFD LBCs	121
7.3.5 Influence of mass of material on total resistive force	124
7.4 Comparison of Field , Laboratory and Simulation Results	124
7.5 Summarized Findings	125

CHAPTER 8 STATISTICAL ANALYSIS	127
8.1 Non-VFD Configured LBC System	127
8.1.1 ANOVA analysis for non-VFD configured LBC system	127
8.1.2 Development of regression model for prediction of the specific energy of a non-VFD configured LBC system	128
8.2 VFD Configured LBC System	130
8.2.1 ANOVA analysis for VFD configured LBC system	130
8.2.2 Development of regression model for prediction of the specific energy of a VFD configured LBC system	131
8.3 Summarized Findings	133
CHAPTER 9 CONCLUSION AND SCOPE FOR FUTURE WORK	135
9.1 Conclusion	135
9.2 Scope of Future Work	136
REFERENCES	139
ANNEXURE – A	147
ANNEXURE – B	155
LIST OF PUBLICATIONS	159
BIODATA	161

LIST OF FIGURES

Figure No.	Description	Page No.
1.1	Energy-saving potential in India	3
2.1	Schematic diagram of belt conveyor	7
2.2	Typical belt conveyor layout	9
2.3	Schematic diagram of an induction motor	11
2.4	Equivalent circuit of an induction motor	12
2.5	Circuit diagram of voltage source inverter	13
2.6	Block diagram of SVM-DTC	18
2.7	Hexagon used to synthesize reference voltage vector	19
5.1	RG-1 Area of M/s. SCCL	25
5.2	Coal handling area of M/s. SCCL (The SSCL Report)	25
5.3	Line diagram of main belt conveyors used in GDK-1&3 incline. (The SCCL Report)	26
5.4	Idler and belt	29
5.5	Belt conveyor system handling coal	29
5.6	Motor drive of belt conveyor	29
5.7	Influence of feed rate on belt speed	32
5.8	Influence of feed rate on annual energy consumption	32
5.9	Influence of feed rate on efficiency	33
5.10	Influence of feed rate on specific energy	34
6.1	Simulink model for conveyor load	40
6.2	Simulation model for non-VFD configured FBC1	42
6.3	Simulation model for non-VFD configured FBC2	43
6.4	Simulation model for non-VFD configured FBC3	44
6.5	Simulation model for non-VFD configured LBC1	45
6.6	Simulation model for non-VFD configured LBC2	46
6.7	Simulation model for non-VFD configured LBC3	47
6.8	Simulation model for VFD configured FBC1	48
6.9	Simulation model for VFD configured FBC2	59

6.10	Simulation model for VFD configured FBC3	50
6.11	Simulation model for VFD configured LBC1	51
6.12	Simulation model for VFD configured LBC2	52
6.13	Simulation model for VFD configured LBC3	53
6.14	Influence of feed rate on belt speed for FBC1 model	58
6.15	Influence of feed rate on annual energy consumption for FBC1 model	58
6.16	Influence of feed rate on efficiency for FBC1 model	59
6.17	Influence of feed rate on specific energy for FBC1 model	60
6.18	Influence of feed rate on belt speed for FBC2 model	62
6.19	Influence of feed rate on energy consumption for FBC2 model	63
6.20	Influence of feed rate on efficiency for FBC2 model	64
6.21	Influence of feed rate on specific energy for FBC2 model	65
6.22	Influence of feed rate on belt speed for FBC3 model	66
6.23	Influence of feed rate on annual energy consumption for FBC3 model	67
6.24	Influence of feed rate on efficiency for FBC3 model	68
6.25	Influence of feed rate on specific energy for FBC3 model	69
6.26	Influence of feed rate on percentage variation in belt speed between non-VFD and VFD configured FBC1, FBC2 and FBC3	71
6.27	Influence of feed rate on percentage variation in annual energy consumption between non-VFD and VFD configured FBC1, FBC2 and FBC3	72
6.28	Influence of feed rate on percentage improvement in efficiency between non-VFD and VFD configured FBC1, FBC2 and FBC3	73
6.29	Influence of feed rate on percentage reduction in specific energy between non-VFD and VFD configured FBC1, FBC2 and FBC3	74
6.30	Influence of mass of the material on belt speed plot for LBC system	75
6.31	Influence of mass of the material on annual energy consumption plot for LBC system	76
6.32	Influence of mass of the material on annual energy consumption plot for LBC system efficiency plot for LBC system	77
6.33	Influence of mass of the material on specific energy plot for LBC system	78
6.34	Influence of feed rate on percentage variation in belt speed between non-VFD and VFD configured LBC1, LBC2 and LBC3	81
6.35	Influence of feed rate on percentage reduction in annual energy consumption between non-VFD and VFD configured LBC1, LBC2 and LBC3	82

6.36	Influence of feed rate on percentage improvement in efficiency between non-VFD and VFD configured LBC1, LBC2 and LBC3	83
6.37	Influence of feed rate on percentage improvement in specific energy between non-VFD and VFD configured LBC1, LBC2 and LBC3	83
6.38	Electromagnetic torque response of FBC1 at different loads	86
6.39	Speed response of FBC1 at different loads	86
6.40	Current response FBC1 at different loads	87
6.41	Electromagnetic torque response of FBC2 at different loads	88
6.42	Speed response of FBC2 at different loads	89
6.43	Current response of FBC2 at different loads	89
6.44	Electromagnetic torque response of FBC3 at different loads	90
6.45	Speed response of FBC3 at different loads	90
6.46	Current response of FBC3 at different loads	91
6.47	Electromagnetic torque response of LBC1 at different loads	93
6.48	Speed response of LBC1 at different loads	94
6.49	Current response of LBC1 at different loads	94
6.50	Electromagnetic torque response of LBC2 at different loads	95
6.51	Speed response of LBC2 at different loads	95
6.52	Current response of LBC2 at different loads	96
6.53	Electromagnetic torque response of LBC3 at different loads	96
6.54	Speed response of LBC3 at different loads	97
6.55	Current response of LBC3 at different loads	97
6.56	Current response for FBC1 model	99
6.57	Current response for FBC2 model	100
6.58	Current response for FBC3 model	101
6.59	Current response of LBC1 system	102
6.60	Current response of LBC2 system	103
6.61	Current response of LBC3 system	104
7.1	Block diagram representation of belt conveyor drive system	106
7.2	Pictorial view of belt conveyor drive system	106
7.3	Fabricated belt conveyor system	106
7.4	Description of laboratory belt conveyor system	107

7.5	Influence of mass of the material on belt speed for LBC1 system	113
7.6	Influence of mass of the material on belt speed for LBC2 system	113
7.7	Influence of mass of the material on belt speed for LBC3 system	114
7.8	Influence of mass of the material on annual energy consumption for LBC1 system	115
7.9	Influence of mass of the material on annual energy consumption for LBC2 system	115
7.10	Influence of mass of the material on annual energy consumption for LBC3 system	116
7.11	Influence of feed rate on percentage variation in annual energy consumption between non-VFD and VFD configured LB1, LBC2 and LBC3	117
7.12	Efficiency of LBC system with respect to material mass	118
7.13	Influence of mass of the material on efficiency for LBC1 system	119
7.14	Influence of mass of the material on efficiency for LBC2 system	120
7.15	Influence of mass of the material on efficiency for LBC3 system	120
7.16	Influence of feed rate on percentage improvement in efficiency between Non-VFD and VFD configured LB1, LBC2 and LBC3	121
7.17	Influence of mass of material on specific energy for LBC1 system	122
7.18	Influence of mass of material on specific energy for LBC2 system	122
7.19	Influence of mass of material on specific energy for LBC3 system	123
7.20	Influence of feed rate on percentage reduction in specific energy between Non-VFD and VFD configured LB1, LBC2 and LBC3	123
7.21	Total resistive force with respect to material mass	124
8.1	Influence of feed rate on percentage contribution of input parameters on specific energy of non-VFD configured LBC system	128
8.2	Relation between predicted and experimental values of specific energy of a non-VFD configured LBC system.	129
8.3	Error plot for specific energy for a non-VFD configured LBC system	130
8.4	Influence of feed rate on percentage contribution of input parameters on specific energy of VFD configured LBC system	131
8.5	Relation between predicted and experimental values of specific energy of a VFD configured LBC system	132
8.6	Error plot for specific energy for a VFD configured LBC system	133

LIST OF TABLES

Table No.	Title	Page No.
2.1	Switching table for a two-level voltage source inverter	14
2.2	Optimal switching vector look-up table	17
5.1	Technical details of belt and rollers of FBC system	27
5.2	Technical details of drive of FBC system	27
5.3	Specifications of FBCs	28
5.4	Calculated energy consumption of FBC1	30
5.5	Calculated energy consumption of FBC2	30
5.6	Calculated energy consumption of FBC3	31
6.1	Specifications of FBC system	35
6.2	Specifications of LBC system	35
6.3	Blocks used in the construction of Simulink models	36
6.4	Simulation parameters of belt and rollers of FBC system	54
6.5	Simulation parameters of FBC drive	54
6.6	Simulation parameters of belt and rollers of LBC system	55
6.7	Simulation parameters of LBC system	55
6.8	Simulation results of non-VFD configured FBC1	61
6.9	Simulation results of VFD configured FBC1	61
6.10	Simulation results of non-VFD configured FBC2	65
6.11	Simulation results of VFD configured FBC2	66
6.12	Simulation results of non-VFD configured FBC3	70
6.13	Simulation results of VFD configured FBC3	70
6.14	Simulation results of non-VFD configured LBC	79
6.15	Simulation results of VFD configured LBC	79
6.16	Simulation results of non-VFD configured LBC2	79
6.17	Simulation results of VFD configured LBC2	80
6.18	Simulation results of non-VFD configured LBC3	80
6.19	Simulation results of VFD configured LBC3	80

6.20	Variation of motor parameters at three different loading conditions	87
6.21	Variation of motor parameters at three different loading conditions	92
6.22	Variation of full load motor current for non-VFD and VFD based FBC	101
6.23	Variation of full load motor current for non-VFD and VFD based LBC	104
7.1	Details of the equipment used	107
7.2	Specifications of belt and rollers of LBCs	110
7.3	Specifications of drive of LBCs	110
7.4	Laboratory results of a non-VFD based LBC system	111
7.5	Laboratory results of a non-VFD based LBC system	112
7.6	Load versus Efficiency of LBC	119
8.1	Results of ANOVA for non-VFD configured LBC system	127
8.2	Model summary for non-VFD configured LBC system	129
8.3	Regression analysis results of a non-VFD based LBC system	129
8.4	Results of ANOVA for VFD configured LBC system	130
8.5	Model summary for VFD configured LBC system	132
8.6	Regression analysis results of a VFD based LBC system	132

NOMENCLATURE

5L	:	5 level
AC	:	Alternating current
ANOVA	:	Analysis of variance
DC	:	Direct current
DIN	:	Douch institute of normalisation
DTC	:	Direct torque control
FBC	:	Field belt conveyor
FOC	:	Field oriented control
IM	:	Induction motor
LBC	:	Laboratory belt conveyor
MATLAB	:	Matrix laboratory
PI	:	Proportional integral
PID	:	Proportional integral derivative
SVM	:	Space vector modulation
VFD	:	Variable frequency drive
VSI	:	Voltage source inverter

CHAPTER 1

INTRODUCTION

1.1 General

Belt conveyor is the most economical means of transport in both surface and underground mines. Transporting a large quantity of material using belt conveyors requires a lot of energy. Within a mining operation, belt conveyors can be responsible for up to 70% of the total energy consumption (Zhang and Xia 2010). This means that reducing the energy consumption of belt conveyors will significantly impact power consumption and the total cost of production in the mines where they are used (Zhang and Xia 2010). Hence, aim should be to minimize the belt conveyor's energy consumption by controlling speed, load and heat generation. DIN 22101 standard indicates that reducing the belt speed and maximizing belt loads always lead to a specific reduction in the required electrical power (Akparibo and Normanyo 2020; Ji et al. 2020; Khurram et al. 2018; Krol et al. 2017; Ristić and Jeftenić 2012; Zhang and Xia 2011).

Variable frequency drives (VFDs) play a vital role in energy conservation (Deepa 2015). VFDs can provide reliable dynamic systems, and at the same time, contribute significantly to the energy usage and costs of induction motor drives (Krishnan 2001). VFDs are inbuilt with a control technology depending upon the type of application. The commonly used control techniques are the scalar control method (SCM) or constant V/f method (Ioannides et al. 2003; TI 2013), Vector control method (VCM) or Field-Oriented Control (FOC) method, and Direct Torque Control (DTC) method. Amongst these, scalar control is simple to implement and suitable for applications where precise speed control is not mandatory. The ratio of the supply voltage to the frequency is maintained as a constant in this method, i.e., the magnitude of voltage will be varying proportionally to frequency changes. Scalar control is incapable of controlling the essential variables in induction motors (IMs), i.e., torque and flux (Bose 1987). Therefore, for applications requiring precise torque control, either FOC or DTC methods usually are adopted. FOC was introduced in the year 1969 by Hasse and Blaschke.

Contrary to the scalar control, the FOC scheme's developments are indulged in the Induction Motor's dynamic model, where the voltage, current, and flux are expressed in space vector forms. In FOC, quantities of the motor, such as voltage, current and flux are transformed to a rotating reference frame (fixed to rotor flux). In this reference frame, all quantities rotating at synchronous speed and appear as Direct Current quantities. The representation of motor quantities using space vectors is valid under both steady-state and transient conditions, and hence, with FOC, an excellent transient response can be achieved. But, the information of rotor position needs to be acquired accurately. Inaccurate rotor flux position causes the torque and flux not to be completely decoupled and consequently resulted in a deterioration in the torque dynamics (Alsofyani and Idris 2013). This major limitation of the FOC scheme has encouraged to development of a new control technique called DTC. Takahashi and Depenbrock (Depenbrock 1988; Takahashi and Noguchi 1986) developed the DTC method as an alternative to the FOC. In DTC, the induction motor drive is supplied by a voltage source inverter. Therefore, it is possible to control the stator flux linkage λ_s (or the rotor flux λ_r or the magnetizing flux λ_m) and the electromagnetic torque by selecting an optimum inverter voltage vector directly. The voltage vector of the voltage source inverter restricts the flux and torque error within their respective flux and torque hysteresis bands. It obtains the fastest torque response and highest efficiency measured at every instant of time. DTC enables quick torque response in the transient operation and reduces harmonic losses and acoustic noise.

Energy is perhaps one of the basic requirements for modern civilization. Energy efficiency is the reduction of energy consumption subjected to key constraints. The importance of energy efficiency is sustainability and cost reduction. According to ISO 50,001, the energy-saving potential in manufacturing sites is 15-20% as shown in Figure 1.1. The Global energy potential is around 36%, and the average saving potential of a plant is 20% (Chan and Kantamaneni 2015).

The energy cost for transportation in underground mines is about 40% of the operational cost; the remaining 60% cost is operation and maintenance (Luo et al. 2015). Therefore, the energy efficiency of the primary transportation system used in underground mines, i.e., belt conveyor, is a significant factor in reducing operational costs (He et al. 2016a; Pang and Lodewijks 2011).

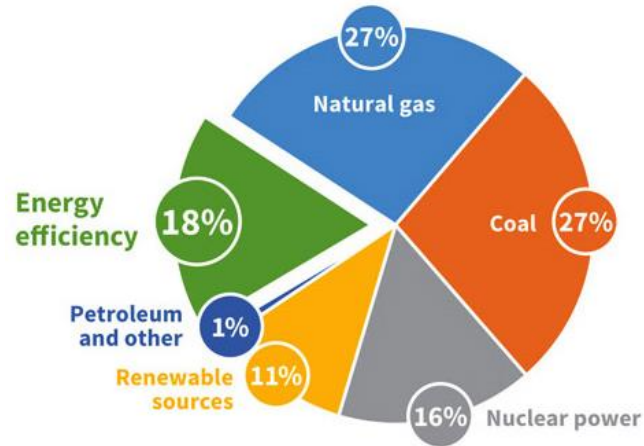


Figure 1.1 Energy-Saving Potential in India (Source: UNNATEE 2019)

Belt conveyor is a safe and efficient transport system used in underground mines. The energy share of belt conveyor in underground mines is up to 60-70% (Rawlinson 1978). DIN 22101 (DIN22101 2011) and ISO 5048 (ISO-5048 1989) are the standards used to model and design the belt conveyor systems for bulk material transfer. According to these standards, there is a scope for achieving energy saving from the belt conveyor's speed control (He et al. 2016a; b, 2017; Hiltermann et al. 2011; Lauhoff 2006; Pang and Lodewijks 2011). The electrical energy given to the conveyor can be converted into useful mechanical energy to run the conveyor, heat energy, noise energy, and other power losses.

The belt conveyor's energy efficiency mainly depends on the belt's speed, material filling profile, dynamic behavior, idler, and belt dimensions (He et al. 2016a; b; Hiltermann et al. 2011). The belt conveyor's energy efficiency can be improved by design, control, and audit methods (Goriparti et al. 2020; Luo et al. 2015; Mathaba and Xia 2017; Popescu et al. 2013; Ristić and Jeftenić 2012)(Luo et al. 2015). The earlier research work was more focused on equipment design (DJL and Calmeyer 2004), i.e., the design of idler (Lech et al. 2016) and drive and speed control (Hiltermann et al. 2011; Lauhoff 2006) of the drive motor. Very little work has been done on the variation in energy efficiency based on the length and height of the belt at which material is transferred. In this study, an attempt is made to illustrate the influence of load carried by the system, length, and height at which material is transferred on the electric motor's energy efficiency.

1.2 Thesis Outline

This research work aims at simulation and experimental studies on the belt conveyor drive system used for transporting the bulk material. An attempt is made to study the different parameters that signify the belt conveyor system's energy consumption and specific energy. The thesis consists of nine chapters. First chapter presents a brief introduction to energy conservation and belt conveyor, i.e., the primary transportation system used in underground mines, available control techniques to increase the belt conveyor system's efficiency, energy scenario in India and importance of energy conservation. Second chapter covers the existing literature on the belt conveyor system, its design, developments and mathematical modelling. It also incorporates literature on induction motor, SVPWM (Space Vector Pulse Width Modulation) and DTC. Third chapter describes the origin, objectives, purpose and scope of the research work. Fourth chapter briefs the methodology used for achieving the objectives of the research work. Fifth chapter illustrates the field investigations carried out at GDK- 1&3 Incline in RG-I area of M\S The Singareni Collieries Company Ltd., Telangana, India. This chapter also describes the technical details/specifications of the belt conveyor, the drive motor and the gear systems used in the mines. This chapter concluded with results and discussions. Sixth chapter presents the Influence of influencing parameters on the belt conveyor performance, such as load acting on the belt, speed of the motor, length of the belt and inclination angle of the belt on specific energy consumption using Simulink. The results and discussions of this chapter is incorporated at the end. Seventh chapter includes studies on the Influence of influencing parameters, such as load acting on the belt, speed of the motor, length of the belt and inclination angle of the belt on specific energy consumption, by experimentation on laboratory belt conveyor system. The experimental results are presented with appropriate discussions. Eighth chapter represents the effect of influencing parameters, such as load acting on the belt, speed of the motor, length of the belt and inclination angle of the belt on specific energy consumption, by statistical analysis on laboratory belt conveyor system. This chapter is also summarized with results and discussions. Ninth chapter gives the overall conclusions of the study and also scope for the future work.

CHAPTER 2

LITERATURE REVIEW

A detailed literature review was done to understand the construction, working principle, operation, and control of a belt conveyor used for transporting the bulk material from one place to another. The literature reviewed was categorized according to various researchers' approaches to improve a belt conveyor's performance and efficiency, using different constructional designs and mathematical models.

2.1 Introduction

Energy conservation is very much essential in mines for extraction of minerals at a low cost. There are several ways of conserving energy. The per-unit energy consumption for a belt conveyor is a scale measure to evaluate the conveyor energy efficiency (Lin et al. 2011) in underground mines where the primary transporting system for ore or minerals is a belt conveyor. An increase in demand for electrical energy for transportation is an economic aspect of any mining operation. The only way to solve this problem is to reduce energy consumption to the possible extent.

Specific energy (kWh/t.km) is an essential factor for any organization, which is using belt conveyor drives for the transportation system (Kawalec et al. 2020; Sarathbabu Goriparti et al. 2019; Suchorab 2019). The main objective of minimizing the specific energy is to increase the profit of an organization and to reduce the pressure on national resources and the environment (He et al. 2017).

Designing conveyors with less friction coefficient provides less wear and tear, no belt stretching, slipping benefits prolonged lifetime, reduced maintenance costs and energy efficiency (Zhang and Xia 2011).

Speed control is another essential aspect to conserve energy and it is necessary for industrial loads, such as pumps, fans and conveyor belts to reduce power losses and achieve energy efficiency (Zhang and Xia 2010). A variable speed drive (VSD) is a system that regulates the speed and output torque of an electric motor. Further, it facilitates minimum start current, smooth acceleration & deceleration, smooth speed-torque response, soft starting and stopping,

per unit energy savings, reverse and braking operation, fewer heating problems for prevention of mechanical drive components. Many researchers have worked on VSDs to achieve the benefits as mentioned above. (Krishnan 2001 and Bose 1987). Various authors have investigated speed control by multiple techniques, like stator voltage control, rotor resistance control, v/f control or frequency control etc. Most of the studies were carried out on the speed control of asynchronous motors since they are workhorses of any industry (ABB 2000; Jefteni et al. 2009; Vas 1998 and Vas 1998).

Almost 90% of the motors used in any industry are asynchronous or induction motors (IMs), because they are highly reliable, less cost, no sparking and commutation problems. However, IMs do not inherently have the capability of adjustable speed operation. Due to this reason, earlier DC (Direct Current) motors are used in most of the drives. But the recent progress in speed control methods is demanding for usage of IMs in almost all electrical drives and some of the popular developments are FOC and DTC. The variable speed drive, namely, DTC of IM, has its advantages but using this method for automatic control of belt conveyor is not easy.

A three-phase induction motor is a highly nonlinear system when compared to a DC motor. The control of induction motor is not easy compared to DC motor because of mutual coupling between stator and rotor parts of IM. DTC is a method widely accepted by industries for motor control. Takahashi and Noguchi (1986) introduced DTC in 1986 as an alternative to the vector control method that controls an IM's speed by controlling the stator magnetic flux and the electromagnetic torque independently. After this work, many researchers have been using the basic concept of DTC with little modifications in controller and inverter circuit designs (i.e, DTC with minimum switching losses, DTC with minimum conduction losses, DTC with different tuning methods, DTC with different modulating techniques, DTC with different level voltage source inverters (VSI), and DTC with different control designs, like PI, PID, Fuzzy, Neural and Neuro-fuzzy etc. (Buja and Kazmierkowski 2004; Depenbrock 1988; Gierse 1992; Reza et al. 2014).

Mathematical models of belt conveyor systems to predict the governing parameters of belt performance are very much necessary. The upcoming sections will present mathematical

models of a total belt conveyor system with a belt conveyor, an induction motor, a voltage source inverter, and available control techniques.

2.2 Modelling of Belt Conveyor

Belt conveyor is a highly mechanized system and has power losses at various parts, like idlers, drums, scrapers etc. Figure 2.1 shows the schematic diagram of the belt conveyor system.

2.2.1 Motional resistance model

The power consumption of the belt conveyor system was estimated by using the Motion Resistance Model.

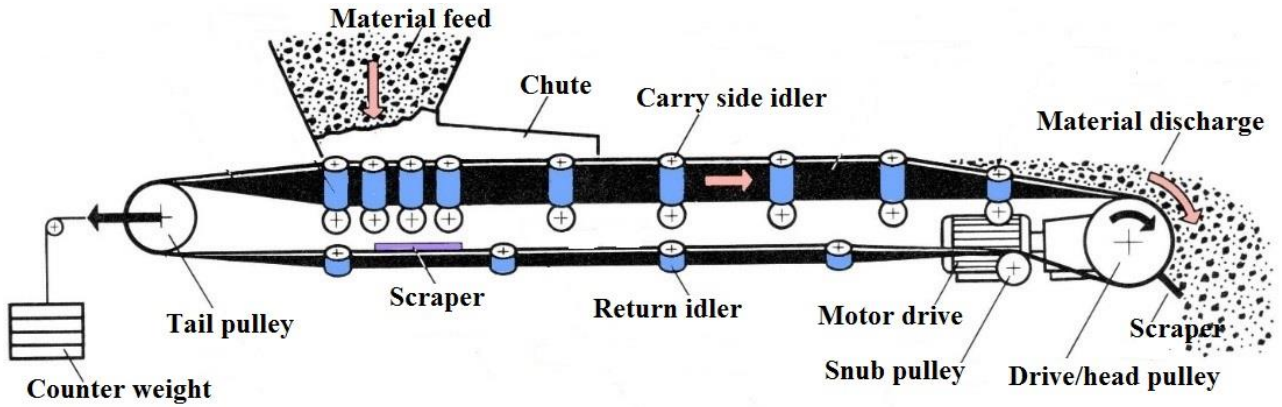


Figure 2.1 Schematic diagram of belt conveyor (*source: <https://conveyorbeltguide.com>*)

The total resistive force (motion resistance) required by the belt conveyor for its run was calculated by using equation (2.1).

$$F = fLg[m_{idler} + (2m_{belt} + m_{load})\cos\delta] + Hm_{load}g \quad (N) \quad (2.1)$$

where, F is the total motion resistance, f is the friction coefficient, L is the conveying length, g is the gravitational constant, m_{idler} is the mass of the running idlers, m_{belt} is the mass per unit length of the belt, m_{load} is the mass of the loaded material on the belt, δ is the inclination of the conveyor and H is the conveying height with respect to ground. For a horizontal conveyor, the conveying height is zero. Therefore the equation (2.1) becomes

$$F = fLg[m_{idler} + (2m_{belt} + m_{load}) \cos \delta] (N) \quad (2.2)$$

The mechanical power required by the belt conveyor is the product of motion resistance and speed of the belt conveyor, which is represented by equation (2.3).

$$P_m = Fv (W) \quad (2.3)$$

Where, P_m is the mechanical power required by the belt conveyor, F is the motion resistance and v is the speed of the belt conveyor.

The electrical power consumed by the belt conveyor depends on the efficiencies of the motor, gear system and the controller, and the net mechanical power required to run the conveyor, which is represented by equation (2.4).

$$P_e = \frac{Fv}{\eta_m \eta_g \eta_c} (W) \quad (2.4)$$

Where, P_e is the electrical power required by the belt conveyor, η_m , η_g and η_c are the efficiencies of the motor, gear system, and controller, respectively.

The energy or Wh (watt-hour) consumed by the belt conveyor system depends on the belt conveyor's operational time and the electrical power required to run the conveyor. When a plant runs 't' hours per day and the material feed on the belt is constant, the energy consumed by the belt conveyor is given by the product of electrical power consumed and operational time of the conveyor. It is given by equation (2.5).

$$E = P_e t (Wh) \quad (2.5)$$

where, E is the energy consumed by the belt conveyor, P_e is the electrical power consumed by the belt conveyor and t is operational time of the conveyor.

2.2.2 Energy conversion model

A belt conveyor model with a minimum friction coefficient is derived using the standard DIN 22101. Based on the energy conversion model, the total energy required by the belt conveyor for its run can be classified into four types (Lin et al. 2011), such as the energy needed to run the empty conveyor, move the material straight, lift the material to a certain elevation and additional energy to overcome skirt friction. The layout of the typical belt conveyor is shown in Figure 2.2.

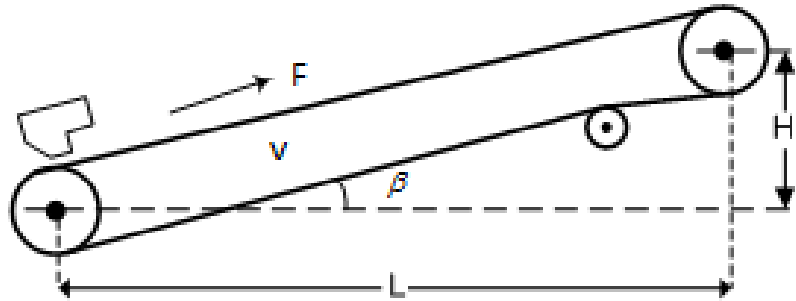


Figure. 2.2 Typical belt conveyor layout (Zhang and Xia 2009)

The total energy required by the belt conveyor for its run is given by equation (2.6).

$$E_t = E_{ec} + E_l + E_h + E_s (Wh) \quad (2.6)$$

where,

E_t = total energy required to run the conveyor (Wh)

E_{ec} = energy required to run the empty conveyor (Wh)

E_l = energy required to move the material straight (Wh)

E_h = energy required to lift the material to a certain elevation (Wh)

E_s = energy to overcome skirt friction (Wh)

The values of E_{ec} , E_l , E_h , and E_s are calculated using the following empirical formulae (Lin et al. 2011), as shown in equation 2.7, equation 2.8, equation 2.9 and equation 2.10.

$$E_{ec} = gCQ(L + L_c) \frac{v}{1000} t \quad (Wh) \quad (2.7)$$

$$E_h = gC \left(\frac{T}{3.6v} \right) (L + L_c) \frac{v}{1000} t \quad (Wh) \quad (2.8)$$

$$E_i = \frac{gTH}{3.6v} \frac{v}{1000} t \quad (Wh) \quad (2.9)$$

$$E_s = 0.2gd^2LM \frac{v}{1000} t \quad (Wh) \quad (2.10)$$

where, g is gravitational acceleration (m/s^2), C is friction factor, Q is mass of the moving parts of the conveyor (kg/m) and it is expressed as $(Q_r + 2Q_b)$ where Q_r is a unit mass of idlers (kg/m) and Q_b is unit mass of the belt (kg/m), L is parallel conveyor length (m), L_c is parallel conveyor length constant due to terminal friction (m), t is the operating period of conveyor (h), T represents material transfer/flow rate (t/h), d represents load depth (m) and M represents material density (kg/m^3).

According to Lin et al. (2011), the belt conveyor's friction depends on several factors, such as tension on the belt, the speed at which it runs, the troughing angle, the idlers' diameter, spacing between idlers and other working conditions. By considering all the above-said variables, an objective function was derived, as given in Equation (2.11), for the minimum friction of the conveyor with the following boundary conditions: The allowable spacing of forwarding idlers is between 1 to 1.5 m, the diameter of the idler is between 108-160 mm, the spacing of return idlers is in between 2.5 to 3.5 m, belt speed is in between 4- 6 m/s and troughing angle is in between 25-35°.

$$C = \sum_{j=1}^n A_j x_j \quad (2.11)$$

where, C is the friction coefficient, n represents the number of variables, A_j Constant matrix of order $(n \times n)$, and x_j is state variable matrix of order $(n \times 1)$.

2.3 Specific Energy

Specific energy of conveyor is defined as the energy required to transfer one ton of material to a distance of one kilometer (Johannes and Marx 2005). It is calculated using equation (2.12) (Kawalec et al. 2020; Krol et al. 2017; Suchorab 2019).

$$W_s = \frac{P_e}{TS} \quad (Kwh/t-km) \quad (2.12)$$

where, W_s is the specific energy of the conveyor ($kWh/t-km$), P_e is the electrical power required to run the conveyor (kW), T is the transfer rate (t/h) and S is the conveying distance (km).

2.4 Space Vector Modulated Direct Torque Control (SVM-DTC) of Induction Motor Drive

In this study, the space vector-based direct torque control technique was used for the belt conveyor's energy efficiency. This technique is more suitable for high torque loads.

2.4.1 Induction motor model

An induction motor is an asynchronous motor, highly used in industries, because of its ruggedness and simplicity (Gupta and Rao 2020). It works on the principle of electromagnetic induction and mainly consists of two parts, namely stator and rotor. Induction motor takes a single-phase or three-phase AC supply and produces mechanical force as an output. The electromechanical torque developed by the motor depends upon the product of stator flux and rotor current. The parts of an induction motor is shown in Figure 2.3.

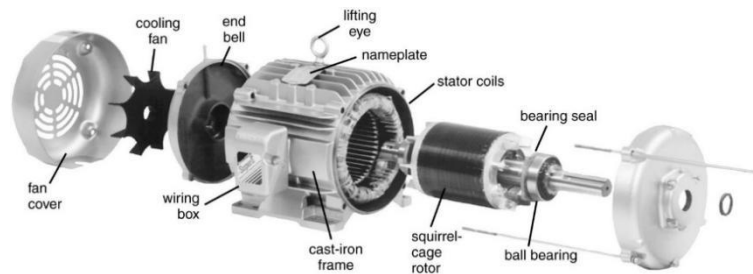


Figure. 2.3 Schematic diagram of an induction motor
(source: B L Theraja and A.K. Theraja, 2005)

The per-phase equivalent circuit of an induction motor represents the ohmic and other losses present in the motor. The per-phase equivalent circuit consists of resistance and inductance values of both stator and rotor windings, and the mutual inductance between stator and rotor, as shown in the Figure 2.4.

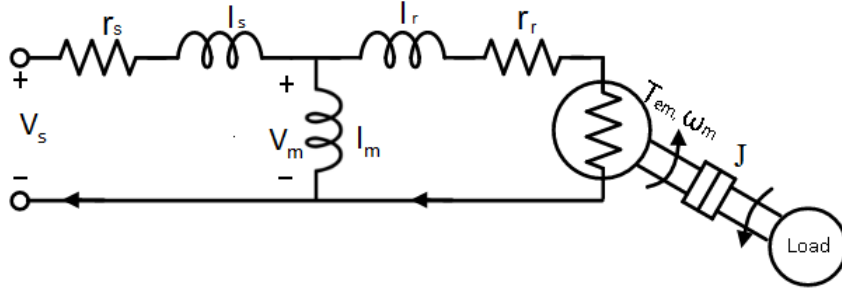


Fig. 2.4 Equivalent circuit of an induction motor
(source: B.K Bose, 1987)

Based on the control phenomena, the three-phase induction motor is modelled in the stationary reference frame using the equation 2.13, equation 2.14, equation 2.15 and equation 2.16 (Pimkumwong et al. 2012).

$$\frac{d}{dt} \begin{bmatrix} i_\alpha \\ i_\beta \\ \lambda_\alpha \\ \lambda_\beta \end{bmatrix} = \begin{bmatrix} -\frac{r_s}{\sigma l_s} & -\omega_r & \frac{r_r}{\sigma l_s l_r} & \frac{\omega_r}{\sigma l_s} \\ \omega_r & -\frac{r_s}{\sigma l_s} & -\frac{\omega_r}{\sigma l_s} & \frac{r_r}{\sigma l_s l_r} \\ -r_s & 0 & 0 & 0 \\ 0 & -r_s & 0 & 0 \end{bmatrix} \begin{bmatrix} i_\alpha \\ i_\beta \\ \lambda_\alpha \\ \lambda_\beta \end{bmatrix} + \begin{bmatrix} \frac{1}{\sigma l_s} & 0 \\ 0 & \frac{1}{\sigma l_s} \\ 1 & 0 \\ 0 & 1 \end{bmatrix} \begin{bmatrix} v_\alpha \\ v_\beta \end{bmatrix} \quad (2.13)$$

$$\sigma = 1 - l_m^2 / l_s l_r \quad (2.14)$$

$$T_e = \frac{3}{2} p (\lambda_\alpha i_\beta - \lambda_\beta i_\alpha) \quad (Nm) \quad (2.15)$$

$$T_e - T_{load} = \frac{2}{p} J \frac{d\omega_r}{dt} \quad (Nm) \quad (2.16)$$

where,

i_α and i_β = current components along α & β axis, respectively (A)

v_α and v_β = voltage components along α & β axis respectively (V)

λ_α and λ_β = flux components along α & β axis respectively (Wb turns)

r_s = stator resistance (Ω)

l_s = stator inductance (H)

r_r = rotor resistance (Ω)

l_r = rotor inductance (H)

l_m = magnetization inductance (H)

ω_r = electrical speed (Rad\sec)

T_e = electromagnetic torque (Nm)

T_{load} = load torque (Nm)

J = rotor inertia constant ($Kg \ m^2$)

p = pair of poles

σ = stray factor.

2.4.2 Voltage source inverter

Voltage source inverters are mainly used in AC motor drives for DC-AC conversion. The circuit diagram of the three-phase 2 level voltage source inverter is shown in the Figure 2.5.

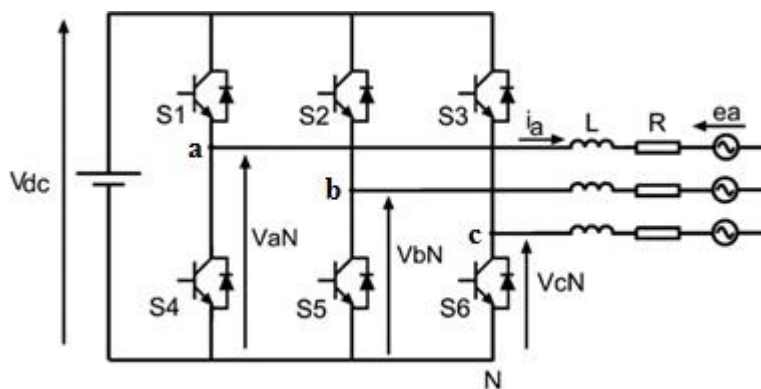


Figure 2.5 Circuit diagram of voltage source inverter
(source: B.K Bose, 1987)

The circuit is built with Insulated Gate Bipolar transistors (IGBTs) as switching devices and diodes as protection devices. The switches S1, S2, S3, S4, S5, and S6 are the IGBTs in

parallel with the diodes. A DC source ‘ V_{dc} ’ is connected as input to the inverter and a three-phase motor is acting as a load. The magnitude of the output voltage depends on the ON and OFF periods of the switching devices. The switching of the power devices is guided by giving the gate pulses to the IGBT gate terminals.

Table 2.1 shows the eight possible combinations of ON and OFF patterns for the three upper power switches (i.e. S1, S2 and S3). The ON and OFF states of the upper power devices are opposite to the lower power devices (i.e. S4, S5 and S6) and are easily determined once the upper power transistors are determined and vice-versa.

Considering a state say ‘ V_0 ’, at which all the upper devices are in the OFF position, so that all the gate pulses are given to the lower devices of the inverter circuit and hence resultant output voltage will be zero.

Table 2.1 Switching table for a two-level voltage source inverter

Switching states			Phase voltages			Line voltages			Output vectors from the inverter
a	b	c	V_{an}	V_{bn}	V_{cn}	V_{ab}	V_{bc}	V_{ca}	
0	0	0	0	0	0	0	0	0	V_0
1	0	0	$2/3$	$-1/3$	$-1/3$	1	0	-1	V_1
1	1	0	$1/3$	$1/3$	$-2/3$	0	1	-1	V_2
0	1	0	$-1/3$	$2/3$	$1/3$	-1	1	0	V_3
0	1	1	$-2/3$	$1/3$	$1/3$	-1	0	1	V_4
0	0	1	$-1/3$	$-1/3$	$2/3$	0	-1	1	V_5
1	0	1	$1/3$	$-2/3$	$1/3$	1	-1	0	V_6
1	1	1	0	0	0	0	0	0	V_7

2.4.3 Concept of DTC

The basic structure of DTC consists of two hysteresis comparators to control the flux and the torque of the motor, torque and flux estimators, a look-up table, and a voltage source inverter (Depenbrock 1988; Gierse 1992; Takahashi and Noguchi 1986). In DTC technique, the output torque and speed of the motor are controlled by the use of the hysteresis comparators. These comparators provide the required voltage to the inverter for the motor control (Belhaouchet et al. 2018; Buja and Kazmierkowski 2004; Casadei et al. 2001; Marino et al. 2001; Reza et al.

2014). The machine's model is expressed in the stationary reference frame, and the stator flux, torque, and stator flux angle are calculated (Tazerart et al. 2015).

The three-phase vector quantities are transformed into equivalent two-phase vector quantities, for making calculation easy, using Park's Transformation (Overlin et al. 2019). Here, the three-phase voltages and currents of the induction motor are transformed into equivalent two-phase quantities using equation 2.17, equation 2.18, equation 2.19 and equation 2.20.

$$v_{\alpha} = \frac{2}{3}(v_a - \frac{1}{2}v_b - \frac{1}{2}v_c) \quad (V) \quad (2.17)$$

$$v_{\beta} = \frac{2}{3}(-\frac{\sqrt{3}}{2}v_b - \frac{\sqrt{3}}{2}v_c) \quad (V) \quad (2.18)$$

where,

v_{α} and v_{β} = two-phase voltages along α and β axis, respectively

v_a , v_b and v_c = three-phase voltages along a, b and c axis, respectively

$$i_{\alpha} = \frac{2}{3}(i_a - \frac{1}{2}i_b - \frac{1}{2}i_c) \quad (A) \quad (2.19)$$

$$i_{\beta} = \frac{2}{3}(-\frac{\sqrt{3}}{2}i_b - \frac{\sqrt{3}}{2}i_c) \quad (A) \quad (2.20)$$

where,

i_{α} and i_{β} = two-phase currents along α and β axis, respectively

i_a , i_b and i_c = three-phase currents along a, b and c axis, respectively

The stator flux components can be estimated by using equations (2.21-2.22)

$$\lambda_{\alpha} = \int (v_{\alpha} - r_s i_{\alpha}) dt \quad (\text{Wb turns}) \quad (2.21)$$

$$\lambda_{\beta} = \int (v_{\beta} - r_s i_{\beta}) dt \quad (\text{Wb turns}) \quad (2.22)$$

where,

λ_{α} and λ_{β} = flux linkages along α and β axis, respectively

i_a , i_b and i_c = three-phase currents along a, b and c axis, respectively

v_{α} and v_{β} = two-phase voltages along α and β axis, respectively

i_α and i_β = two-phase currents along α and β axis, respectively

r_s = per phase stator resistance

The magnitude of the stator flux linkage can then be estimated by using equation (2.23)

$$\lambda_s = \sqrt{(\lambda_\alpha^2 + \lambda_\beta^2)} \text{ (Wb turns)} \quad (2.23)$$

where,

λ_α and λ_β = flux linkages along α and β axis, respectively

λ_s = stator flux linkage

The phase angle of stator flux linkage is estimated by using equation (2.24)

$$\theta_s = \tan^{-1} \left(\frac{\lambda_\beta}{\lambda_\alpha} \right) \text{ (deg)} \quad (2.24)$$

where,

λ_α and λ_β = flux linkages along α and β axis, respectively

θ_s = phase angle of stator flux linkage

And the electromagnetic torque can be estimated by using equation (2.25)

$$T_e = \frac{3}{2} p (\lambda_\alpha i_\beta - \lambda_\beta i_\alpha) \text{ (Nm)} \quad (2.25)$$

where,

T_e = electromagnetic torque

λ_α and λ_β = flux linkages along α and β axis, respectively

i_α and i_β = two-phase currents along α and β axis, respectively

p = number of pole pairs

By the theory of the sector, torque and flux command, an optimum switching voltage vector is obtained by Table 2.2. Here, L_ψ and L_T are the flux and torque commands, respectively. $v_0, v_1, v_2, v_3, v_4, v_5, v_6$ and v_7 are the eight possible voltage vectors. Sectors are I, II, III, IV, V

and VI. According to Table 2.2, if the flux command L_ψ and torque command L_T are equal to '1', and the stator flux is located in sector I, then the required voltage is ' v_2 '.

Table 2.2 Optimal switching vector look-up table

L_ψ	L_T	Sector					
		I	II	III	IV	V	VI
1	1	v_2	v_3	v_4	v_5	v_6	v_1
	0	v_0	v_7	v_0	v_7	v_0	v_7
	-1	v_6	v_1	v_2	v_3	v_4	v_5
0	1	v_3	v_4	v_5	v_6	v_1	v_2
	0	v_7	v_0	v_7	v_0	v_7	v_0
	-1	v_5	v_6	v_1	v_2	v_3	v_4

2.4.4 Space vector modulated DTC

Two of the significant issues that are usually addressed in classical DTC are variations in the inverter switching frequency and torque ripple (Arias et al. 2005; Hassankhan et al. 2008; Swarupa et al. 2009; Tan et al. 2001; Zhang et al. 2009). Space vector modulation (SVM) overcomes the two drawbacks mentioned above. SVM-DTC uses two proportional plus integral controllers to compare flux and torque errors and generate required voltage signals as shown in Figure.2.6. (Ozkop and Okumus 2008).

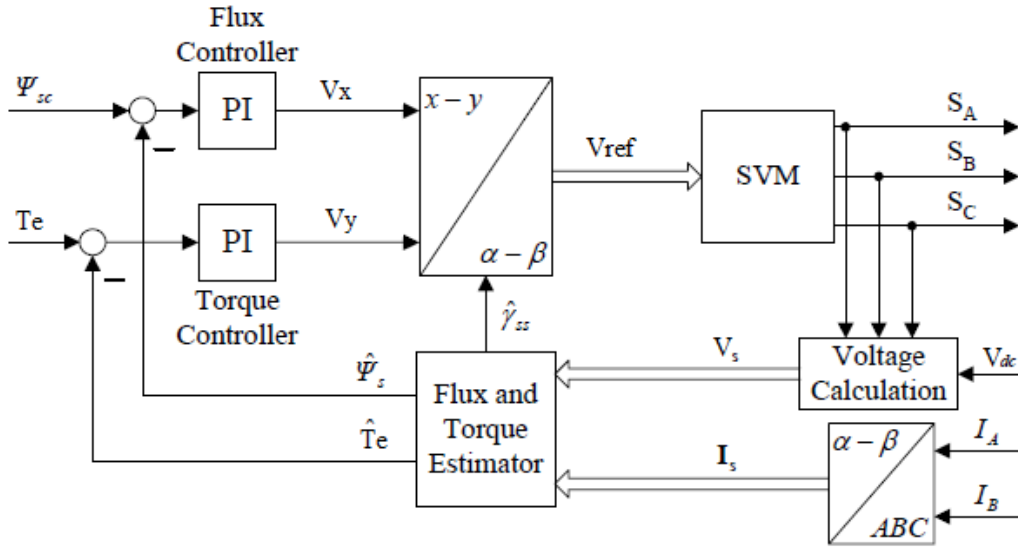


Figure 2.6 Block diagram of SVM-DTC
(source: Arias et al. 2005)

In space vector DTC, the reference voltage vector (v_{ref}) is synthesized by time averaging of the three nearest vectors around it in the hexagon (Sarathbabu Goriparti et al. 2019).

The algorithm for space vector DTC has the following steps:

1. Determination of reference voltage
2. Determination dwell times (ON/OFF state time of chosen switches)

The reference voltage is estimated using Equation (2.26) (Lascu and Trzynadlowski 2004)

$$v_{ref} = (v_{\alpha} + jv_{\beta}) \text{ (V)} \quad (2.26)$$

$$\varphi = \tan^{-1} \left(\frac{v_{\beta}}{v_{\alpha}} \right) \text{ (deg)} \quad (2.27)$$

where,

v_{ref} = reference voltage vector (V)

v_{α} and v_{β} = two-phase voltages along α and β axis, respectively (V)

φ = angle between v_{α} and v_{β} (Degrees)

The dwells can be estimated by using the principle called ‘volt-sec matching.’ This principle tells that the sum of the voltage vectors multiplied by the time interval of chosen space vectors

is the product of reference voltage ‘ v_{ref} ’ and sampling period ‘ T_s ’ (Dharmaprakash and Henry 2015; Gupta and Rao 2020; Manuel and Francis 2013; Motor et al. 2012; Zhang et al. 2011). That is when v_{ref} falls into Sector-I, it can be synthesized by surrounding vectors v_1 , v_2 , and v_z , as depicted in Figure. 2.7.

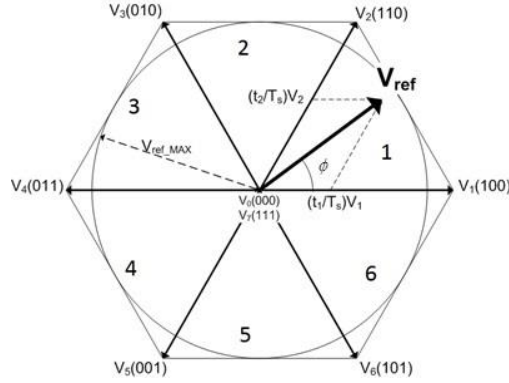


Figure 2.7 Hexagon used to synthesize reference voltage vector
(source: Arias et al. 2005)

The voltage balance condition is given by equation (2.28)

$$v_{ref} T_s = v_1 t_1 + v_2 t_2 + v_z t_z \quad (V \text{ sec}) \quad (2.28)$$

where,

v_{ref} = reference voltage vector (V)

T_s = sampling time (sec)

v_1, v_2 = non-zero voltage vectors at time t_1 and t_2 , respectively (V)

v_z = zero voltage vector (V)

t_1, t_2 and t_z = dwell times (sec)

The dwell times are estimated using the equation (2.24), equation (2.25) and equation (2.26) (G and R 2004; G et al. 1992; Geetha et al. 2009; Wankhade and Salodkar 2016; Yongchang et al. 2009)

$$t_1 = \frac{v_{ref} \sin(60 - \phi)}{v_{dc} \sin \phi} T_s \quad (sec) \quad (2.29)$$

$$t_2 = \frac{v_{ref} \sin \phi}{v_{dc} \sin 60} T_s \quad (sec) \quad (2.30)$$

$$t_z = T_s - t_1 - t_2 \quad (\text{sec}) \quad (2.31)$$

where,

v_{ref} = reference voltage vector (V)

T_s = sampling time (sec)

v_{dc} = DC input voltage to the inverter (V)

t_1 , t_2 and t_z = dwell times (sec)

ϕ = angle between v_1 and v_{ref} (deg)

2.4.5 Proportional-Integral-Derivative (PID) control

A PID control is a strategy widely used in industries to control the process variables, like flow, temperature, speed, position etc. (Bansal et al. 2012). They use a feedback mechanism to control process variables. The three-term PID control scheme provides the three major requirements of the control problems. P-term provides a control action over current errors. I-term mitigates the disturbance from constant errors and provides almost zero steady state error. D-term prevents future control errors. A PID controller is designed either using time-domain specifications (peak overshoot, settling time etc.) or frequency domain specifications (gain margin, phase margin etc.) (Asstrom and Hugglund 2001). However, derivative action is not required for most of the systems. Therefore, 90% of the controllers used in process control are Proportional integral (PI) type. PI control has two design specifications to control (viz. K_p & K_i)- proportional gain constant and integral gain constant.

CHAPTER 3

ORIGIN, OBJECTIVES, PURPOSE, AND SCOPE OF THE RESEARCH WORK

3.1 Origin of the Research Work

Coal clearance systems are very important in order to achieve the maximum benefit from capital investment costs on coal face and further operations to be carried out in mines. The specific energy consumption of a mineral transport system plays a vital role in minimizing the total production cost of the mine. Literature review on belt conveyor transport system indicated that a significant amount of work had been done on the design and selection of type of belt and pulleys, idlers and motor drives. However, very limited studies were done addressing the energy efficiency of belt conveyors by means of speed control. The energy efficiency of belt conveyors used for bulk material transport is not appreciable because of fixed speed run even at a variable feed rate of bulk material flow. Hence, the belt conveyor system demands for incorporation of some techniques to optimize the belt speed according to feed rate, so as to minimize the energy consumption.

In the current research work, field data of belt conveyor has been collected from GDK-1&3 Incline of M/s. The Singareni Collieries Company Limited (The SCCL) and the simulation was done for the collected field data using Matlab-Simulink. Further, experiments were carried out in the laboratory using a fabricated 0.5 hp belt conveyor drive system.

3.2 Objectives of the Research Work

The following are the objectives:

1. To model and estimate the electrical power required for a PVC belt conveyor, under different capacities, with and without connecting a VFD, using Simulink.
2. To investigate the effect of load acting on the belt, speed of the motor, length of the belt, and inclination of the belt on specific energy consumption, by using Simulink.
3. To control the speed and torque of a motor and to study its dynamic response on energy consumption, under different capacities by using a VFD in the laboratory.

4. To estimate the specific energy consumption, daily energy reduction, yearly energy saving under different capacities using proposed control.

3.3 Purpose of the Research Work

The production cost of underground mines rely on transporting extracted raw material from underground to surface. Belt conveyor system is the most common mode of transportation in underground mines. A contribution to optimize the performance of the belt conveyors can cut-down the production cost, thereby maximizing the profit for a particular mine. The purpose of this research study is to demonstrate the importance of optimizing speed of belt conveyor systems for achieving minimum specific energy. The amount of energy savings influence the production cost of underground mines.

3.4 Scope of the Research Work

The focus on energy conservation is very important so as to ensure the minimum operational cost of the mine. This study aims to analyze the characteristics of belt conveyor system, deployed in the underground coal mines, in order to optimize the energy consumption. Specific energy estimations were carried out for field belt conveyors (FBC). Further, improvements was achieved by adopting a feedback control system i.e. variable frequency drive (VFD) to ensure the minimization of energy consumption. Both simulation and laboratory investigations were carried out in order to ensure the minimum amount of energy consumption for both non-VFD and VFD-based models.

CHAPTER 4

RESEARCH METHODOLOGY

The main aim of this study is to analyze the belt conveyor's performance load (i.e., carrying coal) and to achieve energy efficiency using VFD. In underground mines, the primary transportation system is a belt conveyor, so it is essential to minimize the various power losses so as to achieve energy efficiency. The following sections summarize the research work carried out to achieve the above said goal.

4.1 Field Visit

1. The field visit was carried out at the GDK-1&3 incline, RG-I Area of M/s. The Singareni Collieries Company Limited, Telangana, India.
2. Data relevant to the belt conveyor system i.e., technical specifications of belt conveyors, such as belt speed, belt capacity, length and height were collected.
3. From the collected data, energy consumption and specific energy were estimated using standard formulae.
4. Scatter plots were drawn to understand the influence of load (coal) and feed rate on - belt speed, energy consumption, system efficiency and specific energy.

4.2 Simulation Studies

1. Simulation studies were carried out using Matlab-Simulink 2018b.
2. Field data was used for developing simulation models for both non-VFD and VFD. The output of the simulation models are energy consumption and specific energy. The input for simulation models are load torque, voltage of the motor, length and height of the belt conveyor.
5. Similarly, simulation studies were carried out for fabricated laboratory belt conveyor system.
6. Scatter plots were drawn to understand the influence of load (coal) and feed rate on - belt speed, energy consumption, system efficiency and specific energy, for both field and laboratory belt conveyors.

4.3 Laboratory Studies

- 1 A laboratory belt conveyor is fabricated such that it can facilitate the necessary elevations (i.e. 10°, 15° and 20°).
- 2 Energy consumption and specific energy were determined for be with non-VFD and VFD units.
- 3 Scatter plots were drawn to understand the influence of load on belt speed, energy consumption, system efficiency and specific energy.

4.4 Statistical Analysis

- 1 Statistical analysis was carried using Minitab V 18.
- 2 Linear regression models were developed to predict the specific energy for laboratory belt conveyor system. Models were developed individually for both non-VFD and VFD systems.
- 3 Scatter plots were drawn for experimental vs. predicted specific energy for each of the said models.

CHAPTER 5

FIELD INVESTIGATION

5.1 Study Area

Field studies were carried out at GDK-1&3 Incline, RG-I Area of M/s. The Singareni Collieries Company Limited, Telangana, India. The location of the mine is shown in Figure 5.1. The coal handling area of the plant is shown in Figure 5.2.



Figure 5.1 RG-1 Area of M/s. SCCL (source: <https://sclmines.com/sclnew/index.asp>)



Figure 5.2 Coal handling area of M/s. SCCL
(source: <http://www.meritbulkhandling.com/belt-conveyer.php>)

5.2 About Belt Conveyor Systems in GDK 1&3 Incline

This mine consists eight belt conveyor systems to transport the coal from the underground mines to the surface. Out of eight conveyors, three belt conveyors were considered for the study (viz. small, medium, and long length conveyors i.e., length 60 m, 260 m and 420 m, respectively). Figure 5.3 shows the layout of belt conveyors in the GDK 1&3 incline.

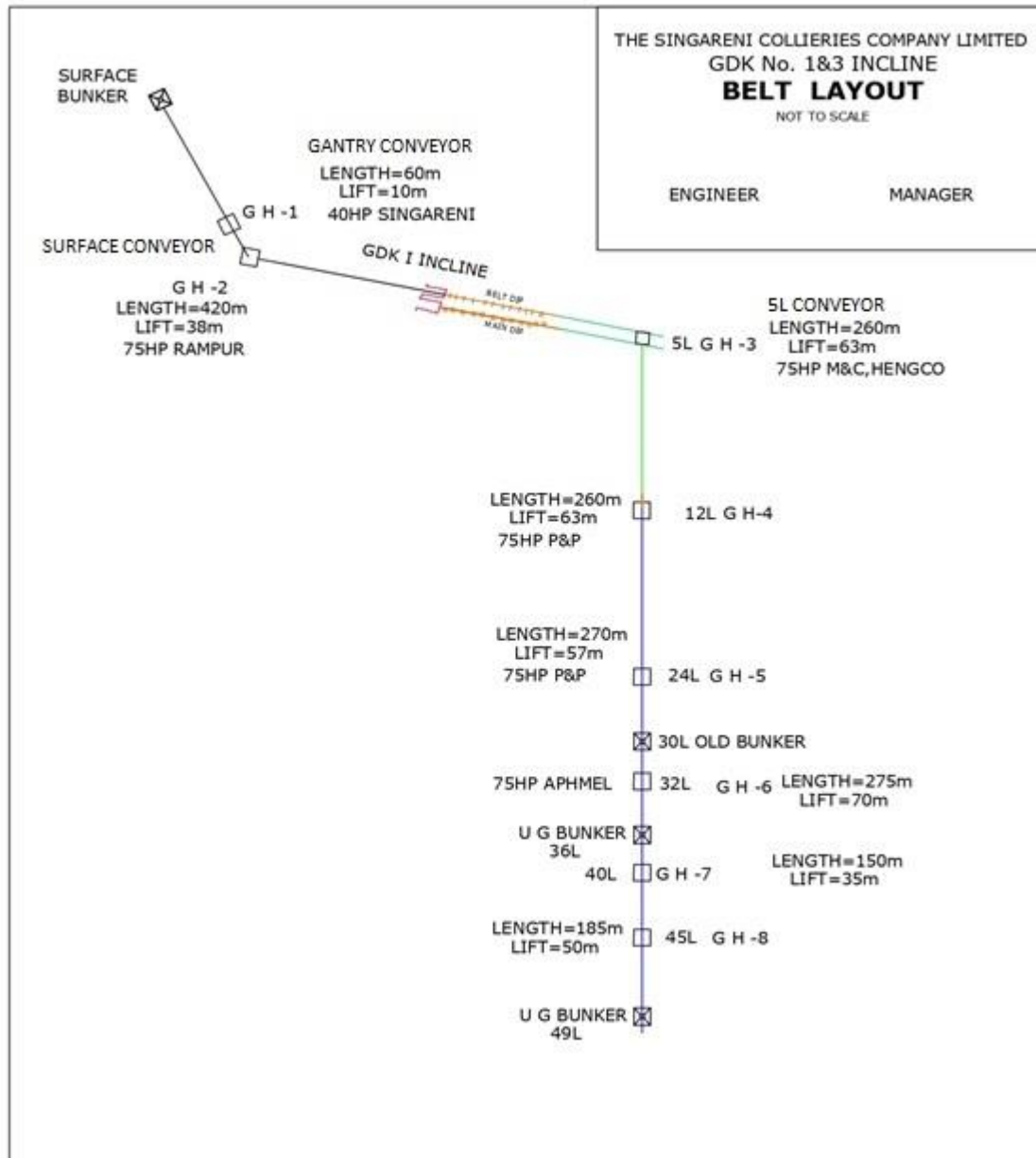


Figure 5.3 Line diagram of main belt conveyors used in GDK-1&3 incline.
(source: The SCCL Report)

5.3 Technical Details and Rated Values

A belt conveyor is a complex system used to transfer material from one end to the other end because of having a large number of moving parts, such as idlers, pulleys, drive motor etc. Therefore, the performance as well as the efficiency of the conveyor system varied, which is mainly depends on the efficiency of the drive motor, efficiency of the gear system and efficiency of the control system used. Thus, for energy estimations, the belt conveyors' technical details were collected from the mine under study, which are listed in Table 5.1.and Table 5.2.

Table 5.1 Technical details of belt and rollers of FBC system

Nominal parameters	Symbol	Value	Unit
Maximum conveying capacity	Q_m	200	t / h
Belt speed	v	2	m / s
Belt width	B	900	mm
Loaded material weight	M_l	30	kg / m
Conveying length	L	60/260/420	m
Conveying height	H	10/63/40	m
Inclination	β	9.46/13.6/5.44	$^\circ$
Belt length	L_b	535	m
Belt thickness	T_b	20	mm
Belt weight	M_b	15	kg / m
idler weight	M_r	54	kg / m
The radius of the drive pulley	R_d	35.1	cm
Friction coefficient	C_f	0.025	-
Made	PVC	Type2	-

Table 5.2 Technical details of drive of FBC system

Nominal parameters	Symbol	Value	Unit
Power	P	75/55	hp / kW
Line Voltage	V	415	$Volt$
Frequency	f	50	Hz
Stator resistance	R_s	0.0862	Ω
Stator inductance	L_s	0.0007829	H
Rotor resistance	R_r	0.0862	Ω
Rotor inductance	L_r	0.0013	H

Mutual inductance	L_m	0.0299	H
Moment of inertia of the rotor	J	0.9818	$kg - m^2$
Friction factor	...	0	---
Pole pairs	p	2	---
Current	I	90	Amp
Power factor	$\cos \phi$	0.88	-
Efficiency	η	94.3	%
Torque at full load	T_{fl}	354	$N - m$
Approximate weight	M_m	540	kg
Rated motor speed	N	1482	rpm
Gear reduction ratio	K	1:30	-
Reduction gear speed	N_{gr}	50	rpm

After collecting the technical details of belt conveyor system from the mine, the calculations w.r.t energy consumption, efficiency and specific energy were done for three belt conveyors: i.e. Gantry (length 60 m), 5L (of length 260 m) and from surface conveyor (length 420 m). These three conveyors (i.e. gantry, 5L and surface) are designated as FBC1, FBC2 and FBC3 in the thesis and some are used in the later sections. The specifications of the FBC1, FBC2 and FBC3 are given in Table 5.3.

Table 5.3 Specifications of FBCs

Name of the conveyor	Length, L, ,m	Height, H, ,m	Inclination, β , ,degree	Capacity ,hp	Belt width ,mm	Voltage ,V
FBC1	60	10	9.46	75	900	440
FBC2	260	63	13.6	75	900	440
FBC3	420	40	5.44	75	900	440



Figure 5.4 Idler and belt



Figure 5.5 Belt conveyor system handling coal



Figure 5.6 Motor drive of belt conveyor

5.4 Results and Discussions

The total driving force, mechanical power required, input power required, the conveyor's efficiency, monthly and annual energy consumption and the conveyor's specific energy were

estimated using standard formulae. The formulae used and details of calculations are given in annexure and the results are tabulated in Table 5.4, Table 5.5 and Table 5.6. The energy consumption of three FBCs was estimated by Motion Resistance Method. The mine working hours are assumed as 8 hours per day while calculating the conveyor's energy consumption. The density of the coal is assumed to be 1350 kg/m³.

The total driving force required by the belt conveyor for its run was calculated using equation (2.1). Similarly, the mechanical required by the drive motor was calculated using equation (2.3). The electrical power required by the conveyor was estimated by adding total power losses of the motor to the mechanical power required by the conveyor. The efficiency of the drive motor was calculated using equation (2.4). And the belt conveyor's energy consumption (kWh) was estimated using equation (2.5). Further, the monthly, and annual energy consumptions were calculated for 200, and 2,400 working hours, respectively. The specific energy was estimated using equation (2.12)

Table 5.4 Calculated energy consumption of FBC1

β	k	Q	F	v	P_o	P_i	η	E_m	E_y	W_s
9.462	0.2	40	2250	2	4500	6790	66.27	1358	16296	2.8292
9.462	0.4	80	4420	1.9	8398	10600	79.23	2120	25440	2.2083
9.462	0.6	120	6279	1.9	11930	14130	84.43	2826	33912	1.9625
9.462	0.8	160	7561	1.9	14365	16560	86.75	3312	39744	1.7250
9.462	1	200	9724	1.8	17504	19702	88.84	3940	47285	1.6418
Note: β = Inclination F = Total driving force P_o = Output/ mechanical power E_y = Energy consumption/year k = Filling rate v = Belt speed η = Efficiency W_s = Specific energy Q = Material discharge P_i = Input/ electrical power E_m = Energy consumption/month										

Table 5.5 Calculated energy consumption of FBC2

β	k	Q	F	v	P_o	P_i	η	E_m	E_y	W_s
13.6	0.2	40	12107	2	24214	26410	91.68	4843	58114	1.5720
13.6	0.4	80	13293	2	26486	28854	91.79	5317	63806	0.8588
13.6	0.6	120	17537	1.9	33320	35525	93.79	6664	79968	0.7049
13.6	0.8	160	23044	1.8	41480	43685	94.95	8296	99552	0.6501
13.6	1	200	26961	1.8	48530	51269	94.66	9706	116472	0.6103
Note: β = Inclination F = Total driving force P_o = Output/ mechanical power k = Filling rate v = Belt speed η = Efficiency W_s = Specific energy Q = Material discharge P_i = Input/ electrical power E_m = Energy consumption/month										

$E_y = \text{Energy consumption/year}$ $W_s = \text{Specific energy}$

Table 5.6 Calculated energy consumption of FBC3

β	k	Q	F	v	P_o	P_i	η	E_m	E_y	W_s
5.44	0.2	40	7263	2	14525	18923	76.76	2905	34860	1.8195
5.44	0.4	80	12016	2	24032	27880	86.20	4806	57677	1.3404
5.44	0.6	120	14827	1.9	28171	31470	89.52	5634	67610	1.0087
5.44	0.8	160	21848	1.8	39326	41520	94.72	7865	94382	0.9981
5.44	1	200	26739	1.8	48130	50881	94.59	9626	115512	0.9785

Note:

$\beta = \text{Inclination}$	$k = \text{Filling rate}$	$Q = \text{Material discharge}$
$F = \text{Total driving force}$	$v = \text{Belt speed}$	$P_i = \text{Input/ electrical power}$
$P_o = \text{Output/ mechanical power}$	$\eta = \text{Efficiency}$	$E_m = \text{Energy consumption/month}$
$E_y = \text{Energy consumption/year}$	$W_s = \text{Specific energy}$	

In general, the speed of any electric motor/ machine will decrease with the increase of load. That means, under no-load condition, the machine runs at its maximum rated speed, and at full-load condition, it runs at minimum speed. However, the speed-load relationship is not linear for all types of loads. The speed-torque waveform is different for different types of loads, such as fans, centrifugal pumps, hoists, conveyors etc. This is due to the requirement of starting torque which is different for each kind of load. Some applications require less torque at starting and some may require high torque. Belt conveyors require a very high starting torque, and it is almost constant throughout their operation. Therefore, it is called a constant torque application, since the load changes doesn't affect the speed of operation considerably.

The belt speed, energy consumption, efficiency and specific energy plots were drawn correspondingly to the varying feed rate (40 t/h to 200 t/h), for all three FBCs, which are shown in figure 5.7, figure 5.8, figure 5.9 and figure 5.10, respectively.

From figure 5.7, it is evident that the speed of all the three belt conveyors is almost constant with varied feed rate and resulting in higher power consumption, which makes the system unreliable. The amount of variation in speed w.r.t. feed rate was found 10%, 10% and 5.2% for FBC1, FBC2 and FBC3, respectively. As shown in figure 5.8, the energy consumption increases with increased feed rate. The energy consumption is less with lower feed rate and higher with highest feed rate. The amount of variation of energy consumption w.r.t. feed rate was found 66.66%, 47.96% and 62.29% for FBC1, FBC3 and FBC3, respectively.

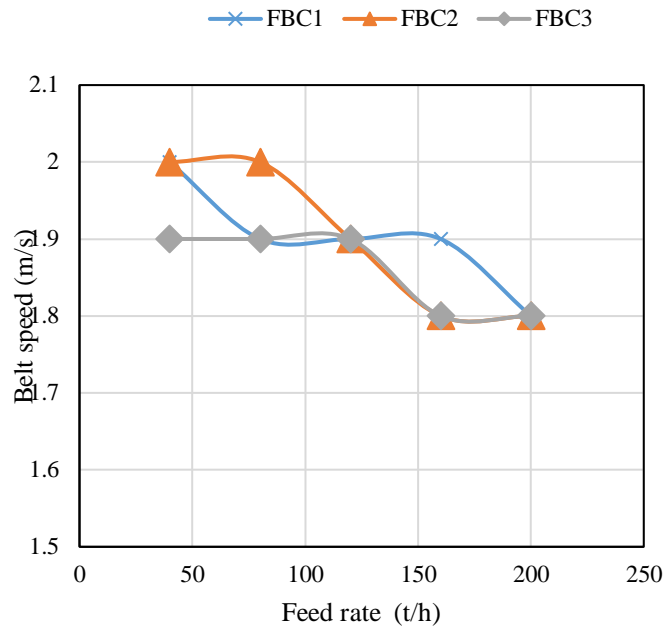


Figure 5.7 Influence of feed rate on belt speed

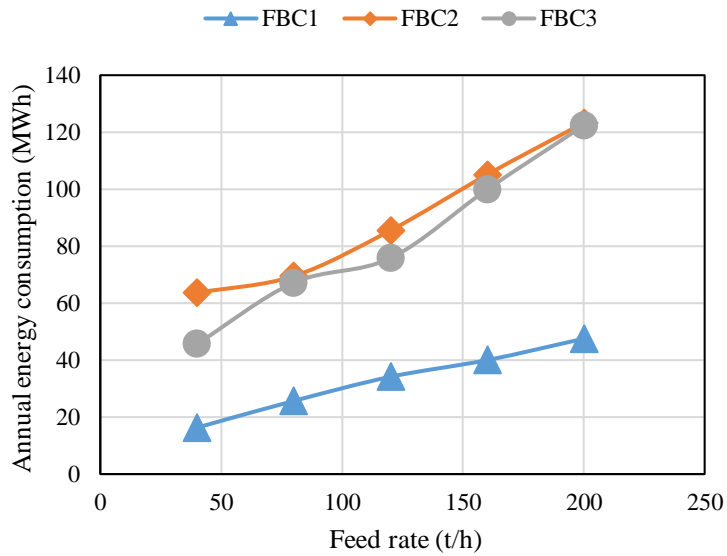


Figure 5.8 Influence of feed rate on annual energy consumption

From figure 5.9, it was observed that the efficiency of the FBCs increases with increase in feed rate and after it is almost constant for the values considered. This is because efficiency is

directly proportional to load applied. The amount of variation of conveyor efficiency w.r.t. feed rate was found 23.92%, 3.14% and 18.75% for FBC1, FBC3 and FBC3, respectively.

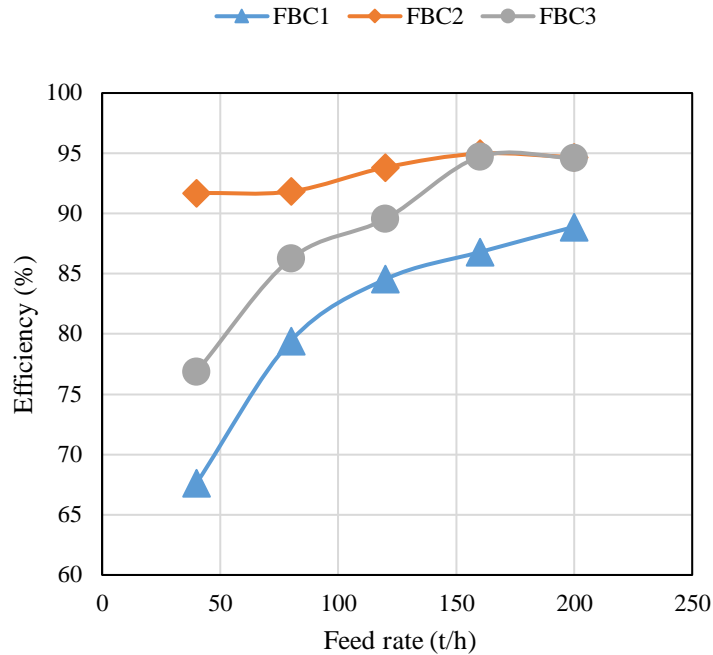


Figure 5.9 Influence of feed rate on efficiency

Figure 5.10 show that the specific energy consumption was found to be in the order FBC1>FBC3>FBC2. This is due to the varying height to which the coal has to be delivered; which is also found to be in the order FBC1>FBC3>FBC2. The amount of variation of specific energy w.r.t. feed rate was found that 41.69%, 59.4% and 46.44% for FBC1, FBC3 and FBC3, respectively.

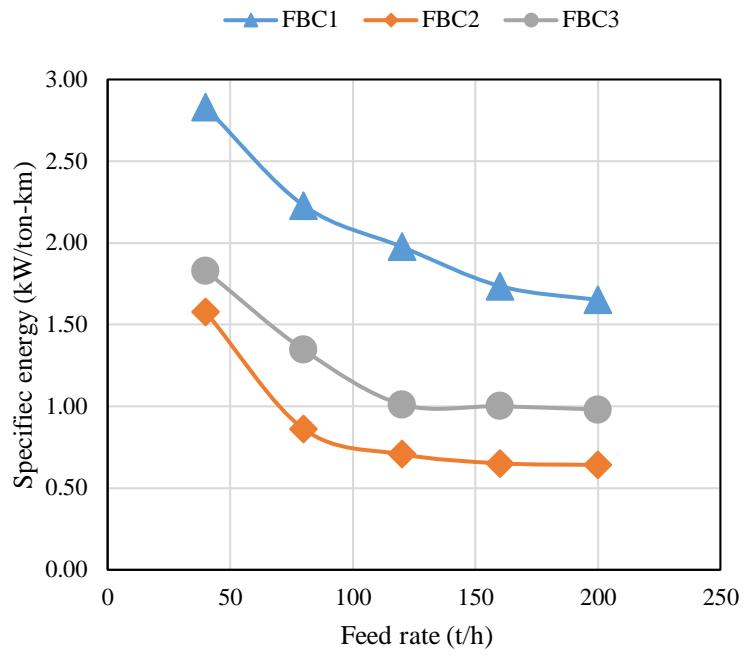


Figure 5.10 Influence of feed rate on specific energy

CHAPTER 6

SIMULATION STUDIES

MATLAB-Simulink R 2016a was used to simulate the efficiency and specific energy of field belt conveyor (FBC) and laboratory belt conveyor (LBC) systems. Input parameters for the simulation include different loading on the belt, inclination of the conveyor, length and height of the conveyor. Simulations were conducted for non-VFD and VFD configured models. The efficiency and specific energy of FBC and LBC were simulated and predicted for three different conditions i.e. FBC1, FBC2 and FBC3 for FBC and LBC1, LBC2 and LBC3 for LBC. The specifications of FBC and LBC models with varying parameters are listed in Table 6.1 and Table 6.2.

Table 6.1 Specifications of FBC system

Name of the conveyor	Length, L ,m	Height, H ,m	Inclination, β ,degree
FBC1	60	10	9.46
FBC2	260	63	13.6
FBC3	420	40	5.44


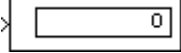
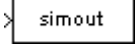
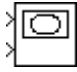







Table 6.2 Specifications of LBC system

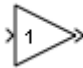
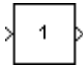
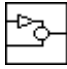

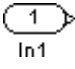
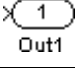
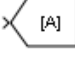
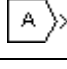
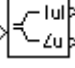
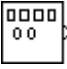

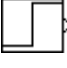


Name of the conveyor	Length, L ,m	Height, H ,m	Inclination, β ,degree
LBC1	2	0.35	10
LBC2	2	0.53	15
LBC3	2	0.72	20

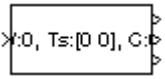
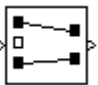
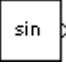
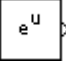


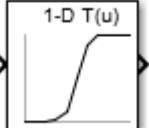
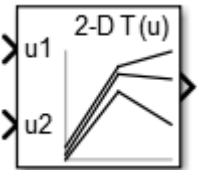
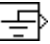

6.1 Blocks Used in the Construction of Simulink Models for FBC and LBC Systems

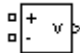
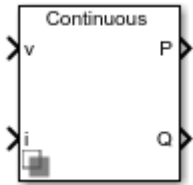

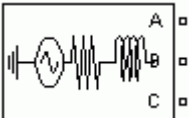
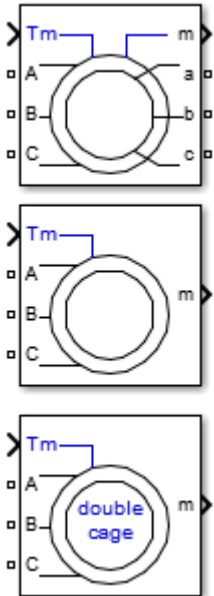
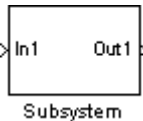
Table 6.3 indicate the various block elements used in constructing the simulation models for all non-VFD and VFD-based FBC and LBC models. These models were similar and hence a single model was developed to obtain the outputs. Different parameters of FBC and LBC are fed to the model and outputs were recorded correspondingly for FBC1, FBC2, FBC3, LBC1, LBC2 and LBC3.

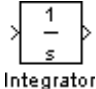
Table 6.3 Blocks used in the construction of Simulink models

S.No.	Name of the block	Symbolic representation	Purpose
1	Scope		Shows the output waveforms.
2	Display		Displays the measured output values.
3	To workspace		Transfers the output data from Simulink to workspace.
4	X-Y Graph		Plots two input variables
5	Mux		Convert many inputs to a single output.
6	Demux		Convert single input to many outputs.
7	Sum	 Sum	It performs the addition/ subtraction of two or more signals and generates a resultant output.
8	Dot product		Dot products the two vector quantities
9	Product		Products the two scalar quantities
10	Clock		Used to set the computation time of any block
11	Terminator		Used to terminate the output signal

12	Gain		It multiplies the input by a gain constant; it may be scalar or vector
13	Slider gain		Used to change the gain between two values
14	Subsystem		Part of the main Simulink block
15	Stop		Used to stop the Simulation
16	Inport		Calls the input value from port1
17	Outport		Returns the output value to port1
18	Goto		Returns the value 'A'
19	From		Calls the value 'A.'
20	Complex to magnitude-angle		Converts a complex value into polar value.
21	Signal generator		It is used to generate required signals; sine, square, sawtooth, etc.
22	Pulse generator		Used to generate pulses of required magnitude and frequency
23	Step signal		It gives a step signal of magnitude A
24	Ramp signal		It gives a ramp signal having the slope dy/dx
25	Repeating sequence		It gives a repeating sequence

26	Probe		Gives the data of displacement, sample time, and the dimensions of the measured quantity
27	Selector		Selects the inputs based on the logic/requirement
28	Trigonometric function		Used to write any trigonometric function; such as sine, cos, tan, etc
29	Math function		Used to write the mathematical equations
30	Relay		The Relay block allows the output to switch between two specified values.
31	Sign function		It is used to find the sign of the input signal. The outputs are 1, 0, and -1 for positive, zero, and negative values of input.
32	1-D Look-up-table		It derives an approximation for a function (1-D) y in terms of x, using interpolation and extrapolation
33	2-D Look-up-table		It derives an approximation for a function (2-D) z in terms of x and y.
34	Ground		Used to grounding the circuit
35	Ammeter		It is used to measure the instantaneous values of current

36	Voltmeter		It is used to measure the instantaneous values of voltage
37	Wattmeter		It is used to measure the active and reactive powers in a single-phase or three-phase circuit.
38	Powergui		This block is used to select the type simulation; continuous, digital, and phasor.
39	Three-Phase Source		It supplies a balanced three-phase ac supply. The three voltages are connected in star fashion with a neutral grounding.
40	Three-phase induction motor		It converts three-phase electrical input into mechanical force. It drives the loads.
41	Subsystem		Group blocks into a subsystem

42	Integrator		It integrates the signal
----	------------	---	--------------------------

6.2 Simulink Models for FBC and LBC

The simulation models have been developed for both the FBC and LBC systems using Simulink library block elements, which is available in MATLAB. Two files namely, a MATLAB file with extension ‘.m’ and a Simulink file with extension ‘.mdl.’ were used for construction of models. The necessary blocks were retrieved to the Simulink workspace through a Simpower System Toolbox. The order in which the blocks were chosen follows as - three-phase ac supply, 3-phase induction motor, conveyor load, ammeter, voltmeter and a wattmeter with interfaced scopes. The necessary parameters for using the blocks were defined by double-clicking on the block.

Since, the conveyor load in Simpower systems is not readily available, an algebraic equation i.e. Equation (2.1) of Chapter 2 was constructed using the ‘Math function’. The representation of conveyor load is shown in Figure 6.1. The algebraic equation parameters are provided as inputs in the MATLAB Command window (i.e. notations along with their magnitudes) and saved as an ‘.m’ file. The output was obtained by compiling the ‘.m’ file and it was stored in MATLAB Workspace.

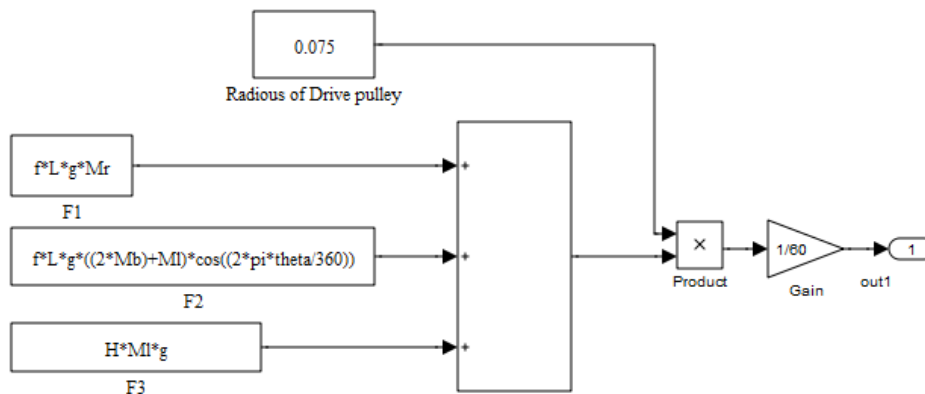


Figure 6.1 Simulink model for conveyor load

The input parameters of conveyor load were varied in the '.m' file and compiled to obtain corresponding outputs. After compiling the '.m' file, the Simulink model was run. However, simulation time has been provided before running the simulation models. The simulated outputs, such as electromagnetic torque, current, voltage, input and output power of a motor, energy consumption of the conveyor, efficiency of the motor, belt speed and motor speed were recorded using their respective displays and scopes.

As this study involves the simulation of both field and lab belt conveyors, the parameters relevant to the conveyors were modified, and each model was made available. The schematic representation of the Simulink model of each conveyor system are presented in figure 6.2 to 6.7 for FBC1, FBC2, FBC3, LBC1, LBC2 and LBC3, respectively for non-VFD configuration. Similarly, Simulink model for VFD configuration are presented in figure 6.8 to 6.13 for FBC1, FBC2, FBC3, LBC1, LBC2 and LBC3, respectively. The Simulation parameters of FBC and LBC models are listed in Tables 6.4 to 6.7. The outputs of each model were recorded and given in Table 6.8 to 6.15, respectively.

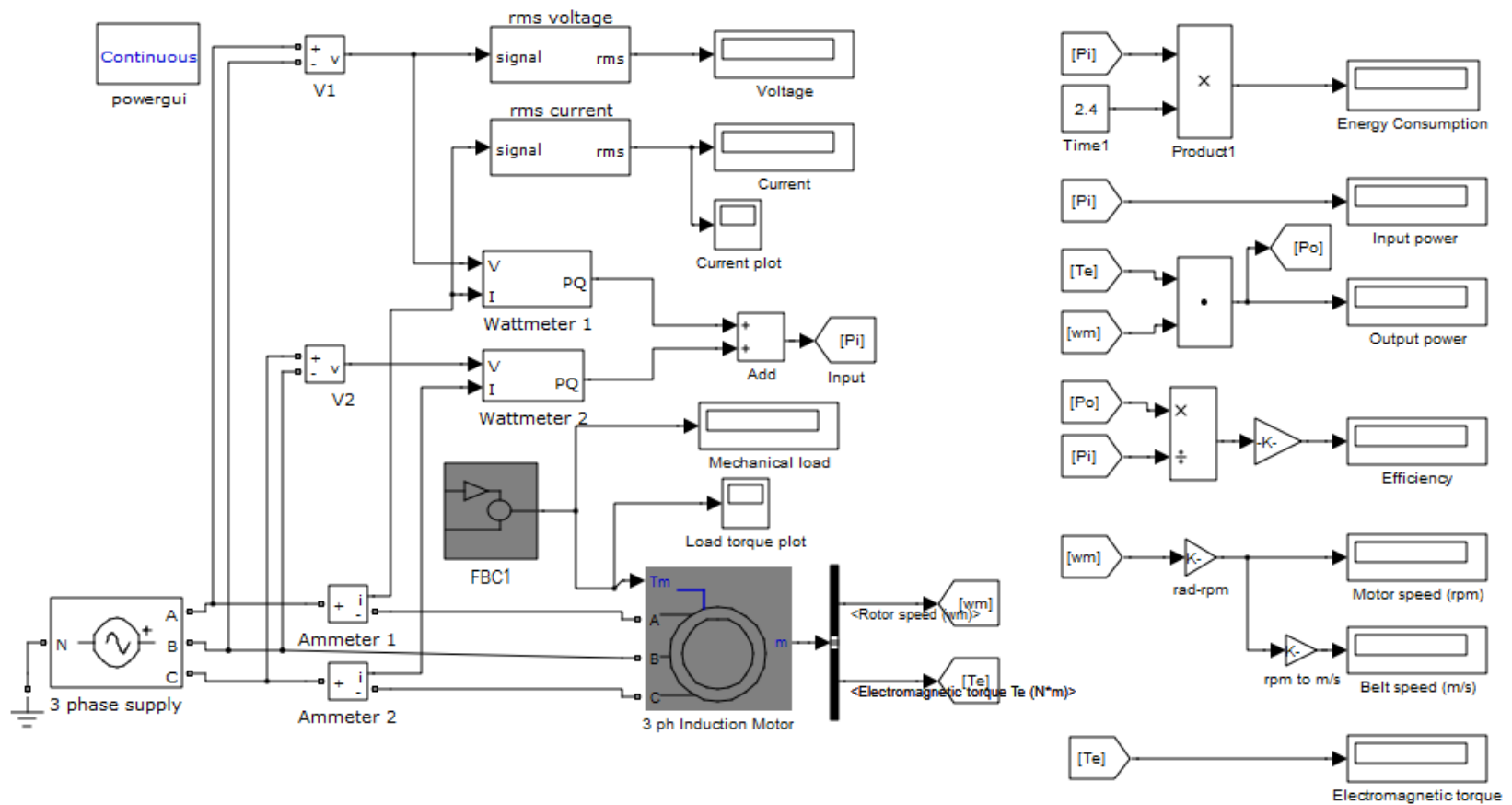


Figure 6.2 Simulation model for non-VFD configured FBC1

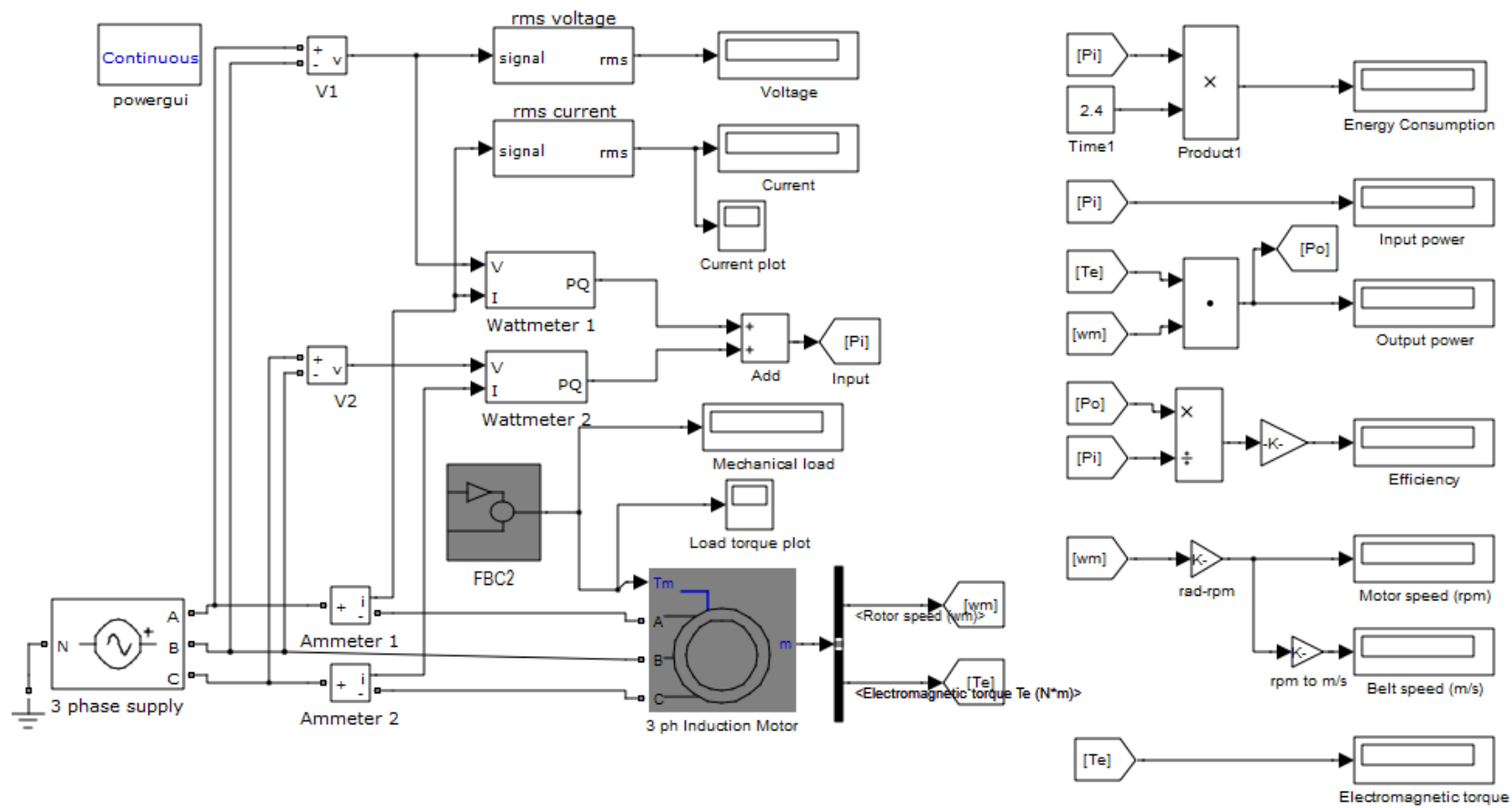


Figure 6.3 Simulation model for non-VFD configured FBC2

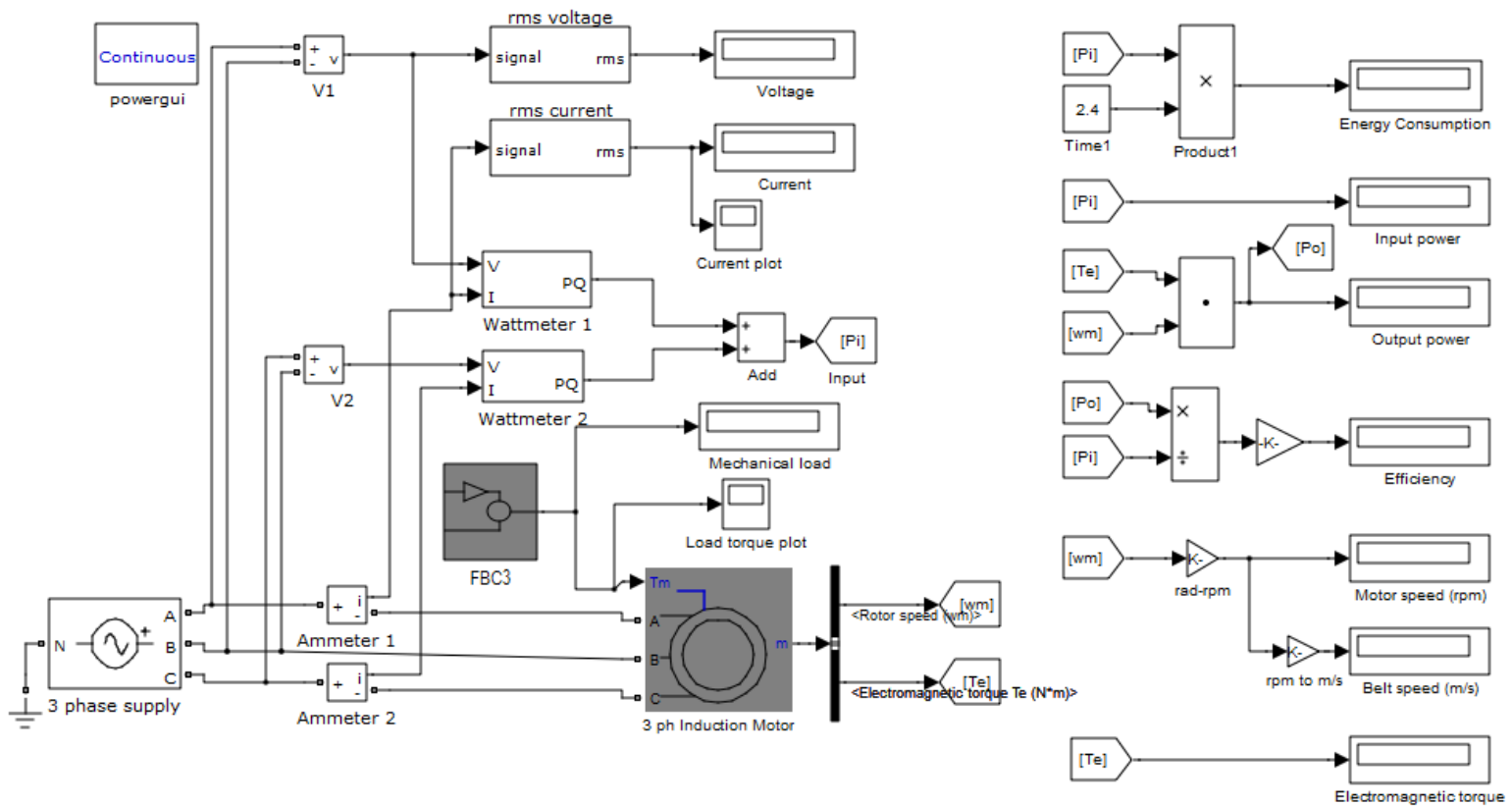


Figure 6.4 Simulation model for non-VFD configured FBC3

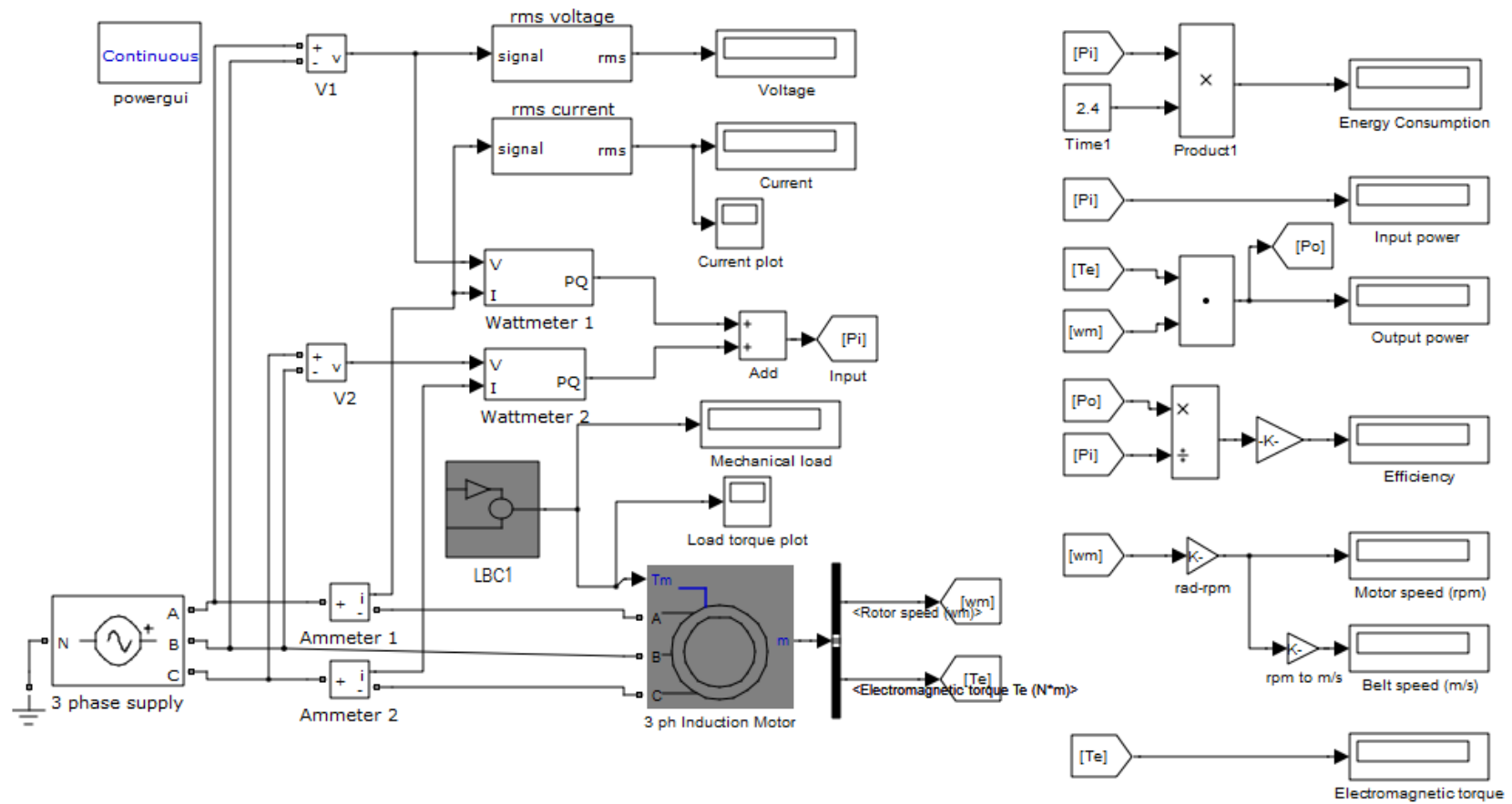


Figure 6.5 Simulation model for non-VFD configured LBC1

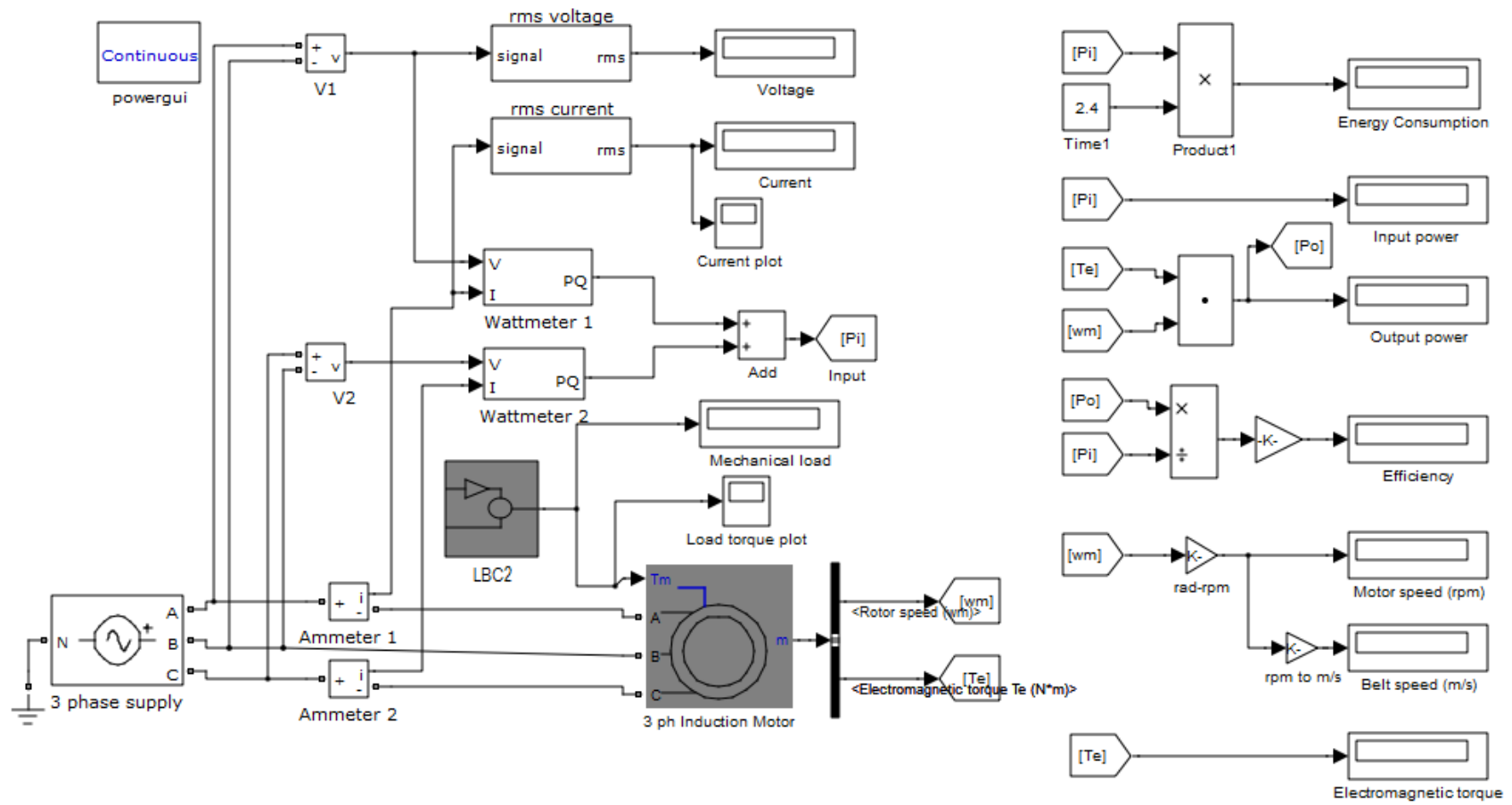


Figure 6.6 Simulation model for non-VFD configured LBC2

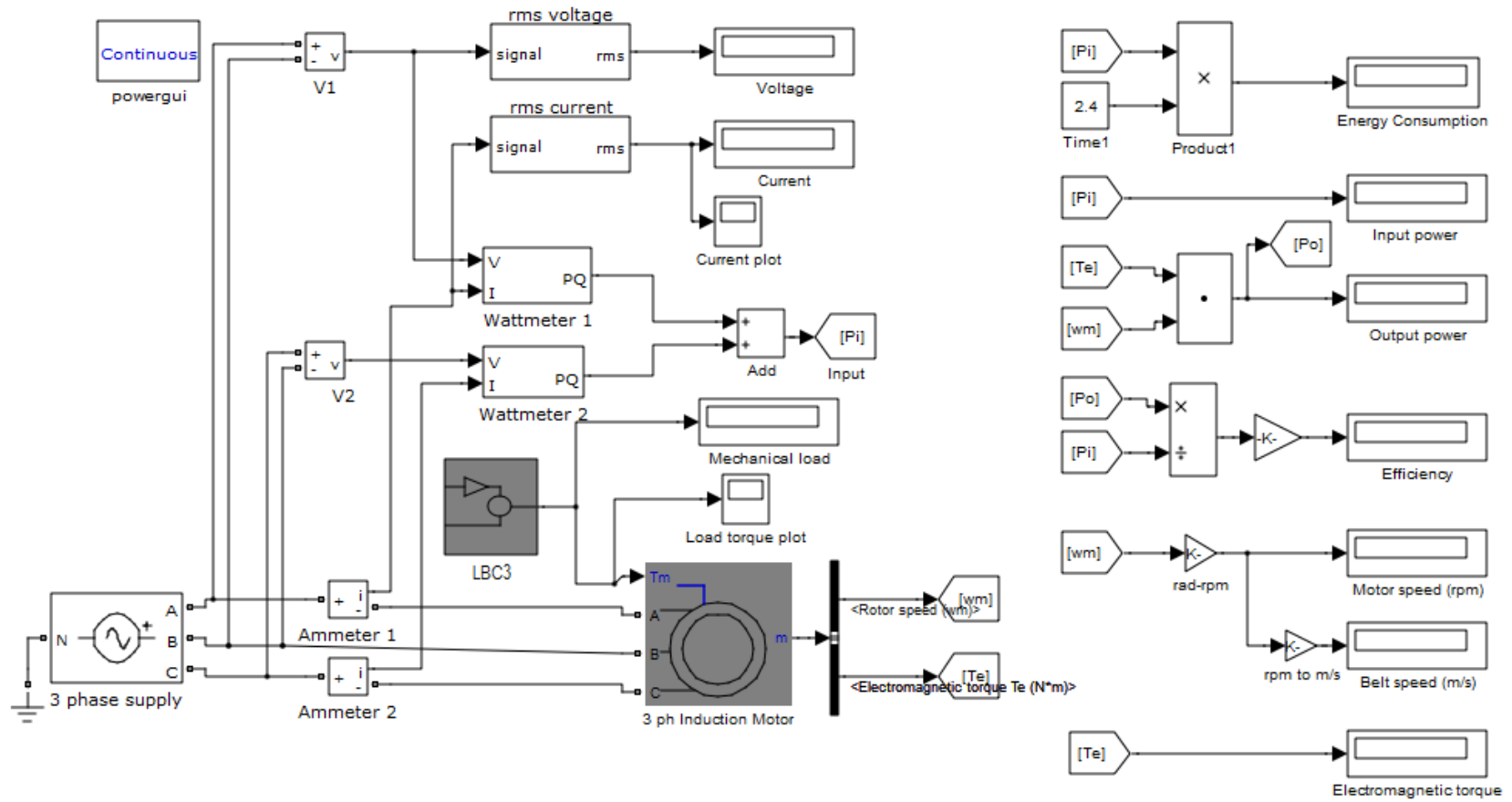


Figure 6.7 Simulation model for non-VFD configured LBC3

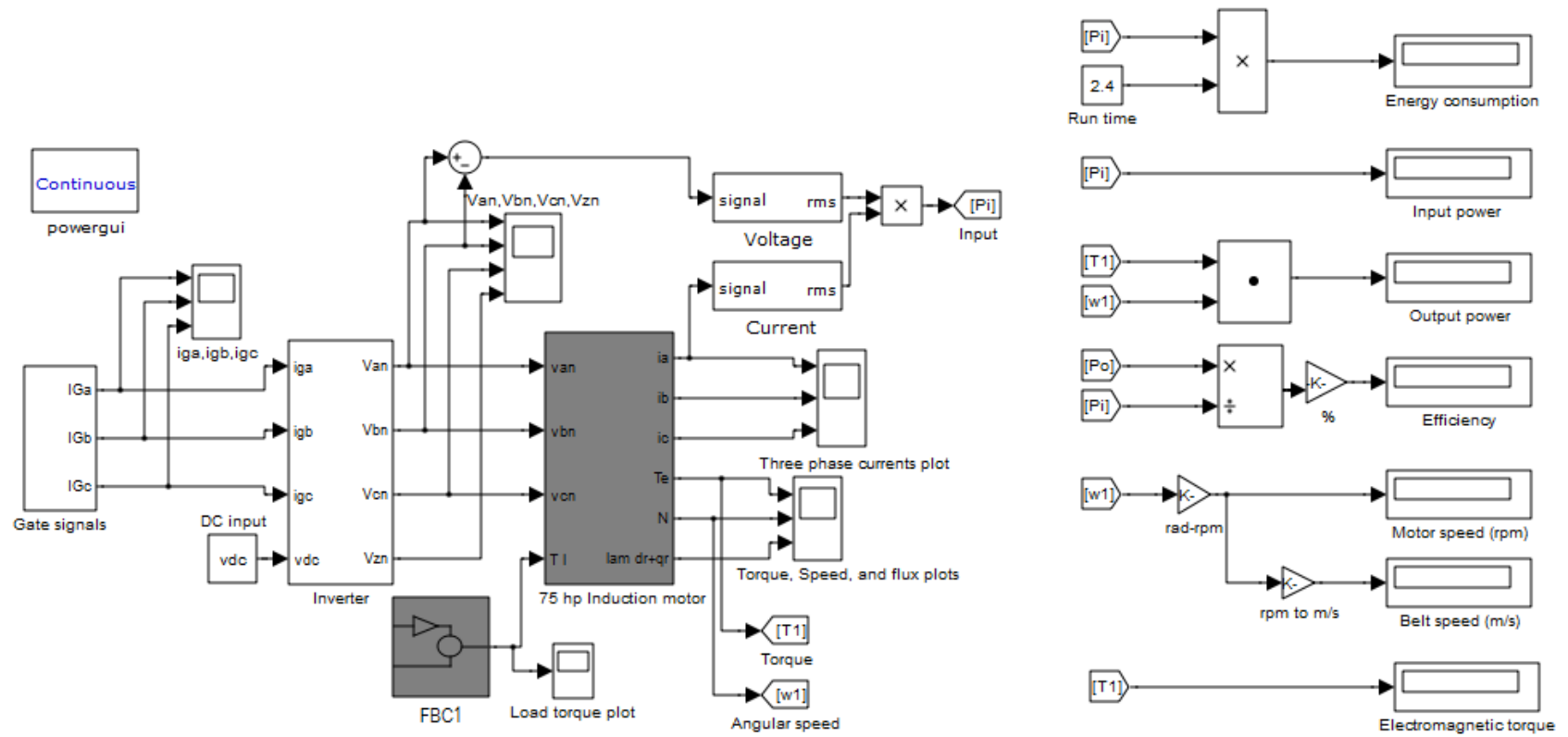


Figure 6.8 Simulation model for VFD configured FBC1

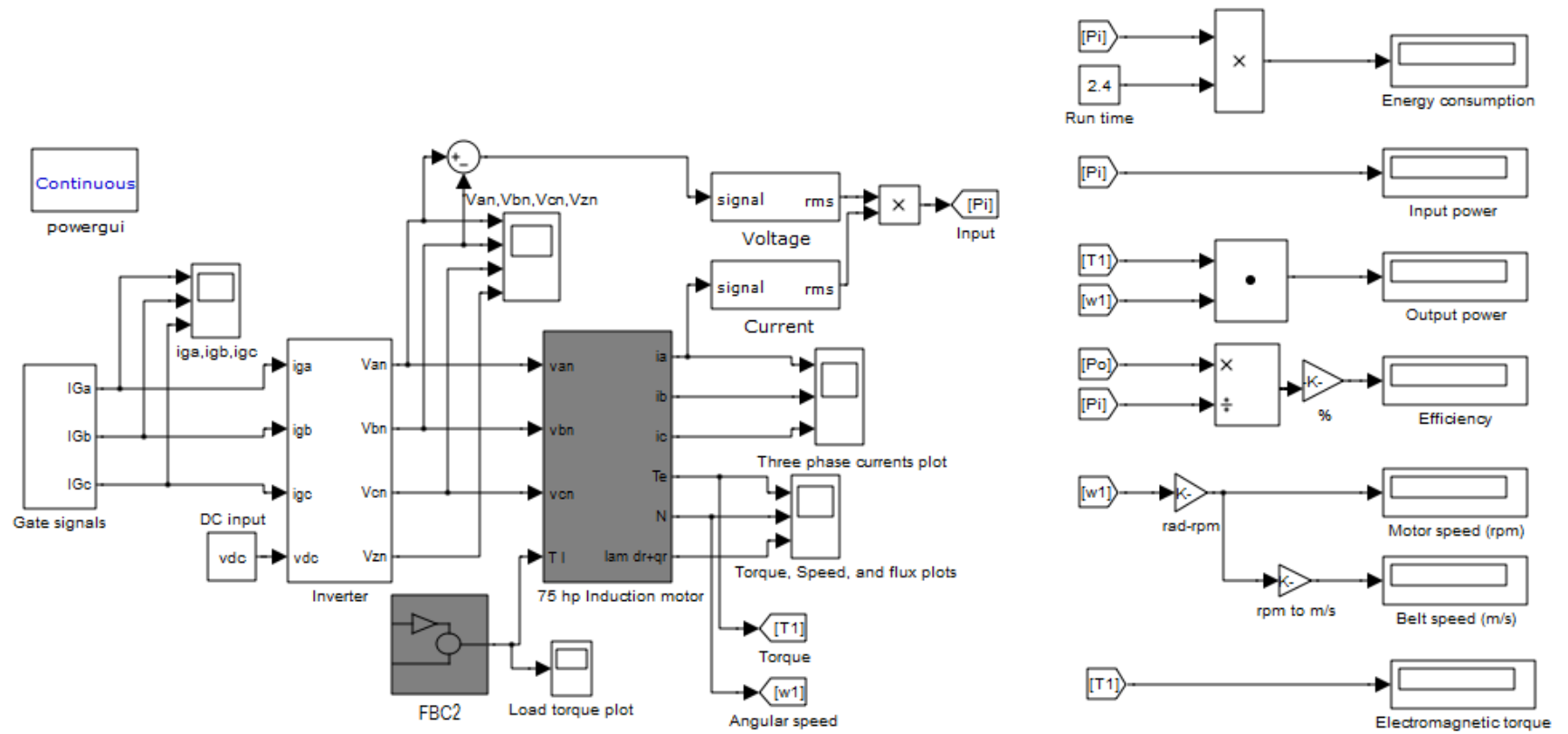


Figure 6.9 Simulation model for VFD configured FBC2

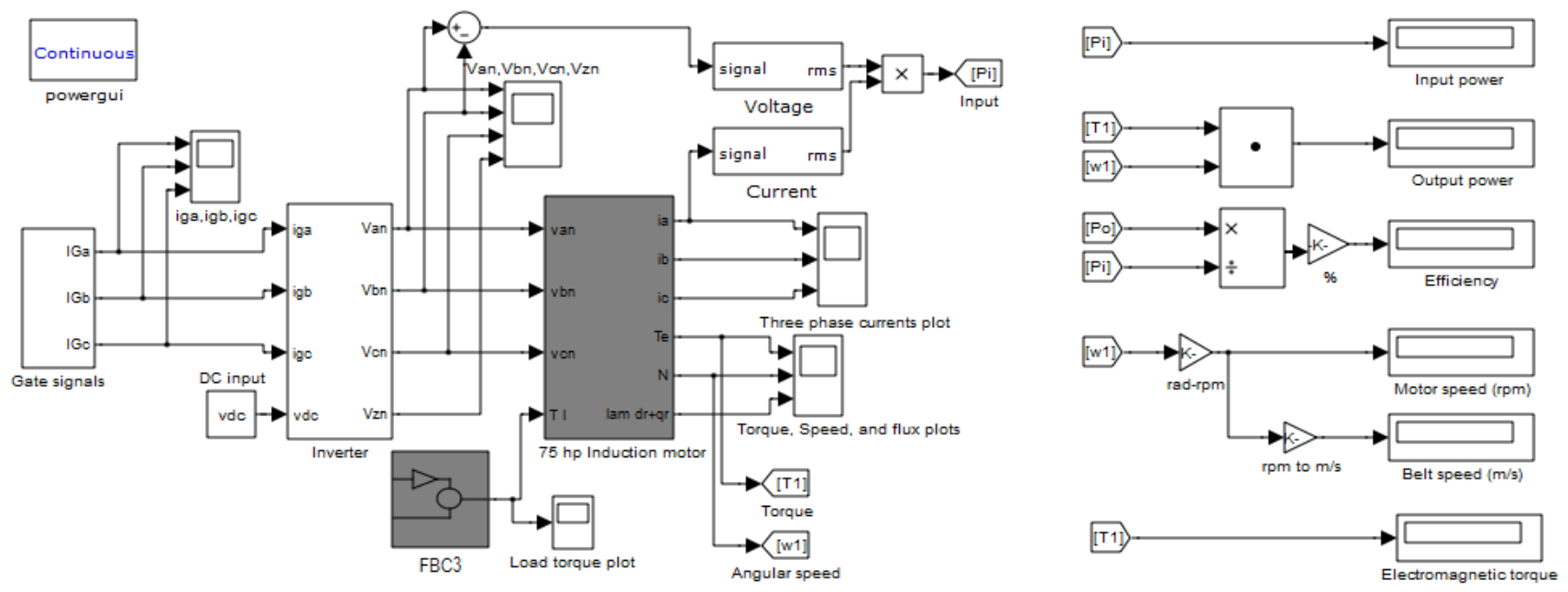


Figure 6.10 Simulation model for VFD configured FBC3

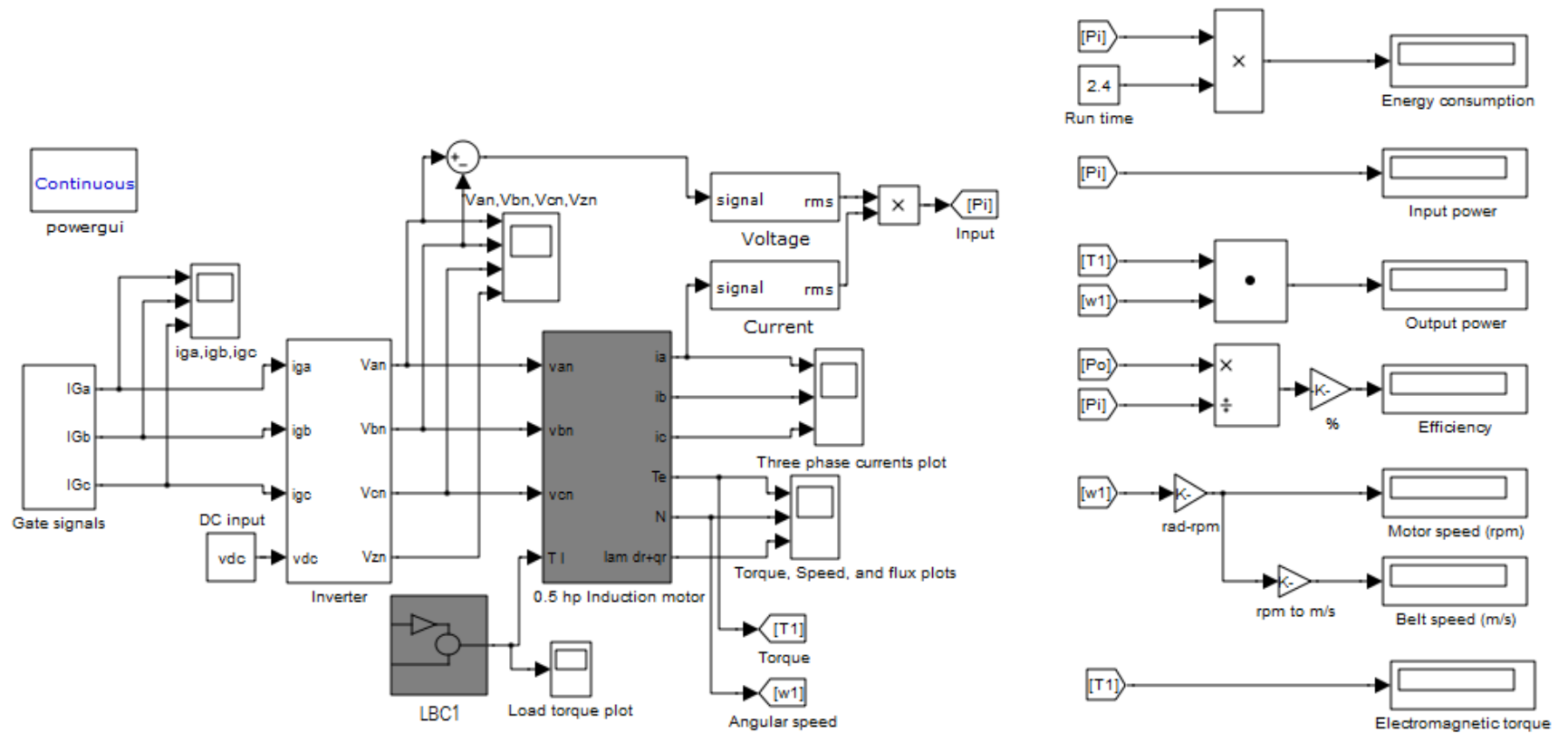


Figure 6.11 Simulation model for VFD configured LBC1

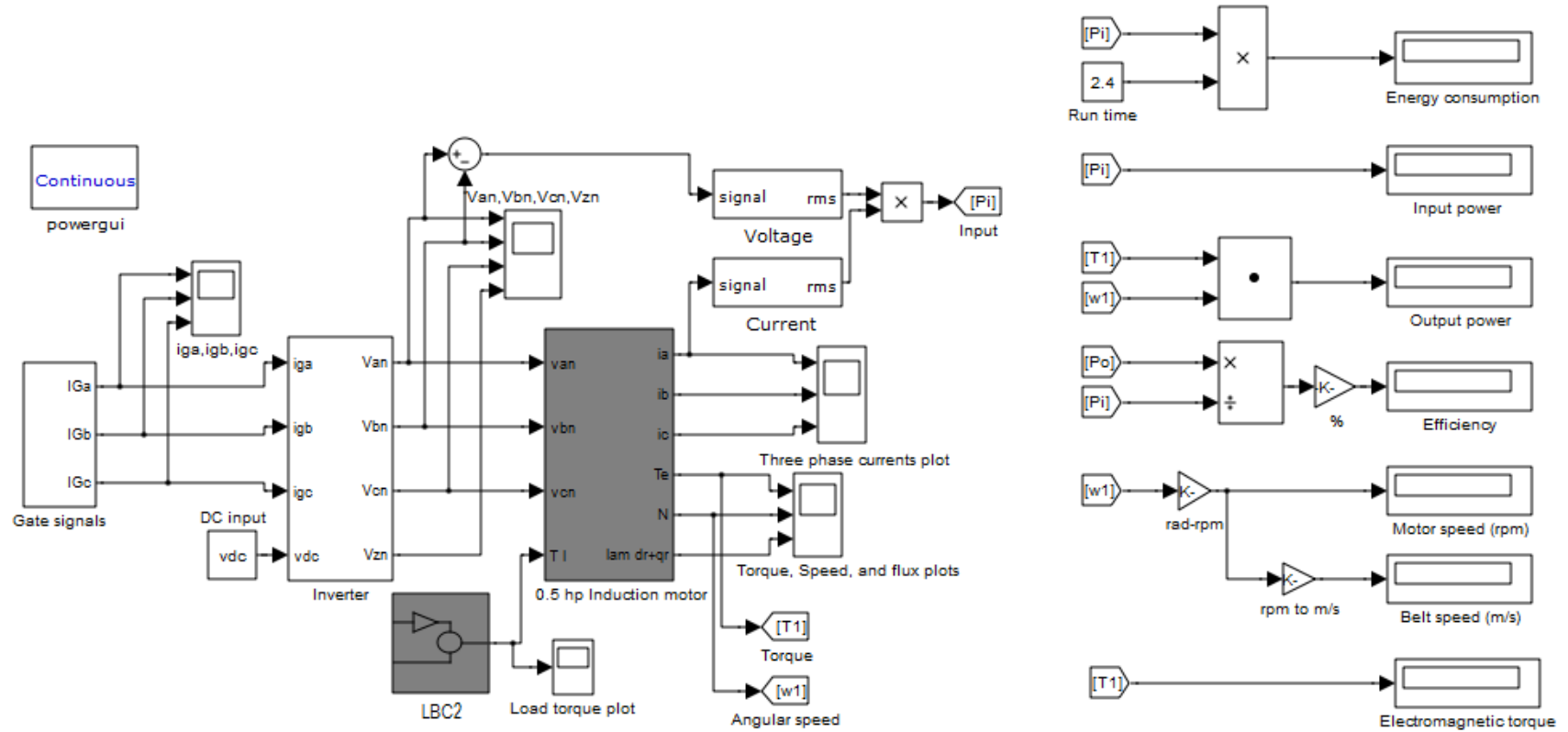


Figure 6.12 Simulation model for VFD configured LBC2

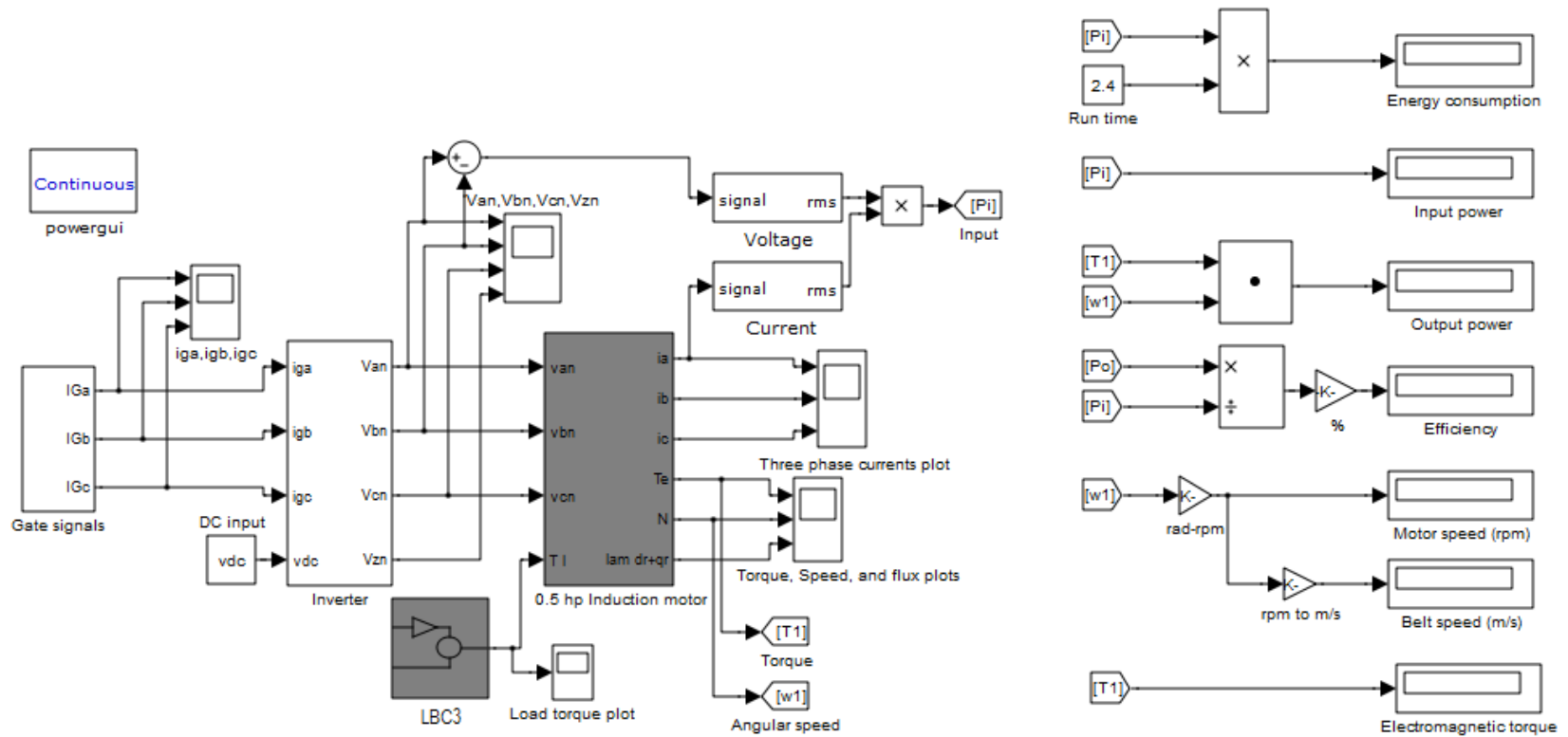


Figure 6.13 Simulation model for VFD configured LBC3

The simulation parameters for FBC and LBC are listed in Table 6.4, Table 6.5, Table 6.6 and Table 6.7.

Table 6.4 Simulation parameters of belt and rollers of FBC system

Nominal parameters	Symbol	Value	Unit
Maximum conveying capacity	Q_m	200	t / h
Belt speed	v	2	m / s
Belt width	B	900	mm
Loaded material weight	M_l	30	kg / m
Conveying length	L	60/260/420	m
Conveying height	H	10/63/40	m
Inclination angle	β	9.46/13.6/5.44	$^\circ$
Belt length	L_b	-	m
Belt thickness	T_b	20	mm
Belt weight	M_b	15	kg / m
Idler weight	M_r	54	kg / m
Radius of drive pulley	R_d	35.1	cm
Friction coefficient	C_f	0.025	-
Made	PVC	Type2	-

Table 6.5 Simulation parameters of FBC drive

Nominal parameters	Symbol	Value	Unit
Power	P	75/55	hp / kW
Line Voltage	V	415	$Volt$
Frequency	f	50	Hz
Stator resistance	R_s	0.0862	Ω
Stator inductance	L_s	0.0007829	H
Rotor resistance	R_r	0.0862	Ω
Rotor inductance	L_r	0.0013	H
Mutual inductance	L_m	0.0299	H
Moment of inertia of the rotor	J	0.9818	$kg - m^2$
Friction factor	...	0	---
Pole pairs	p	2	---
Current	I	90	Amp
Power factor	$\cos \phi$	0.88	-
Efficiency	η	94.3	%
Torque at full load	T_{fl}	354	$N - m$
breakdown torque	T_b	2.5*354	$N - m$
Rated motor speed	N	1482	rpm
Gear reduction ratio	K	1:30	-
Reduction gear speed	N_{gr}	50	rpm

Table 6.6 Simulation parameters of belt and rollers of LBC system

Nominal parameters	Symbol	Value	Unit
Maximum conveying capacity	Q_m	10	t / h
Belt speed	v	0.18	m / s
Belt width	B	300	mm
Loaded material weight	M_l	15	kg / m
Conveying length	L	2	m
Conveying height	H	0.35/ 0.53/ 0.72	m
Inclination angle	β	10/ 15/ 20	$^\circ$
Belt length	L_b	4.2	m
Belt thickness	T_b	12	mm
Belt weight	M_b	3	kg / m
Idler weight	M_r	12	kg / m
Radius of drive pulley	R_d	7	cm
Friction coefficient	C_f	0.1	-
Made	PVC	Type2	-

Table 6.7 Simulation parameters of LBC drive

Nominal parameters	Symbol	Value	Unit
Power	P	0.5/ 0.375	hp / kW
Line Voltage	V	415	$Volt$
Frequency	f	50	Hz
Stator resistance	R_s	25.5	Ω
Stator inductance	L_s	0.168	H
Rotor resistance	R_r	18.54	Ω
Rotor inductance	L_r	0.168	H
Mutual inductance	L_m	2.02	H
Moment of inertia of the rotor	J	0.018	$kg - m^2$
Friction factor	...	0	---
Pole pairs	P	2	---
Current	I	1.1	Amp
Power factor	$\cos \phi$	0.74	-
Efficiency	η	65	%
Torque at full load	T_{fl}	3.856	$N - m$
breakdown torque	T_b	2.6×3.856	$N - m$
Approximate motor weight	M_m	17.5	kg
Rated motor speed	N	1385	rpm
Gear reduction ratio	K	1:60	-

Reduction gear speed	N_{gr}	23	rpm
Slip	s	6	%
Rotor frequency	f_r	3	Hz
Rotational losses	w_1	72	W
Stay load losses	w_2	9	W
Stator copper loss	w_3	36	W
Rotor copper losses	w_4	18	W
Constant losses	$w_1 + w_2$	81	W
Variable losses	$w_3 + w_4$	45	W
Total power losses at Full load	w_t	126	W

6.3 Studies on FBC and LBC systems

Three kind of simulation studies have been carried out on FBC and LBC systems.

In the first study, the belt speed, annual energy consumption, efficiency and specific energy were simulated and predicted for FBC system with respect to feed rate, and for LBC system based on unit mass of the material loaded on the conveyor. Both non-VFD and VFD based configurations for FBC and LBC systems were studied. The simulation results of the study were recorded, which are presented in later section.

In the second study, the dynamic response of FBC and LBC drives were evaluated with respect to electromagnetic torque, speed and current under the following three different loading cases:

Case I: Only with the drive system without conveyor (DS only) or zero-load (ZL)

Case II: Conveyor connected drive system with no load (CCDS with no load) or no-load (NL)

Case III: Conveyor-connected drive system with an external load (CCDS with external load) or full-load (FL)

In the third study, the dynamic response of non-VFD and VFD based FBC and LBC drives were compared with respect to motor current.

The second and third study was carried out with a sample time of 25 s by considering 250 samples (within interval of 0 to 25 s).

6.4 Results and Discussions

The results and discussions of the three studies as stated in Section 6.3 is presented here.

6.4.1 Influence of feed rate on performance parameters of FBCs

In order to establish the optimum performance of the FBCs, the analysis was done based on simulation results (i.e. based on parameters, such as belt speed, annual energy consumption, efficiency and specific energy) for both non-VFD and VFD configuration, and they were compared to understand the behavior of belt conveyors.

6.4.1.1 Influence of feed rate on performance parameters of FBC1

The influence of feed rate on belt speed, annual energy consumption, efficiency and specific energy for non-VFD and VFD based FBC1 are shown in Figure 6.14, Figure 6.15, Figure 6.16 and Figure 6.17, respectively and the results are given in Table 6.8 and Table 6.9.

Figure 6.14 show the influence of feed rate on belt speed for non-VFD and VFD based models. As shown in Figure 6.14, for a non-VFD model the belt speed was decreased from 2 m/s to 1.8 m/s when the feed rate was varied from 40 t/h to 200 t/h, which was due to the increased material loading on the belt. The reduction of speed with respect to minimum and maximum feed rate was found to be 10%. Also, for a VFD based model, the speed was changed from 1 m/s to 2 m/s when the feed rate was varied from 40 t/h to 200 t/h. This is due to the presence of VFD. The VFD controls the motor voltage based on the material feed rate, which helps to optimize the belt speed. Therefore, the reduction of speed with respect to minimum and maximum feed rate was found to be higher when compared to non-VFD model. The reduction of speed with respect to minimum and maximum feed rate for VFD model was 50% whereas it is 10% in case of non-VFD model.

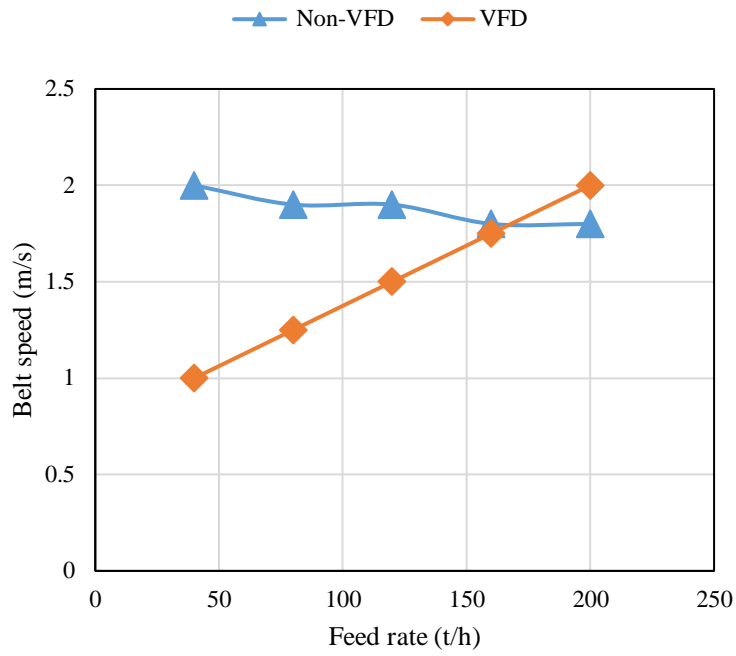


Figure 6.14 Influence of feed rate on belt speed for FBC1 model

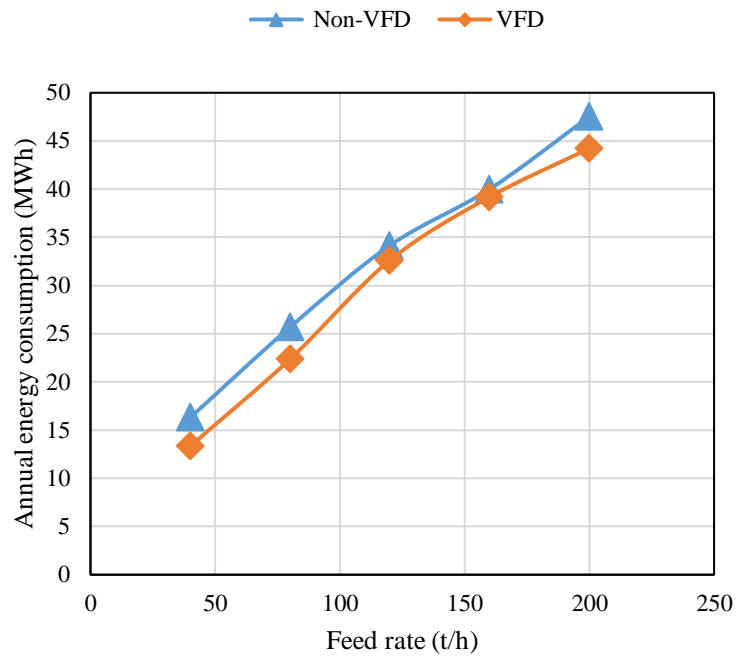


Figure 6.15 Influence of feed rate on annual energy consumption for FBC1 model

Figure 6.15 show the influence of feed rate on annual energy consumption for non-VFD and VFD based models. As depicted in Figure 6.15, for a non-VFD model, the annual energy consumption was increased from 16.3 MWh to 47.5 MWh when the feed rate was varied from 40 t/h to 200 t/h. The increase of annual energy consumption of belt conveyor is due to high power consumption of belt conveyor at higher material feed rate. The variation of annual energy consumption with respect to minimum and maximum feed rate was found to be 65.65%. Also, for a VFD based model, the annual energy consumption was increased from 13.3 MWh to 44.2 MWh when the feed rate was varied from 40 t/h to 200 t/h. The increment of annual energy consumption with respect to minimum and maximum loading was found to be 69.84%.

Figure 6.16 show the influence of feed rate on variation of efficiency of FBC1 system for non-VFD and VFD based models.

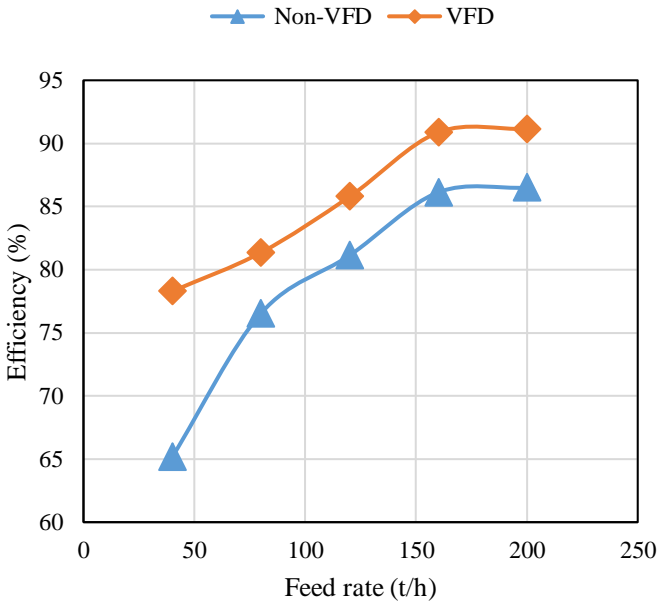


Figure 6.16 Influence of feed rate on efficiency for FBC1 model

As shown in Figure 6.16, for a non-VFD model, the efficiency was increased from 67.62% to 88.89% when the feed rate was varied from 40 t/h to 200 t/h. This is due to increase of power factor of the system. In general, the power factor of the system will be high when it is fully loaded. The variation of efficiency with respect to minimum and maximum loading was found

to be 23.9%. Also, for a VFD based model, the efficiency was increased from 78.29% to 90.62% when the feed rate was varied from 40 t/h to 200 t/h. The maximum efficiency was achieved at a feed rate of 200 t/h. The increment of efficiency with respect to minimum and maximum loading was found to be 13.62%. The variation of efficiency with respect to minimum and maximum loading was higher for non-VFD model when compared to VFD based model.

Figure 6.17 demonstrates the influence of feed rate on specific energy consumption of FBC1 system for non-VFD and VFD based models. As shown in Figure 6.17, for a non-VFD model, the specific energy of FBC1 was reduced from 2.83 kW/ton-km to 1.65 kW/ton-km when the feed rate was changed from 40 t/h to 200 t/h. The reduction of specific energy consumption of FBC1 was due to reduced power consumption of FBC1 at higher material feed rate. The variation of specific energy with respect to minimum and maximum loading was found to be 41.6%. And for a VFD based model, the specific energy consumption was decreased from 2.31 kW/ton-km to 1.53 kW/ton-km when the feed rate was varied from 40 t/h to 200 t/h. The reduction of specific energy with respect to minimum and maximum loading was found to be 33.67%.

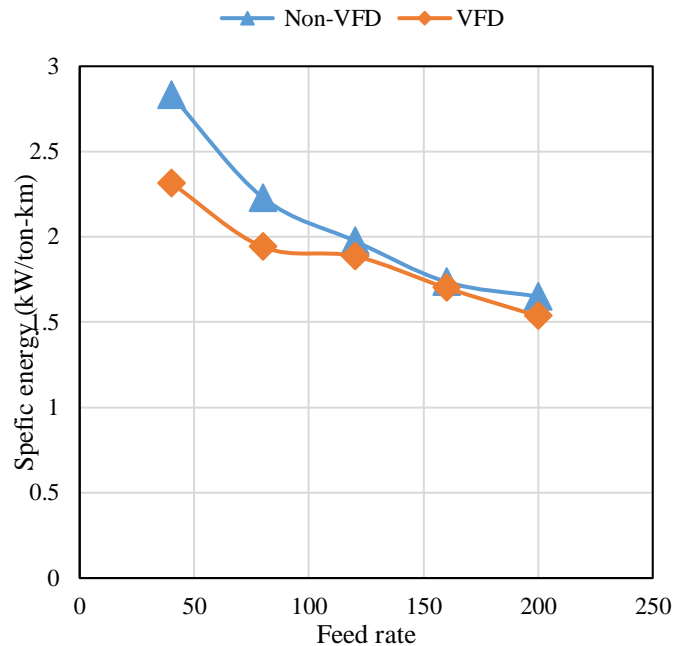


Figure 6.17 Influence of feed rate on specific energy for FBC1 model

Table 6.8 Simulation results of non-VFD configured FBC1

β	Q	F	v	V	I	cos ϕ	P _i	P _o	η	E _m	E _y	W _s
9.462	40	2250	2	397	38	0.26	6794	4594	67.62	1359	16305	2.8307
9.462	80	4420	1.9	395	46	0.34	10700	8500	79.44	2140	25681	2.2292
9.462	120	6279	1.9	395	52	0.4	14231	12031	84.54	2846	34153	1.9765
9.462	160	7561	1.9	395	58	0.42	16666	14466	86.80	3333	39999	1.7361
9.462	200	9724	1.8	397	60	0.48	19804	17604	88.89	3961	47529	1.6503

Note:
 β = Inclination (in degrees) P_i = Input/ electrical power (in W)
 Q = Material discharge rate (in t/h) P_o = Output/ mechanical power (in W)
 F = Total driving force (in N.m) η = Efficiency (%)
 v = Belt speed (in m/s) E_m = Energy consumption/month (in kWh)
 V = Voltage (in V) E_y = Energy consumption/year (in kWh)
 I = Current (in A) W_s = Specific energy (in kWh/ton km)
 cos ϕ = Power factor

Table 6.9 Simulation results of VFD configured FBC1

β	Q	F	v	V	I	cos ϕ	P _i	P _o	η	E _m	E _y	W _s
9.462	40	2250	1.00	401	10	0.8	5556	4350	78.29	1111	13335	2.3152
9.462	80	4420	1.25	405	16	0.83	9316	7485	80.35	1863	22358	1.9408
9.462	120	6279	1.50	406	23	0.84	13586	11654	85.78	2717	32607	1.8870
9.462	160	7561	1.75	406	27	0.86	16329	15002	91.88	3266	39189	1.7009
9.462	200	9724	2.00	403	30	0.88	18428	16700	90.62	3686	44226	1.5356

Note:
 β = Inclination (in degrees) P_i = Input/ electrical power (in W)
 Q = Material discharge rate (in t/h) P_o = Output/ mechanical power (in W)
 F = Total driving force (in N.m) η = Efficiency (%)
 v = Belt speed (in m/s) E_m = Energy consumption/month (in kWh)
 V = Voltage (in V) E_y = Energy consumption/year (in kWh)
 I = Current (in A) W_s = Specific energy (in kWh/ton km)
 cos ϕ = Power factor

6.4.1.2 Influence of feed rate on performance parameters of FBC2

Figure 6.18 show the influence of feed rate on belt speed for non-VFD and VFD based FBC2 models. As shown in Figure 6.18, for a non-VFD model, the belt speed was decreased from 1.9 m/s to 1.8 m/s when the feed rate was varied from 40 t/h to 200 t/h due to increased material loading on the belt. The reduction of speed with respect to minimum and maximum feed rate was found to be 5.26%. Also, for a VFD based model, the speed was changed almost from 1 m/s to 2 m/s when the feed rate was varied from 40 t/h to 200 t/h. This is due to the

presence of VFD. The VFD controls the motor voltage based on the material feed rate, which helps to optimize the belt speed. Therefore, the reduction of speed with respect to minimum and maximum feed rate was found to be higher when compared to non-VFD model. The reduction of speed with respect to minimum and maximum feed rate for VFD model was 50% whereas 5.26% in case of non-VFD model.

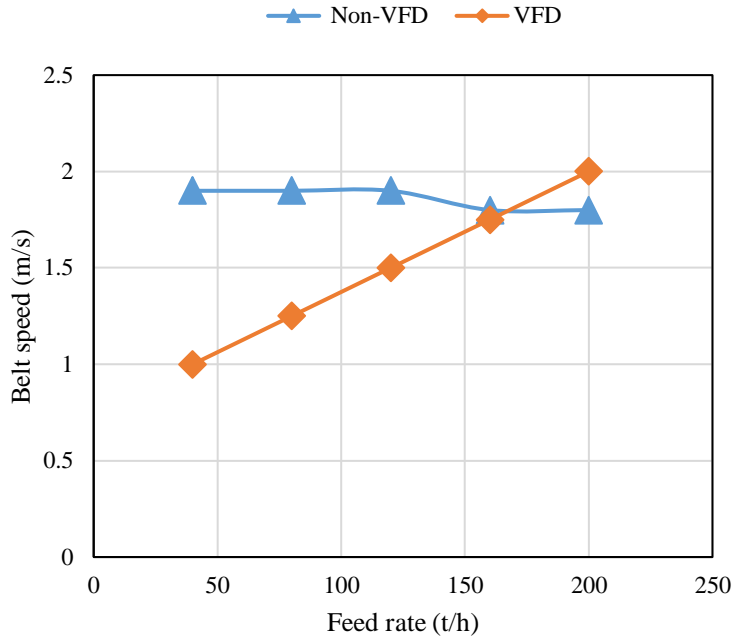


Figure 6.18 Influence of feed rate on belt speed for FBC2 model

Figure 6.19 show the influence of feed rate on annual energy consumption for non-VFD and VFD based models. As depicted in Figure 6.19, for a non-VFD model, the annual energy consumption was increased from 63.63 MWh to 123.29 MWh when the feed rate was varied from 40 t/h to 200 t/h. The increase of annual energy consumption of belt conveyor is due high power consumption belt conveyor at higher material feed rate. The variation of annual energy consumption with respect to minimum and maximum feed rate was found to be 48.38%. Also, for a VFD based model, the annual energy consumption was increased from 56.006 MWh to 120.96 MWh when the feed rate was varied from 40 t/h to 200 t/h. The increment of annual energy consumption with respect to minimum and maximum loading was found to be 53.69%.

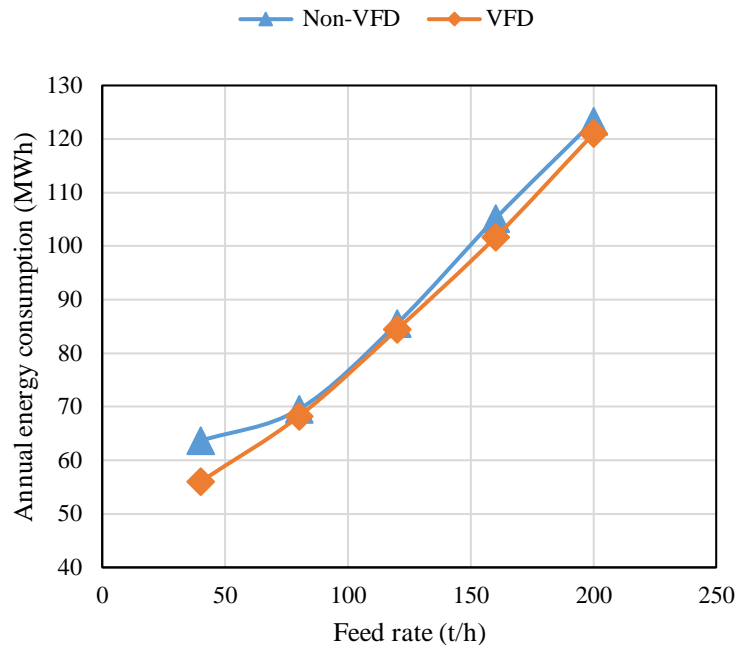


Figure 6.19 Influence of feed rate on energy consumption for FBC2 model

Figure 6.20 show the influence of feed rate on efficiency of FBC2 system for non-VFD and VFD based models. As shown in Figure 6.20, for a non-VFD model, the efficiency was increased from 91.70% to 94.97% when the feed rate was varied from 40 t/h to 160 t/h. This is due to increase of power factor of the system. The power factor of the system is high when it is fully loaded. The variation of efficiency with respect to minimum and maximum loading was found to be 23.9%. The maximum efficiency was achieved at a feed rate of 160 t/h. After that the efficiency was slightly decreased from 94.97% to 94.66% when the feed rate varied from 160 t/h to 200 t/h. This reduction of efficiency was due high power losses in the system. Also, for a VFD based FBC2 model, the efficiency was increased from 91.93% to 95.39% when the feed rate was varied from 40 t/h to 160 t/h. The maximum efficiency was achieved at a feed rate of 160 t/h. After that the efficiency was slightly decreased from 95.39% to 95.00% when the feed rate varied from 160 t/h to 200 t/h. This reduction of efficiency was also due high power losses in the system. The increment of efficiency with respect to minimum and maximum loading was found to be 3.23%. The variation of efficiency with respect to minimum and maximum loading was higher for non-VFD model when compared to VFD based model.

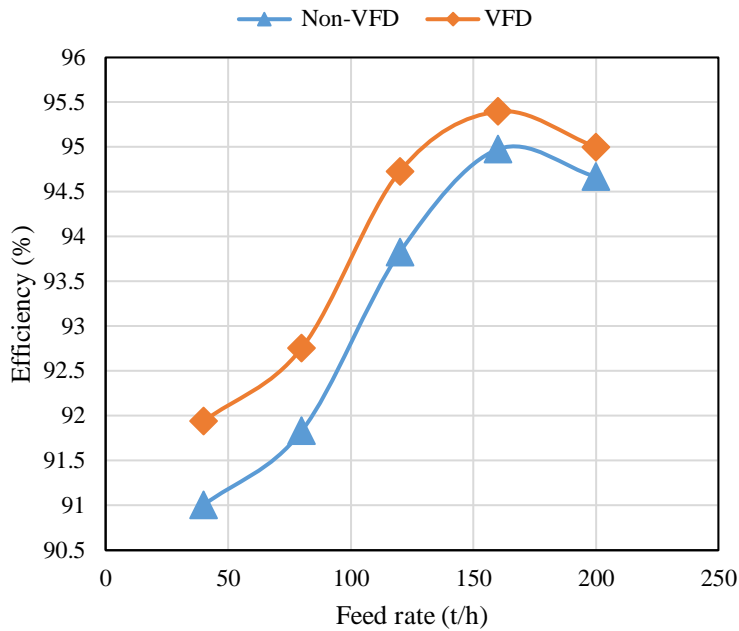


Figure 6.20 Influence of feed rate on efficiency for FBC2 model

Figure 6.21 show the influence of feed rate specific energy consumption of FBC2 system for non-VFD and VFD based models. As illustrated in Figure 6.21, for a non-VFD model, the specific energy of FBC2 was reduced from 1.57 kW/ton-km to 0.61 kW/ton-km when the feed rate was changed from 40 t/h to 200 t/h. The reduction of specific energy consumption of FBC2 is due to the reduced per unit power consumption of FBC2 at higher material feed rate. The variation of specific energy with respect to minimum and maximum loading was found to be 61.14%. And for a VFD based model, the specific energy consumption was decreased from 1.39 kW/ton-km to 0.60 kW/ton-km when the feed rate was varied from 40 t/h to 200 t/h. The reduction of specific energy with respect to minimum and maximum loading was found to be 56.83%.

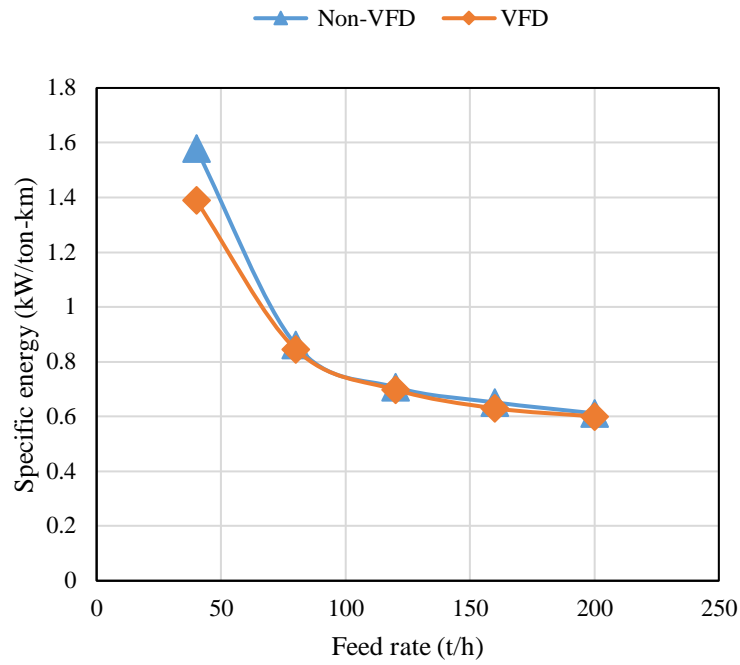


Figure 6.21 Influence of feed rate on specific energy for FBC2 model

Table 6.10 Simulation results of non-VFD configured FBC2

β	Q	F	v	V	I	cos ϕ	P _i	P _o	η	E _m	E _y	W _s
13.6	40	12107	1.9	402	68	0.56	26515	24315	91.70	5303	63635	1.5782
13.6	80	13293	1.9	398	70	0.60	28953	26588	91.83	5791	69487	0.8617
13.6	120	17537	1.9	398	76	0.68	35626	33426	93.82	7125	85502	0.7069
13.6	160	23044	1.8	396	84	0.76	43787	41587	94.97	8757	105090	0.6516
13.6	200	26961	1.8	398	92	0.81	51371	48632	94.67	10274	123290	0.6116
Note:												
β = Inclination (in degrees)							P _i = Input/ electrical power (in W)					
Q = Material feed rate (in t/h)							P _o = Output/ mechanical power (in W)					
F = Total driving force (in N.m)							η = Efficiency (%)					
v = Belt speed (in m/s)							E _m = Energy consumption/month (in kWh)					
V = Voltage (in V)							E _y = Energy consumption/year (in kWh)					
I = Current (in A)							W _s = Specific energy (in kWh/ton km)					
cos ϕ = Power factor												

Table 6.11 Simulation results of VFD configured FBC2

β	Q	F	v	V	I	cos ϕ	P _i	P _o	η	E _m	E _y	W _s
13.6	40	12107	1.00	401	42	0.8	23337	21456	91.94	4667	56009	1.3891
13.6	80	13293	1.25	405	50	0.81	28410	26210	92.26	5682	68184	0.8455
13.6	120	17537	1.50	406	61	0.82	35175	33320	94.73	7035	84419	0.6979
13.6	160	23044	1.75	406	70	0.86	42333	40300	95.20	8467	101600	0.6300
13.6	200	26961	2.00	403	83	0.87	50404	48204	95.64	10081	120969	0.6000
		Note:										
		β = Inclination (in degrees)					P _i = Input/ electrical power (in W)					
		Q = Material feed rate (in t/h)					P _o = Output/ mechanical power (in W)					
		F = Total driving force (in N.m)					η = Efficiency (%)					
		v = Belt speed (in m/s)					E _m = Energy consumption/month (in kWh)					
		V = Voltage (in V)					E _y = Energy consumption/year (in kWh)					
		I = Current (in A)					W _s = Specific energy (in kWh/ton km)					
		cos ϕ = Power factor										

6.4.1.3 Influence of feed rate on performance parameters of FBC3

Figure 6.22 show the influence of feed rate on belt speed for non-VFD and VFD based FBC3 models.

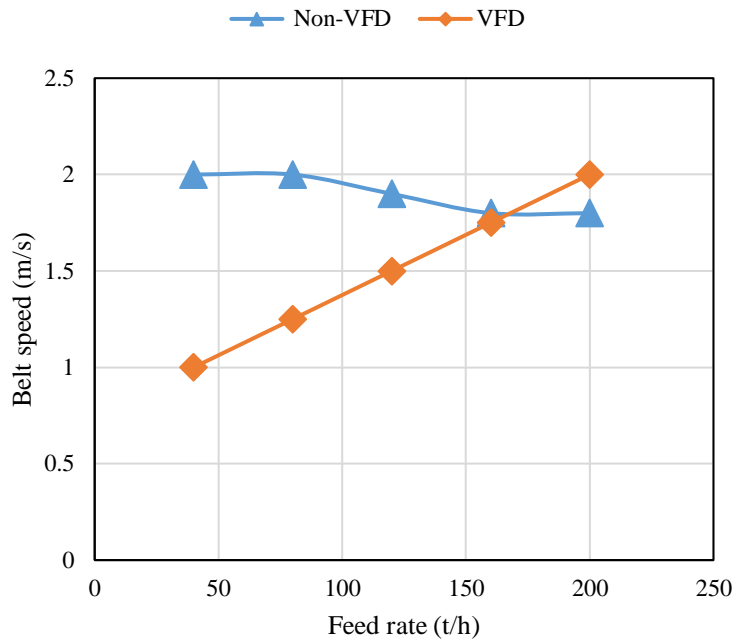


Figure 6.22 Influence of feed rate on belt speed for FBC3 model

As demonstrated in Figure 6.22, for a non-VFD model, the belt speed was decreased from 2 m/s to 1.8 m/s when the feed rate was varied from 40 t/h to 200 t/h, this reduction in belt speed was due to the increased material loading on the belt. The reduction of belt speed with respect to minimum and maximum feed rate was found to be 10%. Also, for a VFD based model, the speed was changed almost from 1 m/s to 2 m/s when the feed rate was varied from 40 t/h to 200 t/h. This high change in belt speed was due to the presence of VFD. The VFD controls the motor voltage based on the material feed rate, this helps to optimize the belt speed. Therefore, the reduction of speed with respect to minimum and maximum feed rate was found to be higher when compared to non-VFD model. The reduction of speed with respect to minimum and maximum feed rate for VFD model was 50% whereas 10% in case of non-VFD model.

Figure 6.23 show the influence of feed rate on annual energy consumption for non-VFD and VFD based FBC3 models. As shown in Figure 6.23, for a non-VFD model, the annual energy consumption was increased from 45.66 MWh to 122.36 MWh when the feed rate was varied from 40 t/h to 200 t/h.

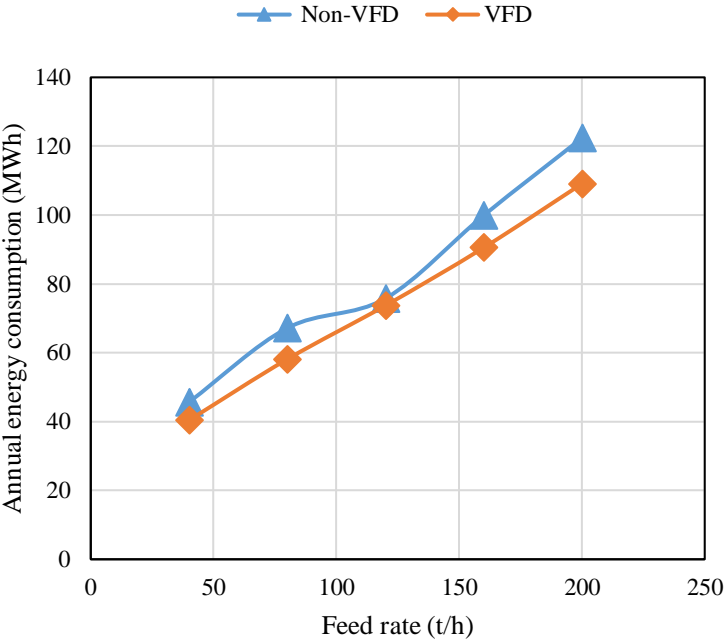


Figure 6.23 Influence of feed rate on annual energy consumption for FBC3 model

The increase of annual energy consumption of belt conveyor is due high power consumption belt conveyor at higher material feed rate. The variation of annual energy consumption with respect to minimum and maximum feed rate was found to be 62.68%. Also, for a VFD based model, the annual energy consumption was increased from 40.4 MWh to 109.09 MWh when the feed rate was varied from 40 t/h to 200 t/h. The increment of annual energy consumption with respect to minimum and maximum loading was found to be 62.9%.

Figure 6.24 show the influence of feed rate on efficiency of FBC3 system for non-VFD and VFD based models. As depicted in Figure 6.24, for a non-VFD model, the efficiency was increased from 76.87% to 94.71% when the feed rate was varied from 40 t/h to 160 t/h. This is due to increase of power factor of the system since, the power factor of the system is high when it is fully loaded. The variation of efficiency with respect to minimum and maximum loading was found to be 18.74%. The maximum efficiency was achieved at a feed rate of 160 t/h. After that the efficiency was slightly decreased from 94.71% to 94.60% when the feed rate varied from 160 t/h to 200 t/h.

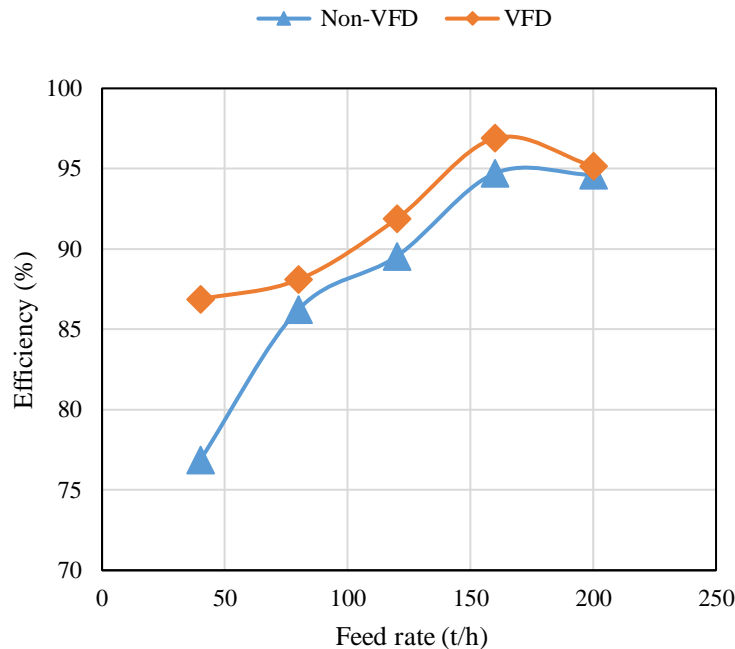


Figure 6.24 Influence of feed rate on efficiency for FBC3 model

This reduction of efficiency was due to high power losses in the system. Also, for a VFD based FBC2 model, the efficiency was increased from 86.87% to 96.89% when the feed rate was varied from 40 t/h to 160 t/h. The maximum efficiency was achieved at a feed rate of 160 t/h. After that the efficiency was slightly decreased from 96.89% to 95.15% when the feed rate varied from 160 t/h to 200 t/h. This reduction of efficiency was also due to high power losses in the system. The increment of efficiency with respect to minimum and maximum loading was found to be 8.7%. The variation of efficiency with respect to minimum and maximum loading was higher for non-VFD model when compared to VFD based model.

Figure 6.25 show the influence of feed rate on specific energy consumption of FBC3 system for non-VFD and VFD based models.

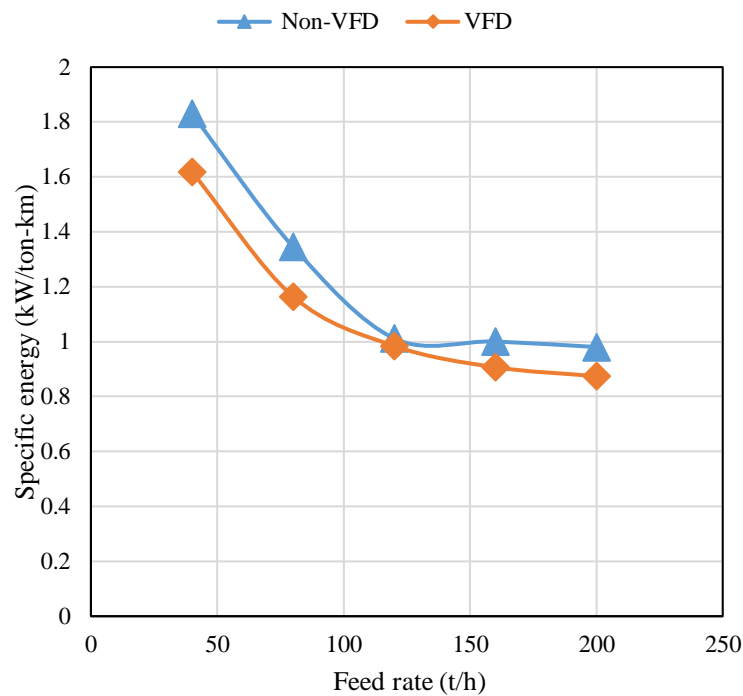


Figure 6.25 Influence of feed rate on specific energy for FBC3 model

As demonstrated in Figure 6.25 for a non-VFD model, the specific energy of FBC3 was reduced from 1.829 kW/ton-km to 0.980 kW/ton-km when the feed rate was changed from 40 t/h to 200 t/h. The reduction of specific energy consumption of FBC3 is due to the reduced per unit power consumption of FBC3 at higher material feed rate. The variation of specific energy

with respect to minimum and maximum loading was found to be 46.39%. And for a VFD based model, the specific energy consumption was decreased from 1.618 kW/ton-km to 0.874 kW/ton-km when the feed rate was varied from 40 t/h to 200 t/h. The reduction of specific energy with respect to minimum and maximum loading was found to be 45.98%.

Table 6.12 Simulation results of non-VFD configured FBC3

β	Q	F	v	V	I	cos ϕ	P _i	P _o	η	E _m	E _y	W _s
5.44	40	7263	2	398	60	0.46	19026	14626	76.87	3805	45663	1.8294
5.44	80	12016	2	396	68	0.60	27984	24134	86.24	5597	67163	1.3454
5.44	120	14827	1.9	395	71	0.65	31574	28274	89.55	6315	75778	1.0120
5.44	160	21848	1.8	395	78	0.78	41624	39436	94.74	8325	99898	1.0006
5.44	200	26739	1.8	398	86	0.86	50985	48235	94.61	10197	122363	0.9805

Note:
 β = Inclination (in degrees) P_i = Input/ electrical power (in W)
 Q = Material feed rate (in t/h) P_o = Output/ mechanical power (in W)
 F = Total driving force (in N.m) η = Efficiency (%)
 v = Belt speed (in m/s) E_m = Energy consumption/month (in kWh)
 V = Voltage (in V) E_y = Energy consumption/year (in kWh)
 I = Current (in A) W_s = Specific energy (in kWh/ton km)
 cos ϕ = Power factor

Table 6.13 Simulation results of VFD configured FBC3

β	Q	F	v	V	I	cos ϕ	P _i	P _o	η	E _m	E _y	W _s
5.44	40	7263	1.00	405	30	0.8	16836	14626	86.88	3367	40405	1.6188
5.44	80	12016	1.25	406	42	0.82	24219	21336	88.10	4844	58125	1.1644
5.44	120	14827	1.50	406	52	0.84	30716	28223	91.88	6143	73719	0.9845
5.44	160	21848	1.75	402	63	0.86	37725	36553	96.89	7545	90539	0.9068
5.44	200	26739	2.00	405	72	0.9	45456	43252	95.15	9091	109094	0.8742

Note:
 β = Inclination (in degrees) P_i = Input/ electrical power (in W)
 Q = Material feed rate (in t/h) P_o = Output/ mechanical power (in W)
 F = Total driving force (in N.m) η = Efficiency (%)
 v = Belt speed (in m/s) E_m = Energy consumption/month (in kWh)
 V = Voltage (in V) E_y = Energy consumption/year (in kWh)
 I = Current (in A) W_s = Specific energy (in kWh/ton km)
 cos ϕ = Power factor

6.4.1.4 Influence of feed rate on percentage variation in belt speed, annual energy consumption, efficiency and specific energy between non-VFD and VFD based FBCs

The influence of feed rate on percentage variation of speed, annual energy consumption, efficiency and specific energy for Non-VFD and VFD based FBCs were studied, which are shown in Figure 6.26, Figure 6.27, Figure 6.28 and Figure 6.29.

Figure 6.14, Figure 6.18 and Figure 6.22 shows the influence of feed rate on belt speed for FBC1, FBC2 and FBC3 systems, respectively. It was observed that speed of a FBC system can be optimized by incorporating a VFD to a belt conveyor system. Figure 6.26 show the percentage variation in belt speed between non-VFD and VFD configured FBC1, FBC2 and FBC3. The highest variation in belt speed achieved was found during the initial stage of material loading which is 50%, 47.36% and 50% for FBC1, FBC2 and FBC3, respectively. The percentage variation in belt speed was found to be zero for all the three FBCs at feed rate of 200 t/h.

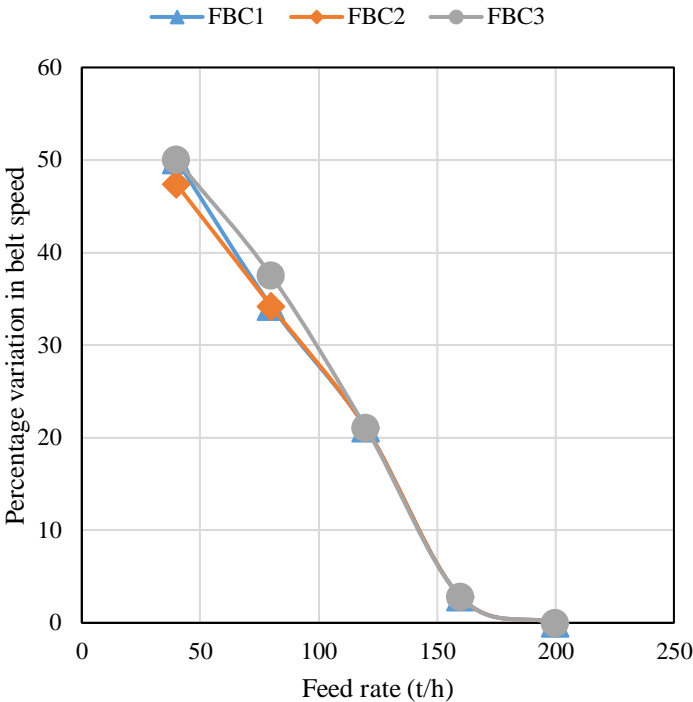


Figure 6.26 Influence of feed rate on percentage variation in belt speed between non-VFD and VFD configured FBC1, FBC2 and FBC3

Figure 6.15, Figure 6.19 and Figure 6.23 depict the influence of feed rate on annual energy consumption for FBC1, FBC2 and FBC3 systems, respectively. Figure 6.27 shows the influence of feed rate on percentage variation in annual energy consumption between non-

VFD and VFD configured FB1, LBC2 and LBC3. The highest variation in annual energy consumption was achieved during the initial stage of material loading which is 18%, 11.5% and 12% for FBC1, FBC2 and FBC3, respectively. The average percentage reductions in annual energy consumption for FBC1, FBC2 and FBC3 was also estimated from the Figure 6.27, which was found to be 9.4%, 2.31% and 7.3% with respect to FBC1, FBC2 and FBC3. The average percentage reductions were estimated using Equation (6.1)

Average percentage reductions = sum of percentage reductions / number of samples

(6.1)

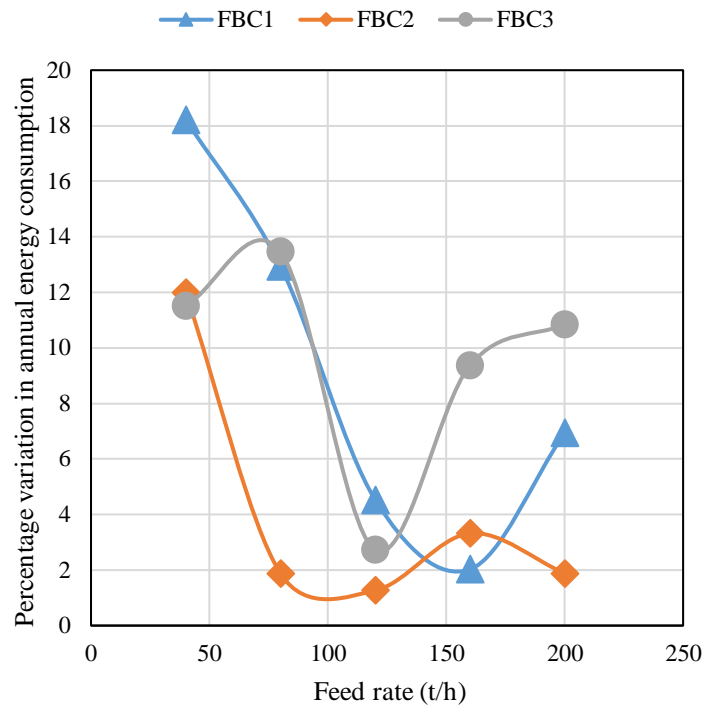


Figure 6.27 Influence of feed rate on percentage variation in annual energy consumption between non-VFD and VFD configured FBC1, FBC2 and FBC3

Figure 6.16, Figure 6.20 and Figure 6.24 show influence of feed rate on conveyor's efficiency for FBC1, FBC2 and FBC3 systems, respectively. It can be observed that the efficiency of a FBC system can be improved by incorporating VFD to belt conveyor systems. The variation in efficiency between non-VFD and VFD configured FBC1, FBC2 and FBC3 are given in Table 6.18, Table 6.19 and Table 6.20, respectively. The trend of efficiency with feed rate is same for FBC1, FBC2 and FBC3 systems, but with the change in magnitudes of output. From

the Figure 6.28, Table 6.18, Table 6.19 and Table 6.20 the highest improvement in efficiency achieved is found during the initial stage of material loading which is 16.76%, 1.01% and 11.51% for FBC1, FBC2 and FBC3, respectively. The percentage variation in efficiency between non-VFD and VFD configured FBC1, FBC2 and FBC3 are indicated in Table 6.18, Table 6.19 and Table 6.20, which are given in Annexure A.

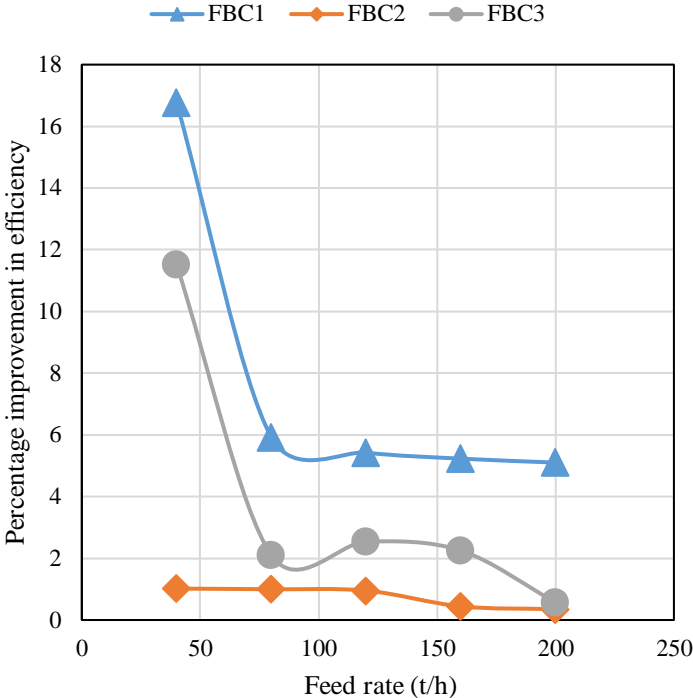


Figure 6.28 Influence of feed rate on percentage variation in efficiency between non-VFD and VFD configured FBC1, FBC2 and FBC3

Figure 6.17, Figure 6.21 and Figure 6.25 influence of feed rate on specific energy for FBC1, FBC2 and FBC3 systems, respectively. Figure 6.29 show the influence of feed rate on percentage reduction in specific energy between non-VFD and VFD based FBCs. As observed in Figure 6.29, the highest reduction in specific energy was achieved during the initial stage of material feed rate, which was 18%, 11.7% and 11.8% for FBC1, FBC2 and FBC3, respectively. The average percentage reduction in specific energy for FBC1, FBC2 and FBC3 was also estimated from the Figure 6.29, which was 10.4%, 2.55% and 5.93% with respect to FBC1, FBC2 and FBC3.

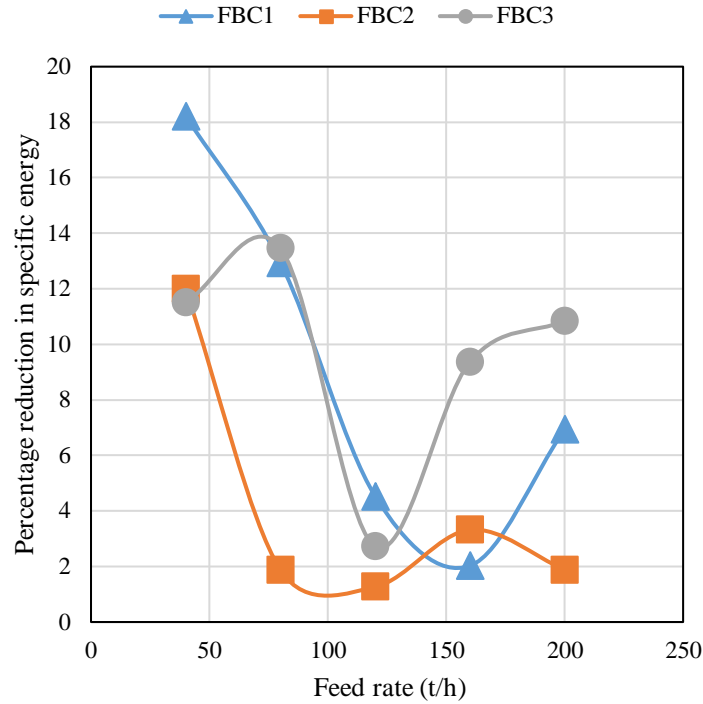


Figure 6.29 Influence of feed rate on percentage reduction in specific energy between non-VFD and VFD configured FBC1, FBC2 and FBC3

6.4.2 Influence of feed rate on performance parameters of LBCs

The analysis of non-VFD and VFD based LBCs were carried out similar to that of FBCs, as explained in Section 6.4.1.

6.4.2.1 Influence of feed rate on performance parameters of LBC1, LBC2 and LBC3

The influence of feed rate on belt speed, annual energy consumption, efficiency and specific energy for non-VFD and VFD based LBCs are shown in Figure 6.30, Figure 6.31, Figure 6.32 and Figure 6.33. The simulations results of non-VFD and VFD models for LBCs were listed in Table 6.14 to Table 6.19.

Figure 6.30 show the influence of feed rate on belt speed for non-VFD and VFD based LBC1, LBC2 and LBC3 models. Observations reveal that, for a non-VFD model, when the unit mass of material was varied from 3 kg/m to 15 kg/m, the belt speed was reduced from 0.178 m/s to 0.175 m/s for LBC1, 0.177 m/s to 0.174 m/s for LBC2 and 0.175 m/s to 0.174 m/s for LBC3. This speed reduction is due to the increased material loading on the belt. The percentage

reduction of belt speed with respect to minimum and maximum loadings was found to be 1.68, 1.69 and 0.57, respectively for LBC1, LBC2 and LBC3. However, for a VFD based LBC1, LBC2 and LBC3 models, when the unit mass of material was varied from 3 kg/m to 15 kg/m, the belt speed was changed almost from 0.144 m/s to 0.189 m/s for LBC1, 0.13 m/s to 0.17 m/s for LBC2 and 0.12 m/s to 0.16 m/s for LBC3. This high change in belt speed is mainly due to the presence of VFD. The VFD controls the motor voltage based on the unit mass of material, which helps to optimize the belt speed. Therefore, the percentage reduction of belt speed with respect to minimum and maximum loading was found to be higher when compared to non-VFD models. The percentage reduction of belt speed with respect to minimum and maximum loading for VFD based LBC1, LBC2 and LBC3 models was found to be 23.5, 23.8 and 25.

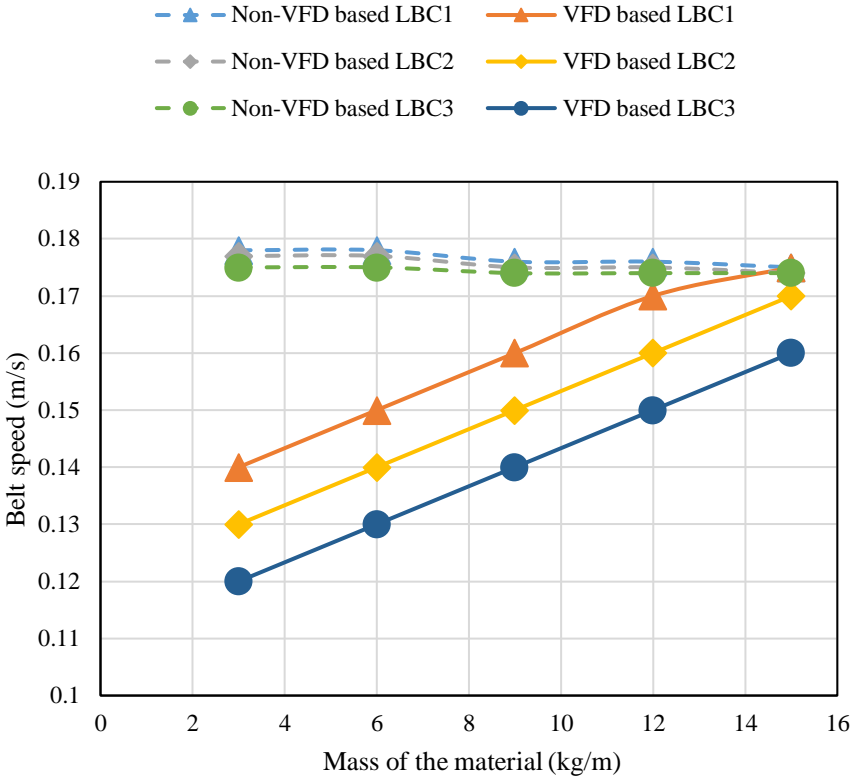


Figure 6.30 Influence of mass of the material on belt speed plot for LBC system

Figure 6.31 show the influence of mass of the material on annual energy consumption for non-VFD and VFD based LBC1, LBC2 and LBC3 models. It was observed that, for a non-VFD based LBC1, LBC2 and LBC3 models, when the unit mass of material was varied from 3 kg/m to 15 kg/m, the annual energy consumption was increased from 259 kWh to 706 kWh for LBC1, 301 kWh to 769 kWh for LBC2 and 330 kWh to 806 kWh for LBC3 models. The increase of annual energy consumption of belt conveyor is due to high power consumption of belt conveyor at higher unit mass of material. The percentage variation of annual energy consumption with respect to minimum and maximum loading was found to be 63.3, 60.85 and 59 for non-VFD based LBC1, LBC2 and LBC3 models, respectively. For a VFD based models, when the feed rate was varied from 3 kg/m to 15 kg/m, the annual energy consumption was increased from 206 kWh to 661 kWh. The percentage increment of annual energy consumption with respect to minimum and maximum loading was found to be 68.83, 65.61 and 63.7 for VFD based LBC1, LBC2 and LBC3 models, respectively.

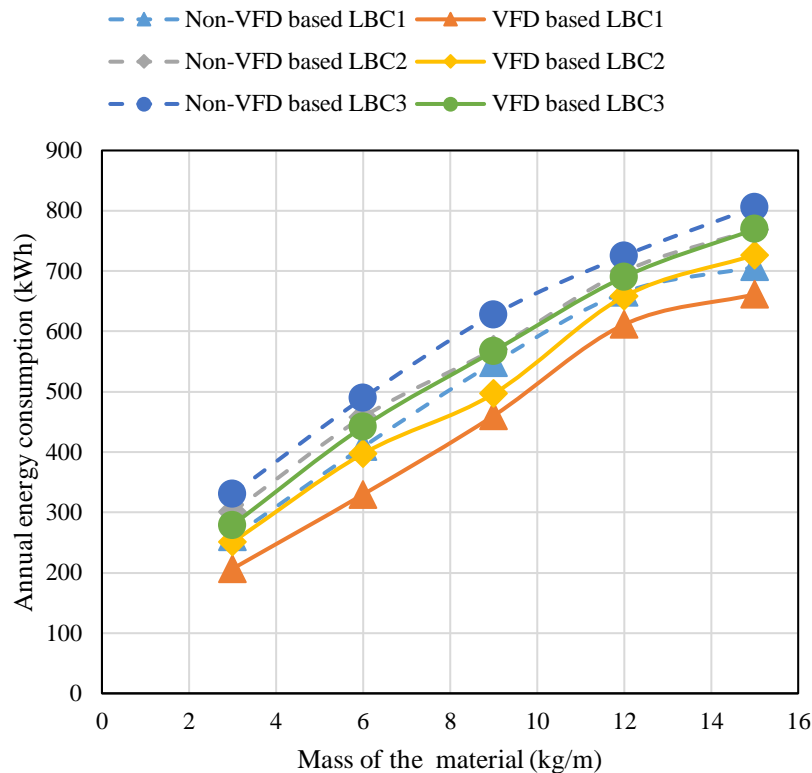


Figure 6.31 Influence of mass of the material on annual energy consumption plot for LBC system

Figure 6.32 show the influence of mass of the material on efficiency for non-VFD and VFD based LBC1, LBC2 and LBC3 models. It was observed that for a non-VFD based LBC1, LBC2 and LBC3 models, when the unit mass of material was varied from 3 kg/m to 15 kg/m, the efficiency was increased from 26.33% to 61.78% for LBC1, 28.73% to 63.92% for LBC2 and 29.06% to 65.51% for LBC3. This is due to increase in power factor of the system, since the power factor of the system will be high when it is fully loaded. The percentage variation of efficiency with respect to minimum and maximum loading was found to be 57.38, 55.05 and 55.6 for non-VFD based LBC1, LBC2 and LBC3, respectively. For VFD based LBC1, LBC2 and LBC3 models, when the unit mass of material was varied from 3 kg/m to 15 kg/m the efficiency was increased from 33.86% to 63.13% for LBC1, 34.8% to 65.25% for LBC2 and 34.43% to 66.7% for LBC3. The maximum efficiency was achieved at a unit mass of material of 15 kg/m for all the three conveyors. The percentage increment of efficiency with respect to minimum and maximum loading was found to be 46.36, 46.66 and 48.38 for VFD based LBC1, LBC2 and LBC3, respectively. The percentage variation of efficiency with respect to minimum and maximum loading was higher for non-VFD LBC models when compared to VFD based LBC models.

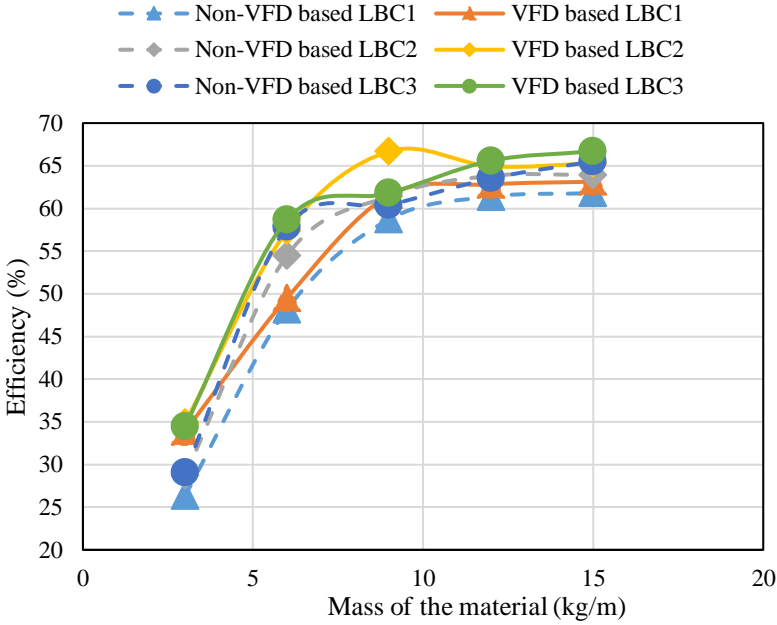


Figure 6.32 Influence of mass of the material on annual energy consumption plot for LBC system efficiency plot for LBC system

Figure 6.33 show the influence of mass of the material on specific energy consumption for non-VFD and VFD based LBC1, LBC2 and LBC3 models. It was observed that, for a non-VFD based LBC1, LBC2 and LBC3 models, when the unit mass of material was changed from 3 kg/m to 15 kg/m, the specific energy was reduced from 2.69 kW/ton-km to 1.472 kW/ton-km for LBC1, 3.133 kW/ton-km to 1.60 kW/ton-km for LBC2 and 3.44 kW/ton-km to 1.67 kW/ton-km for LBC3. This reductions of specific energy consumption of LBC systems is due to lower value of per unit power consumption of LBC systems at higher material loadings. The percentage variation of specific energy with respect to minimum and maximum loading was found to be 45.27, 48.99 and 51.45 for a non-VFD based LBC1, LBC2 and LBC3 models, respectively. For a VFD based model, when the unit mass of material was varied from 3 kg/m to 15 kg/m, the specific energy consumption was decreased from 2.51 kW/ton-km to 1.378 kW/ton-km for LBC1, 2.61 kW/ton-km to 1.51 kW/ton-km for LBC2 and 2.9 kW/ton-km to 1.6 kW/ton-km for LBC3. The percentage reduction of specific energy with respect to minimum and maximum loading was found to be 45.1, 41.9 and 44.82.

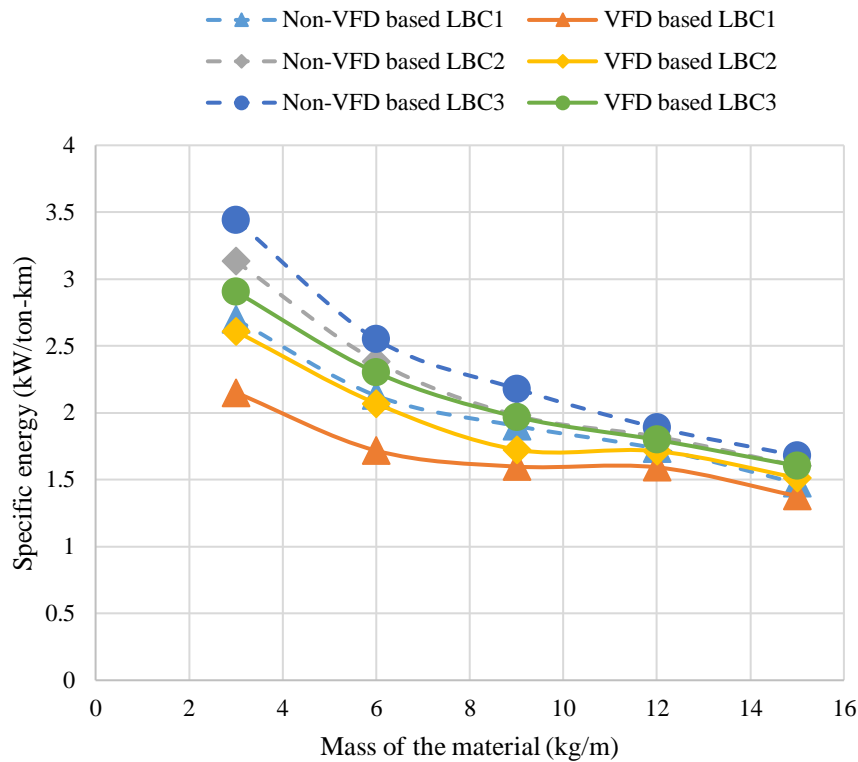


Figure 6.33 Influence of mass of the material on specific energy plot for LBC system

Table 6.14 Simulation results of non-VFD configured LBC1

β	M_l	F	v	V	I	cos ϕ	P_i	P_o	η	E_m	E_y	Q	W_s
10	3	129	0.178	412	0.72	0.21	108	28	25	21.58	259	2	2.70
	6	455	0.178	408	0.73	0.33	170	82	48.2	34.05	409	4	2.13
	9	750	0.176	414	0.74	0.43	228	134	58.7	45.63	548	6	1.90
	12	955	0.176	410	0.75	0.52	277	170	61.4	55.39	665	8	1.73
	15	1029	0.175	409	0.77	0.54	295	182	61.8	58.91	707	10	1.47
<p>Note: β = Inclination (in degrees) P_i = Input/ electrical power (in W) M_l = Unit mass of material (in kg/m) P_o = Output/ mechanical power (in W) F = Total driving force (in N.m) η = Efficiency (in %) v = Belt speed (in m/s) E_m = Energy consumption/month (in kWh) V = Voltage (in V) E_y = Energy consumption/year (in kWh) I = Current (in A) Q = Material feed rate (in t/h) cosϕ = Power factor W_s = Specific energy (in kWh/ton km)</p>													

Table 6.15 Simulation results of VFD configured LBC1

β	M_l	F	v	V	I	cos ϕ	P_i	P_o	η	E_m	E_y	Q	W_s
10	3	129	0.144	414	0.5	0.24	86	30	34.9	17.21	207	2	2.15
	6	455	0.153	412	0.55	0.35	137	68	49.5	27.47	330	4	1.72
	9	750	0.162	410	0.6	0.45	192	118	61.5	38.35	460	6	1.60
	12	955	0.171	409	0.62	0.58	255	160	62.8	50.95	611	8	1.59
	15	1029	0.189	408	0.65	0.6	276	174	63.1	55.12	661	10	1.38
<p>Note: β = Inclination (in degrees) P_i = Input/ electrical power (in W) M_l = Unit mass of material (in kg/m) P_o = Output/ mechanical power (in W) F = Total driving force (in N.m) η = Efficiency (in %) v = Belt speed (in m/s) E_m = Energy consumption/month (in kWh) V = Voltage (in V) E_y = Energy consumption/year (in kWh) I = Current (in A) Q = Material feed rate (in t/h) cosϕ = Power factor W_s = Specific energy (in kWh/ton km)</p>													

Table 6.16 Simulation results of non-VFD configured LBC2

β	M_l	F	v	V	I	cos ϕ	P_i	P_o	η	E_m	E_y	Q	W_s
15	3	152	0.177	413	0.73	0.24	125	32	26.3	25.07	301	2	3.13
	6	576	0.177	408	0.73	0.37	191	104	54.5	38.17	458	4	2.39
	9	817	0.175	412	0.74	0.45	238	146	61.4	47.53	570	6	1.98
	12	1023	0.175	410	0.76	0.54	291	186	63.8	58.29	699	8	1.82
	15	1138	0.174	409	0.78	0.58	320	202	63.0	64.10	769	10	1.60
<p>Note: β = Inclination (in degrees) P_i = Input/ electrical power (in W) M_l = Unit mass of material (in kg/m) P_o = Output/ mechanical power (in W) F = Total driving force (in N.m) η = Efficiency (in %) v = Belt speed (in m/s) E_m = Energy consumption/month (in kWh) V = Voltage (in V) E_y = Energy consumption/year (in kWh) I = Current (in A) Q = Material feed rate (in t/h) cosϕ = Power factor W_s = Specific energy (in kWh/ton km)</p>													

Table 6.17 Simulation results of VFD configured LBC2

β	M_l	F	v	V	I	cos ϕ	P_i	P_o	η	E_m	E_y	Q	W_s
15	3	152	0.135	414	0.52	0.28	104	27	25.9	20.88	251	2	2.61
	6	576	0.144	412	0.58	0.4	166	95	57.4	33.11	397	4	2.07
	9	817	0.154	410	0.62	0.47	207	138	66.7	41.39	497	6	1.72
	12	1023	0.161	409	0.68	0.569	274	178	64.9	54.82	658	8	1.71
	15	1138	0.172	408	0.69	0.621	303	197	65.1	60.56	727	10	1.51
<p>Note: β = Inclination (in degrees) P_i = Input/ electrical power (in W) M_l = Unit mass of material (in kg/m) P_o = Output/ mechanical power (in W) F = Total driving force (in N.m) η = Efficiency (in %) v = Belt speed (in m/s) E_m = Energy consumption/month (in kWh) V = Voltage (in V) E_y = Energy consumption/year (in kWh) I = Current (in A) Q = Material feed rate (in t/h) cosϕ = Power factor W_s = Specific energy (in kWh/ton km)</p>													

Table 6.18 Simulation results of non-VFD configured LBC3

β	M_l	F	v	V	I	cos ϕ	P_i	P_o	η	E_m	E_y	Q	W_s
20	3	274	0.175	413	0.74	0.26	138	50	36.3	27.53	330	2	3.44
	6	651	0.175	408	0.74	0.39	204	118	57.9	40.79	489	4	2.55
	9	885	0.174	414	0.76	0.48	262	158	60.4	52.32	628	6	2.18
	12	1069	0.174	410	0.76	0.56	302	192	63.5	60.45	725	8	1.89
	15	1207	0.174	409	0.79	0.6	336	222	66.1	67.16	806	10	1.68
<p>Note: β = Inclination (in degrees) P_i = Input/ electrical power (in W) M_l = Unit mass of material (in kg/m) P_o = Output/ mechanical power (in W) F = Total driving force (in N.m) η = Efficiency (in %) v = Belt speed (in m/s) E_m = Energy consumption/month (in kWh) V = Voltage (in V) E_y = Energy consumption/year (in kWh) I = Current (in A) Q = Material feed rate (in t/h) cosϕ = Power factor W_s = Specific energy (in kWh/ton km)</p>													

Table 6.19 Simulation results of VFD configured LBC3

β	M_l	F	v	V	I	cos ϕ	P_i	P_o	η	E_m	E_y	Q	W_s
20	3	274	0.126	414	0.54	0.3	116	40	34.4	23.23	279	2	2.90
	6	651	0.136	412	0.6	0.43	184	108	58.7	36.23	442	4	2.30
	9	885	0.144	410	0.64	0.52	236	146	61.8	47.27	567	6	1.97
	12	1069	0.152	409	0.7	0.58	288	180	62.6	57.52	690	8	1.80
	15	1207	0.161	408	0.72	0.63	321	201	62.7	64.11	769	10	1.60
<p>Note: β = Inclination (in degrees) P_i = Input/ electrical power (in W) M_l = Unit mass of material (in kg/m) P_o = Output/ mechanical power (in W) F = Total driving force (in N.m) η = Efficiency (in %) v = Belt speed (in m/s) E_m = Energy consumption/month (in kWh) V = Voltage (in V) E_y = Energy consumption/year (in kWh) I = Current (in A) Q = Material feed rate (in t/h) cosϕ = Power factor W_s = Specific energy (in kWh/ton km)</p>													

6.4.2.2 Influence of mass of material on percentage variation in belt speed, annual energy consumption, efficiency and specific energy between non-VFD and VFD based LBCs

Figure 6.30 show the influence of mass of material on belt speed for LBC1, LBC2 and LBC3 systems. Observations reveal that the belt speed of a LBC system can be optimized by incorporating a VFD. The highest variation in belt speed was achieved during the initial stage of material loading, which is 21.34%, 26.55% and 31.42% for LBC1, LBC2 and LBC3, respectively as shown in Figure 6.34.

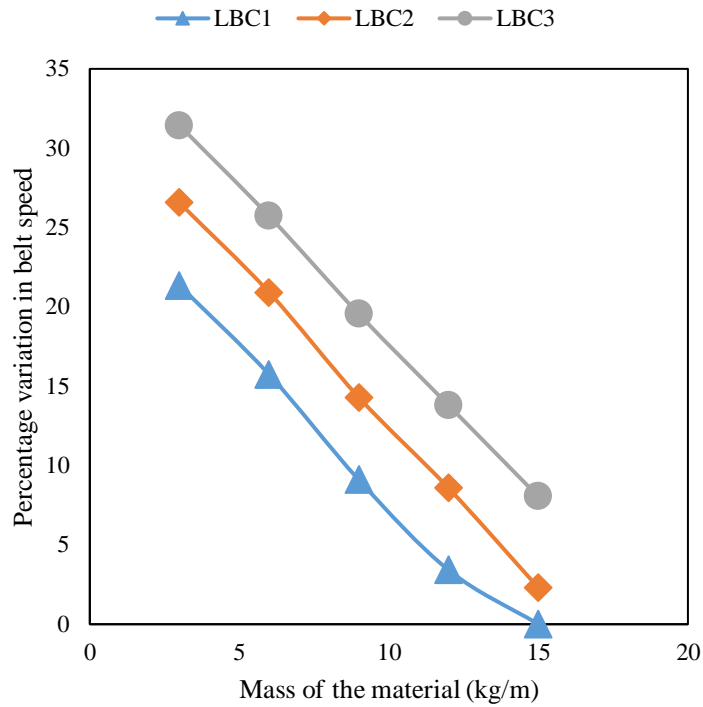


Figure 6.34 Influence of feed rate on percentage variation in belt speed between non-VFD and VFD configured LBC1, LBC2 and LBC3

Figures 6.31 depict the influence of mass of material on annual energy consumption for LBC1, LBC2 and LBC3 systems. Observations reveals that the minimization in annual energy consumption is achieved on interfacing VFD to belt conveyor system, which is 20.24%, 16.69% and 15.52% with respect to LBC1, LBC2 and LBC3 as shown in Figure 6.35.

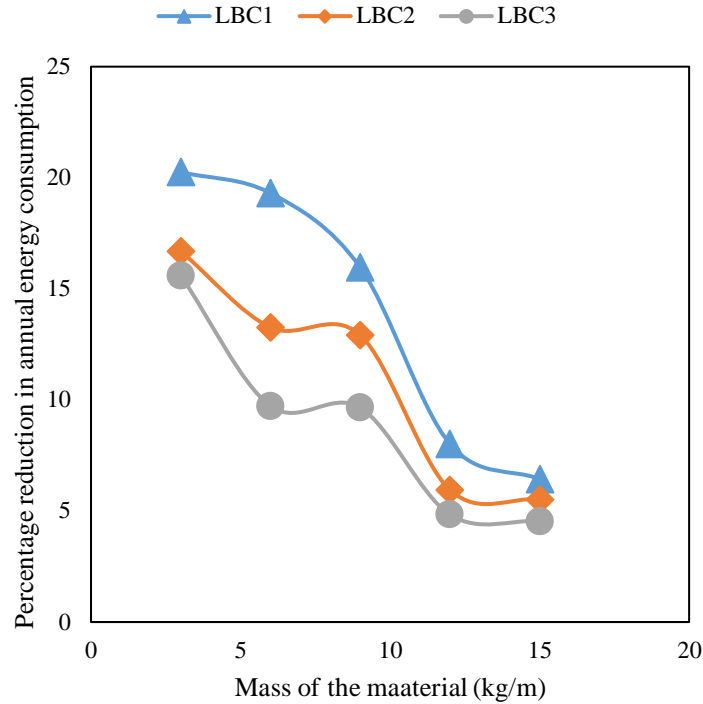


Figure 6.35 Influence of feed rate on percentage reduction in annual energy consumption between non-VFD and VFD configured LBC1, LBC2 and LBC3

Figure 6.32 show the influence of mass of material on conveyor's efficiency for LBC1, LBC2 and LBC3 systems. It can be observed that efficiency of a LBC system can be improved by incorporating a VFD. Also, the highest improvement in efficiency was achieved during the initial stage of material loading which is 22.24%, 17.58% and 15.59% for LBC1, LBC2, and LBC3, respectively as shown in Figure 6.36.

Figure 6.33 show the influence of mass of material on specific energy for LBC1, LBC2 and LBC3 systems. It is found that specific energy is indirectly proportional to material loading. Specific energy can be reduced with implementation of VFD to belt conveyor system. The highest amount of reduction in specific energy was achieved at the initial stage of material loading which is 20.24%, 16.69% and 15.52% for LBC1, LBC2 and LBC3, respectively as shown in Figure 6.37.

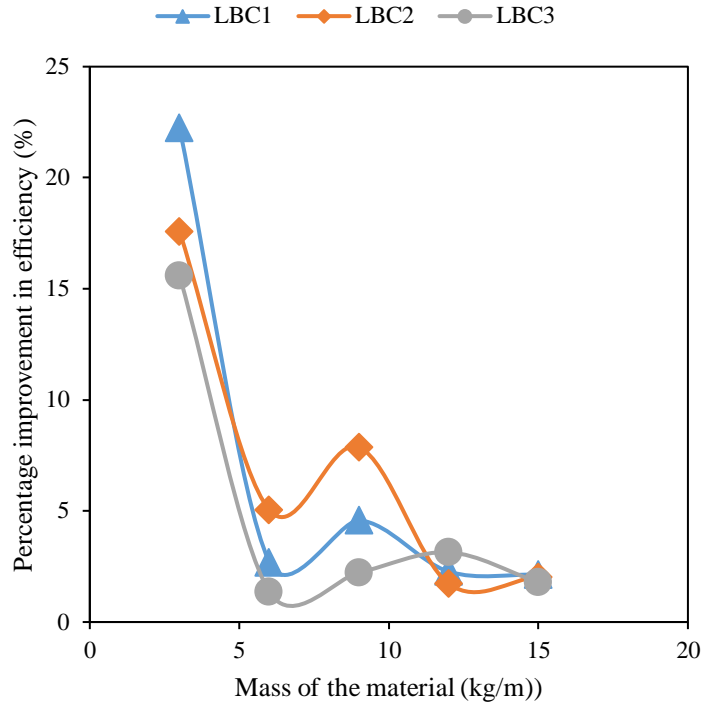


Figure 6.36 Influence of feed rate on percentage improvement in efficiency between non-VFD and VFD configured LBC1, LBC2 and LBC3

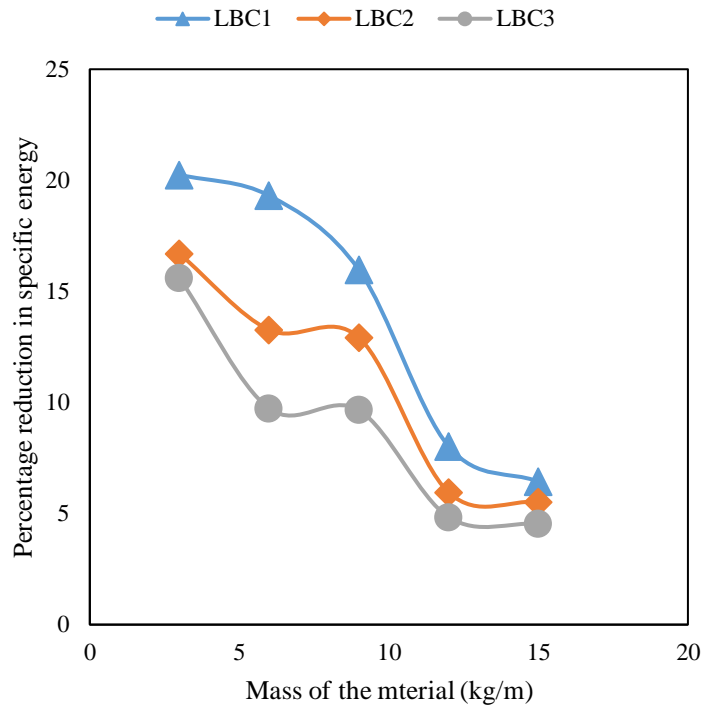


Figure 6.37 Influence of feed rate on percentage improvement in specific energy between non-VFD and VFD configured LBC1, LBC2 and LBC3

6.4.3 Dynamic response of field and laboratory drive motors – An analysis

Simulation analysis was carried out for both field and laboratory drive motors to know the dynamic behavior of the motors. This analysis was carried at three different loading cases i.e. Case I: DS only, Case II: CCDS with no load and Case III: CCDS with external load) as presented in Section 6.3. The three parameters, such as electromagnetic torque, speed and current were considered in this analysis. This analysis doesn't involve any VFD.

6.4.3.1 Dynamic response of field drive motor at varied load

The analysis was carried out on field drive motor with respect to three FBC models (i.e. FBC1, FBC2 and FBC3). Each model was tested for three cases (i.e. Case I: DS only, Case II: CCDS with no load and Case III: CCDS with external load).

Figure 6.38 represents electromagnetic torque of field drive motor with respect to FBC1. From Figure 6.38 it is observed that, the electromagnetic torque of the motor for Case I, Case II and Case III is 38 N m, 42.66 N m and 51.58 N m, respectively at steady state. In Case I (i.e. motor is not connected to any FBC), the motor draws a minimum amount of power from the supply mains to overcome the power losses, therefore, the required torque was minimum, which is 38 N m. In Case II (i.e. motor is connected to FBC1 with no material load on the belt), the FBC1 acts as load on the motor, hence, electromagnetic torque of the motor is high when compared to the Case I. In Case III (i.e. motor is connected to FBC1 with external material load on the belt), the FBC1 along with feed material on FBC1 acts as a load, hence the electromagnetic torque of the motor is high when compared to both Case I and Case II. From the Figure 6.38, it is also observed that, for all three cases (i.e. Case I, Case II and Case III) the electromagnetic torque intensity is high during the interval 0-15 s, after 15 s interval it reaches steady state. The electromagnetic torque reaches its peak value of x, y and z for Case I, Case II and Case III, respectively at 2s interval.

Figure 6.39 represents motor speed with respect to FBC1. From Figure 6.39 it is observed that, the speed of the motor for Case I, Case II and Case III is 1482 rpm, 1460 rpm and 1455 rpm, respectively at steady state. In Case I, the motor is not connected to any FBC, therefore, it runs at its speed, which was 1482 rpm. In Case II, the FBC1 acts as load on the motor, hence, the motor speed was reduced when compared to the Case I. And in Case III, the motor

is connected to FBC1 with external material load on FBC1, therefore the motor speed was as low as when compared to both Case I and Case II. The percentage variation in speed between Case I and Case II was 1.48 and between Case II and Case III was 0.34 (i.e. almost zero). This low percentage variation in speed was due to the tendency of conveyor and causes high power consumption of the conveyor system.

Figure 6.40 represents motor current with respect to FBC1. From Figure 6.40 it is observed that, the motor current for Case I, Case II and Case III is 24 A, 30 A and 60 A, respectively at steady state. In Case I, the motor was ran alone (i.e. zero load on the motor), therefore it drawn very less amount of current. In Case II, the FBC1 was connected to the motor, therefore the motor current was increased when compared to the Case I. And in Case III, the motor is connected to fully loaded FBC1, therefore the motor drawn high amount current when compared to both Case I and Case II. The percentage variation in current between Case I and Case II was 20 and between Case II and Case III was 50. From the Figure 6.40, it is also observed that the motor draws a very high starting current (i.e. about 10-15 times the full load current) for all the three cases. This is due to zero back electromotive force at time of starting. The back electromotive force is directly proportional to the speed. At the time of starting the motor speed is zero, so the back electromotive force is also zero, causing high starting current. The peak value of current drawn by the motor at the time of starting was 1100 A, 550 A and 450 A in Case I, Case II and Case III, respectively. This values of currents observed at 2 s. After 2 s, the current start decaying and reaches a steady state at 10 s interval. The state in between 0-10 s is called transient state of the system, where the oscillations of waveform are completely settle down.

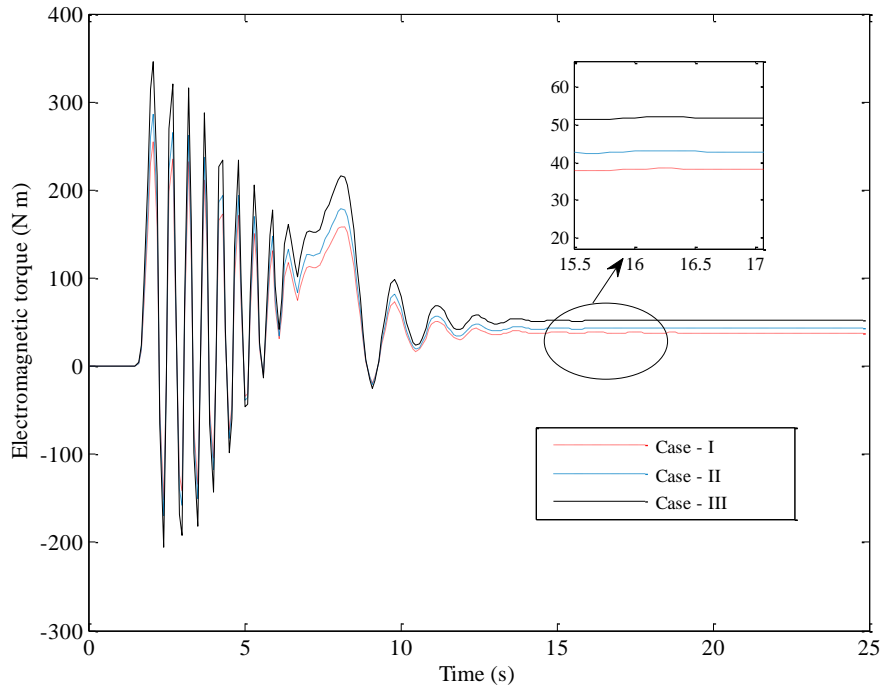


Figure 6.38 Electromagnetic torque response of FBC1 at different loads

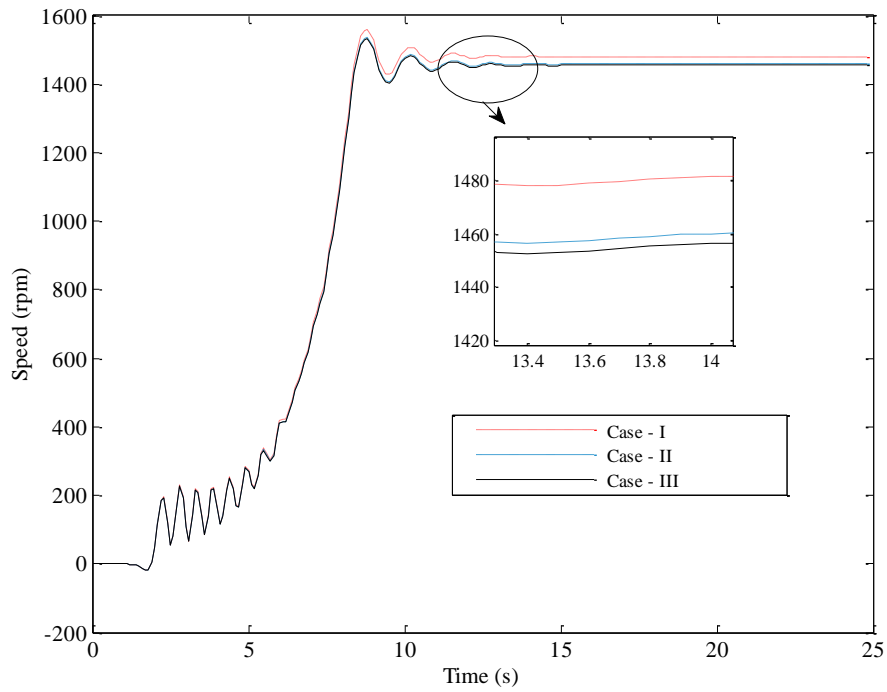


Figure 6.39 Speed response of FBC1 at different loads

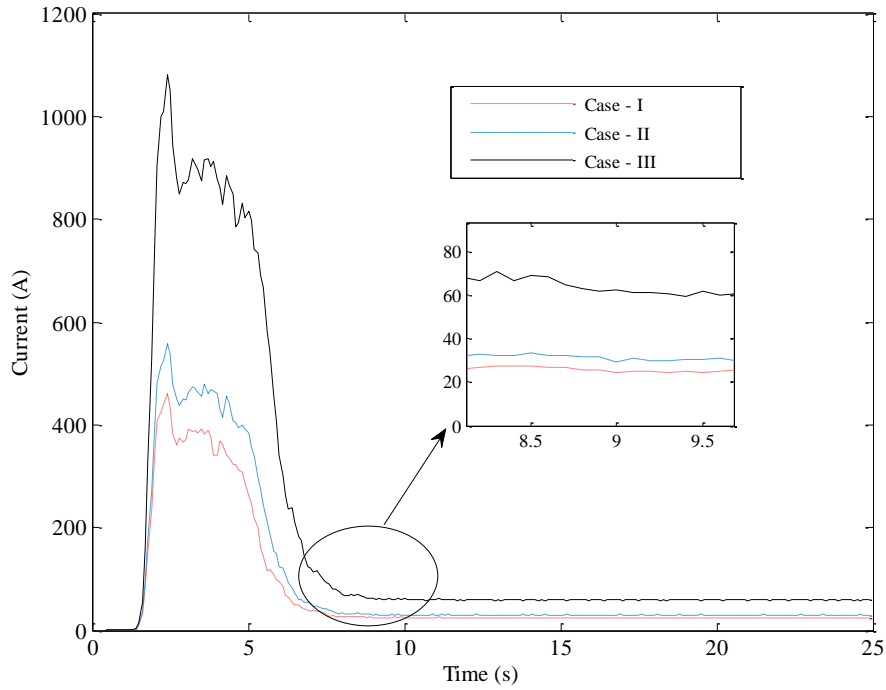


Figure 6.40 Current response FBC1 at different loads

Similarly, the study was carried for FBC2 and FBC3. From this analysis it was observed that the trends in waveforms related to electromagnetic torque, current and speed are same for FBC1, FBC2 and FBC3, but with the change in magnitudes of output. The results of the simulation (i.e. electromagnetic torque, speed and current) of FBC1, FBC2 and FBC3 for three different cases (i.e. Case I - DS only; Case II - CCDS with no load and Case III - CCDS with external load) were listed in Table 6.20

Table 6.20 Variation of motor parameters at three different loading conditions

Conveyor	Load	Electromagnetic torque in (in N m)	Speed (in rpm)	Current (in A)
FBC1	Case I	38	1482	24
	Case II	42.66	1460	30
	Case III	51.58	1455	60
FBC2	Case I	38	1482	24
	Case II	54.59	1450	42
	Case III	294	1430	92
FBC3	Case I	38	1482	24
	Case II	88.94	1445	48
	Case III	258	1435	86

For FBC2, the electromagnetic torque, speed and current response plots were shown in Figure 6.41, Figure 6.42 and Figure 6.43. From Figure 6.41 it is observed that, the electromagnetic torque of the motor for Case I, Case II and Case III is 38 N m, 54.6 N m and 294 N m, respectively at steady state. From Figure 6.42 it is observed that, the speed of the motor for Case I, Case II and Case III is 1482 rpm, 1450 rpm and 1430 rpm, respectively at steady state. From Figure 6.43 it is observed that, the motor current for Case I, Case II and Case III is 24 A, 30 A and 60 A, respectively at steady state.

For FBC3, the electromagnetic torque, speed and current response plots were shown in Figure 6.44, Figure 6.45 and Figure 6.46. From Figure 6.44 it is observed that, the electromagnetic torque of the motor for Case I, Case II and Case III is 38 N m, 88.94 N m and 258 N m, respectively at steady state. From Figure 6.45 it is observed that, the speed of the motor for Case I, Case II and Case III is 1482 rpm, 1450 rpm and 1430 rpm, respectively at steady state. From Figure 6.46 it is observed that, the motor current for Case I, Case II and Case III is 24 A, 30 A and 60 A, respectively at steady state.

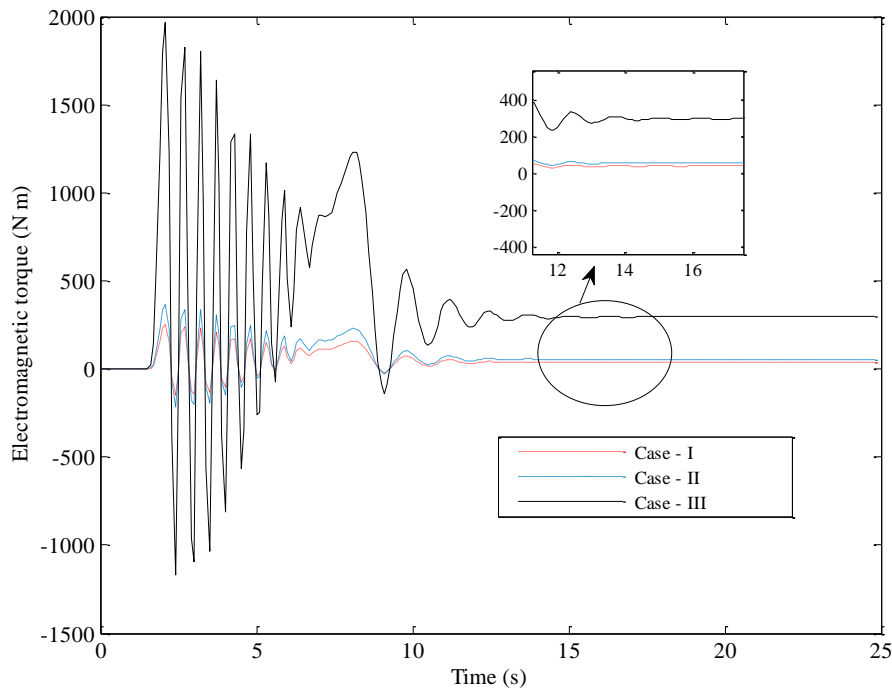


Figure 6.41 Electromagnetic torque response of FBC2 at different loads

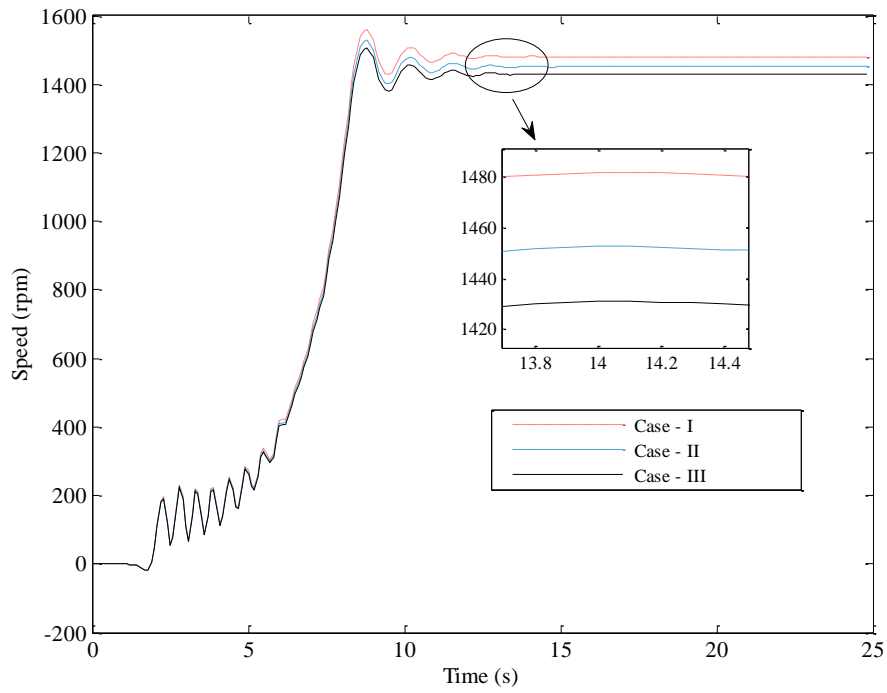


Figure 6.42 Speed response of FBC2 at different loads

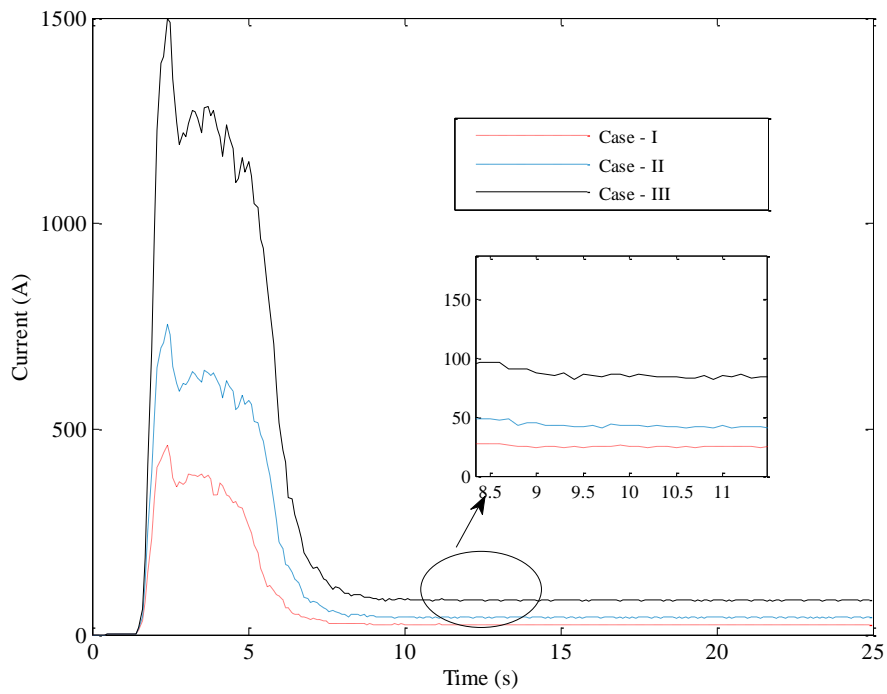


Figure 6.43 Current response of FBC2 at different loads

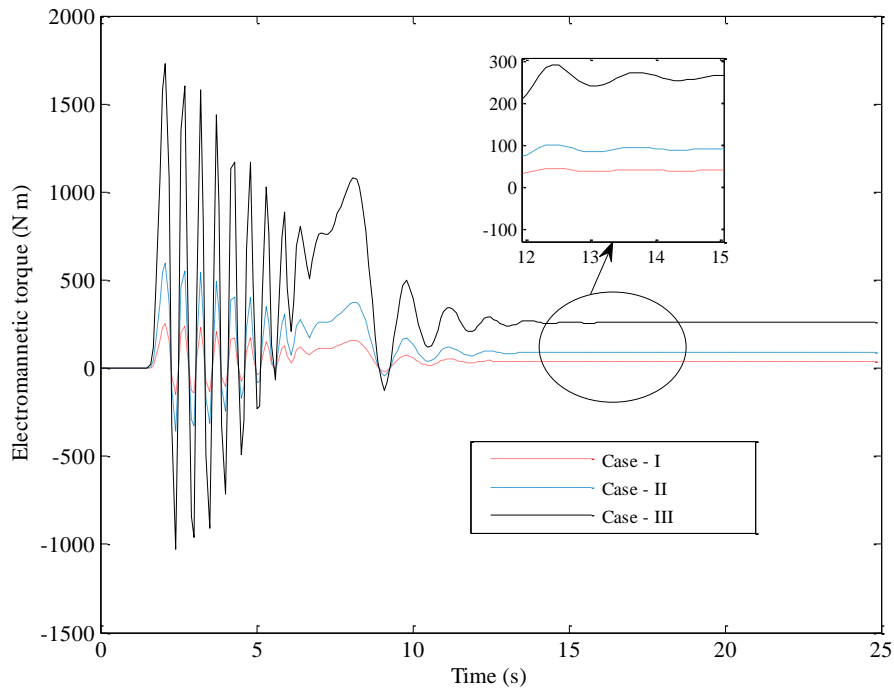


Figure 6.44 Electromagnetic torque response of FBC3 at different loads

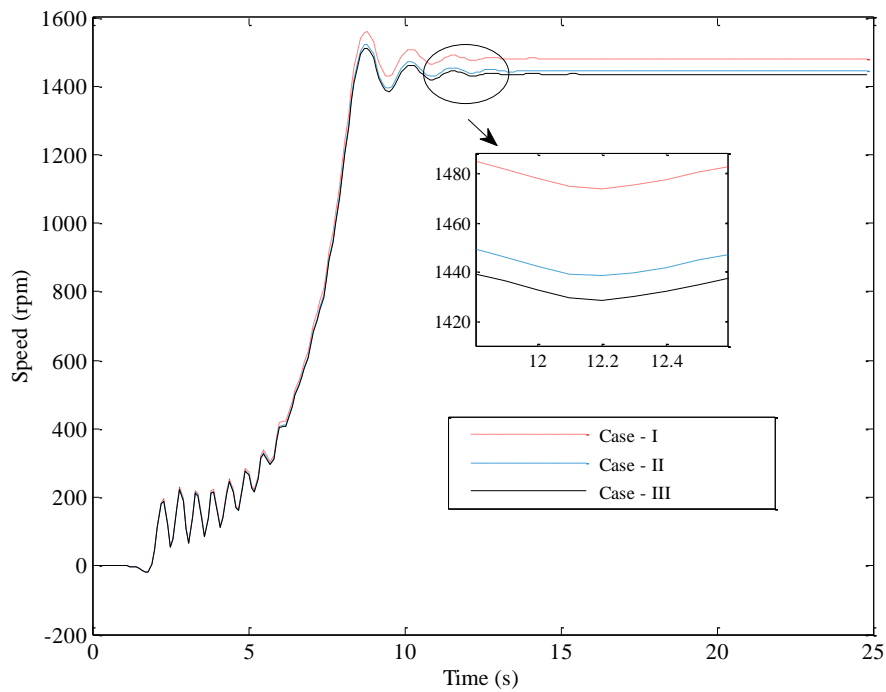


Figure 6.45 Speed response of FBC3 at different loads

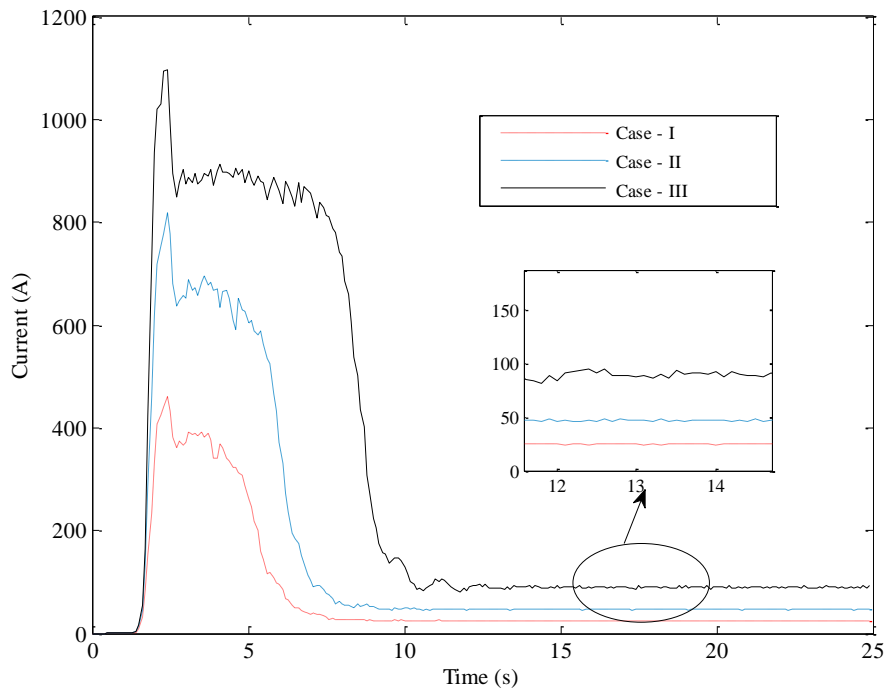


Figure 6.46 Current response of FBC3 at different loads

From the above analysis it is concluded that, the electromagnetic torque developed in the motor at a steady state is 38 N m when it is not connected to the belt conveyor. The nature of electromagnetic is pulsating decay. The no-load torque of the FBC1, FBC2, and FBC3 are 42.66 N m, 54.59 N m and 88.9 N m, respectively. The no-load torque was found to be in the order $FBC1 < FBC2 < FBC3$. This is due to the varying length of conveyor; which is found to be in the order $FBC1 < FBC2 < FBC3$. The full load torque of the FBC1, FBC2, and FBC3 are 51.58 N m, 294 N m and 258 N m, respectively. The full load torque was found to be in the order $FBC1 > FBC3 > FBC2$. This is due to the varying height to which the material has to be delivered; which is also found to be in the order $FBC1 > FBC3 > FBC2$.

6.4.3.2 Dynamic response of laboratory drive motor at varied load

The analysis was carried out on drive motor of LBC system, with similar to FBC system, for all the three LBC models (i.e. LBC1, LBC2 and LBC3). Each model was tested for three cases

(i.e. Case I: DS only, Case II: CCDS with no load and Case III: CCDS with external load). The results of the simulation study were recorded and given in Table 6.21.

Table 6.21 Variation of motor parameters at three different loading conditions

Conveyor	Load	Electromagnetic torque (in N m)	Speed (in rpm)	Current (in A)
LBC1	Case I	1.66	1380	0.68
	Case II	2.62	1357	0.72
	Case III	3.19	1341	0.77
LBC2	Case I	1.66	1380	0.68
	Case II	2.78	1349	0.73
	Case III	3.49	1326	0.78
LBC3	Case I	1.66	1380	0.68
	Case II	2.85	1341	0.74
	Case III	3.86	1311	0.79

For LBC1, the electromagnetic torque, speed and current response plots were shown in Figure 6.47, Figure 6.48 and Figure 6.49. From Figure 6.47 it is observed that, the electromagnetic torque of the motor for Case I, Case II and Case III is 1.66 N m, 2.62 N m and 3.19 N m, respectively at steady state. From Figure 6.48 it is observed that, the speed of the motor for Case I, Case II and Case III is 1380 rpm, 1357 rpm and 1341 rpm, respectively at steady state. From Figure 6.49 it is observed that, the motor current for Case I, Case II and Case III is 0.68 A, 0.72 A and 0.77 A, respectively at steady state.

For LBC2, the electromagnetic torque, speed and current response plots were shown in Figure 6.50, Figure 6.51 and Figure 6.52. From Figure 6.50 it is observed that, the electromagnetic torque of the motor for Case I, Case II and Case III is 1.66 N m, 2.78 N m and 3.49 N m, respectively at steady state. From Figure 6.51 it is observed that, the speed of the motor for Case I, Case II and Case III is 1380 rpm, 1349 rpm and 1326 rpm, respectively at steady state. From Figure 6.52 it is observed that, the motor current for Case I, Case II and Case III is 0.68 A, 0.73 A and 0.7 A, respectively at steady state.

For LBC3, the electromagnetic torque, speed and current response plots were shown in Figure 6.53, Figure 6.54 and Figure 6.55. From Figure 6.53 it is observed that, the electromagnetic torque of the motor for Case I, Case II and Case III is 1.66 N m, 2.85 N m and 3.86 N m, respectively at steady state. From Figure 6.54 it is observed that, the speed of the motor for Case I, Case II and Case III is 1380 rpm, 1341 rpm and 1311 rpm, respectively at steady state.

From Figure 6.55 it is observed that, the motor current for Case I, Case II and Case III is 0.68 A, 0.74 A and 0.79 A, respectively at steady state.

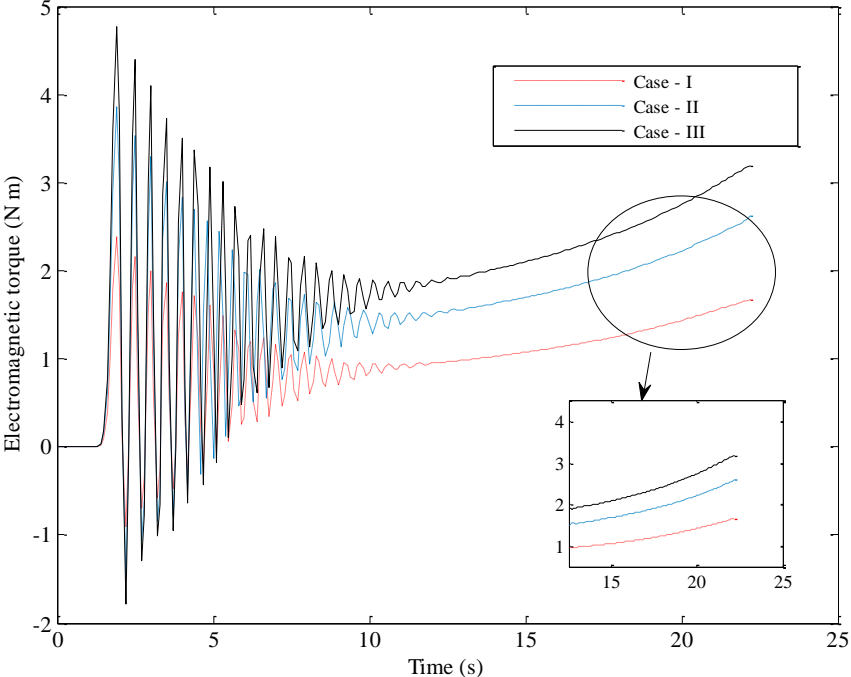


Figure 6.47 Electromagnetic torque response of LBC1 at different loads

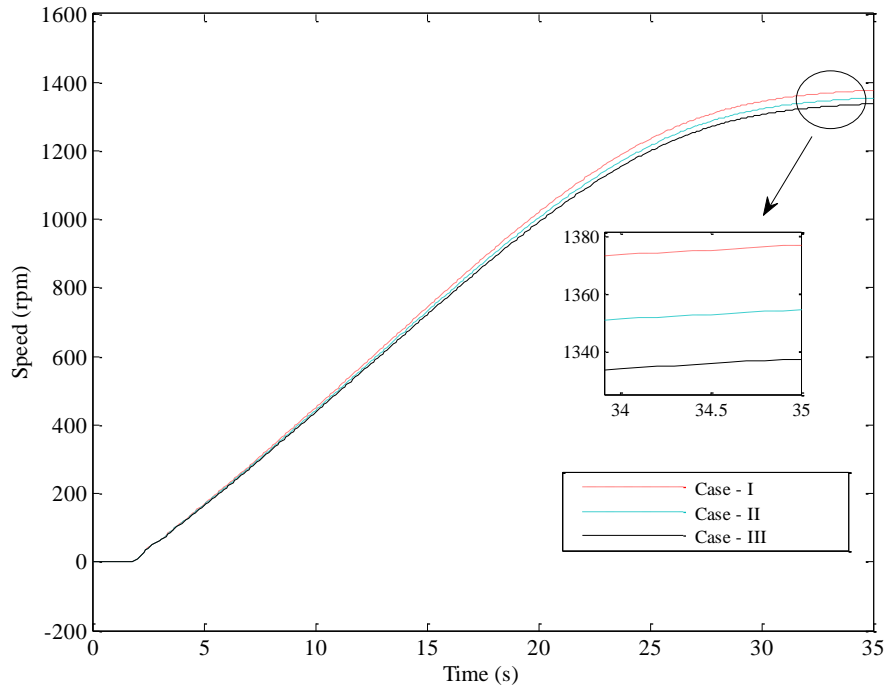


Figure 6.48 Speed response of LBC1 at different loads

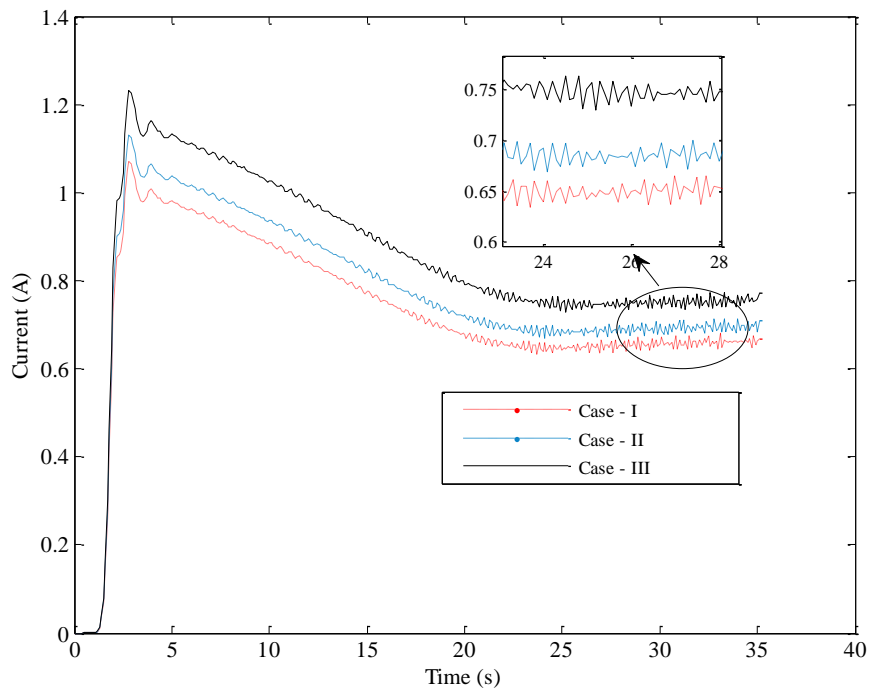


Figure 6.49 Current response of LBC1 at different loads

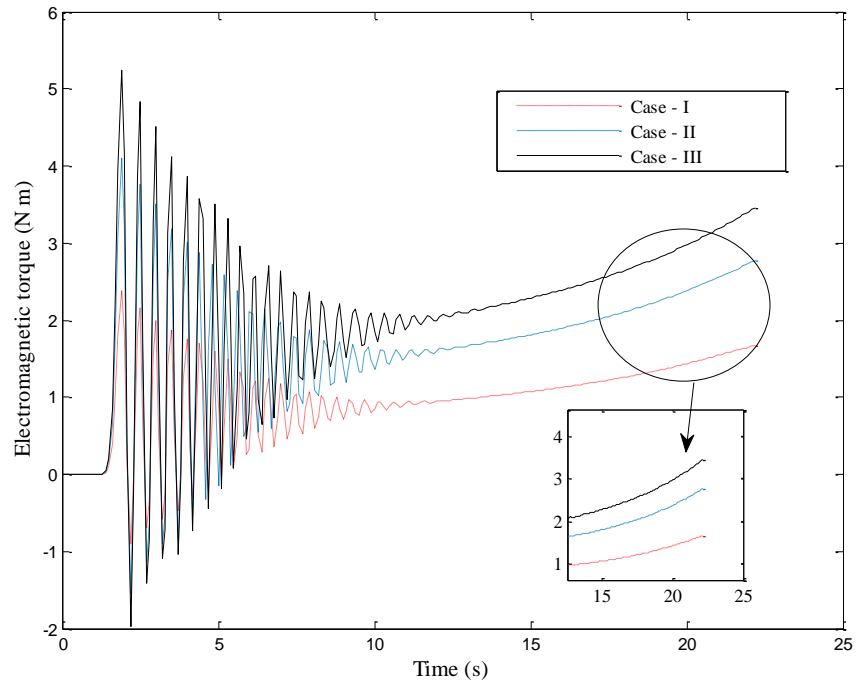


Figure 6.50 Electromagnetic torque response of LBC2 at different loads

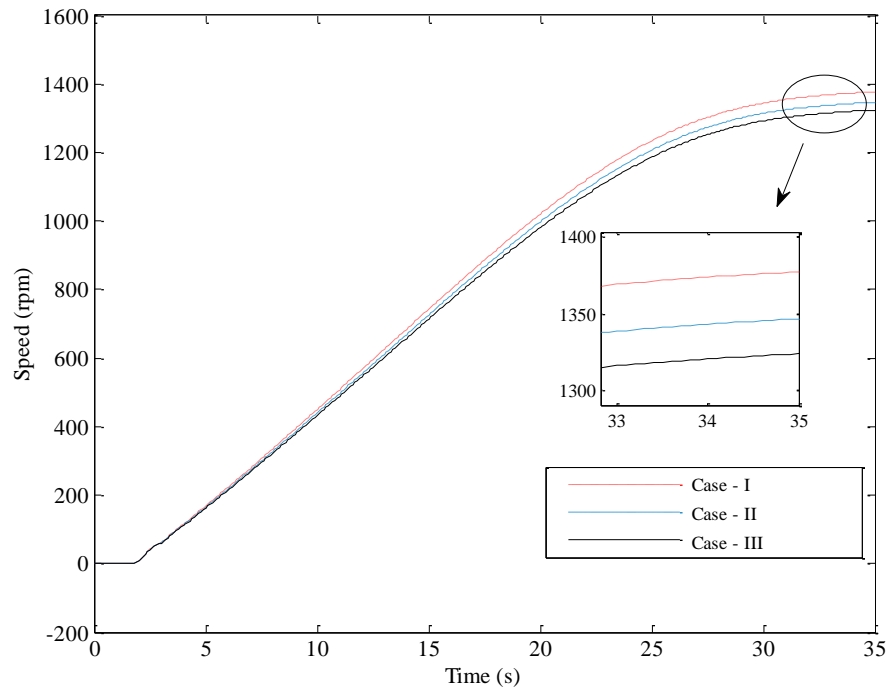


Figure 6.51 Speed response of LBC2 at different loads

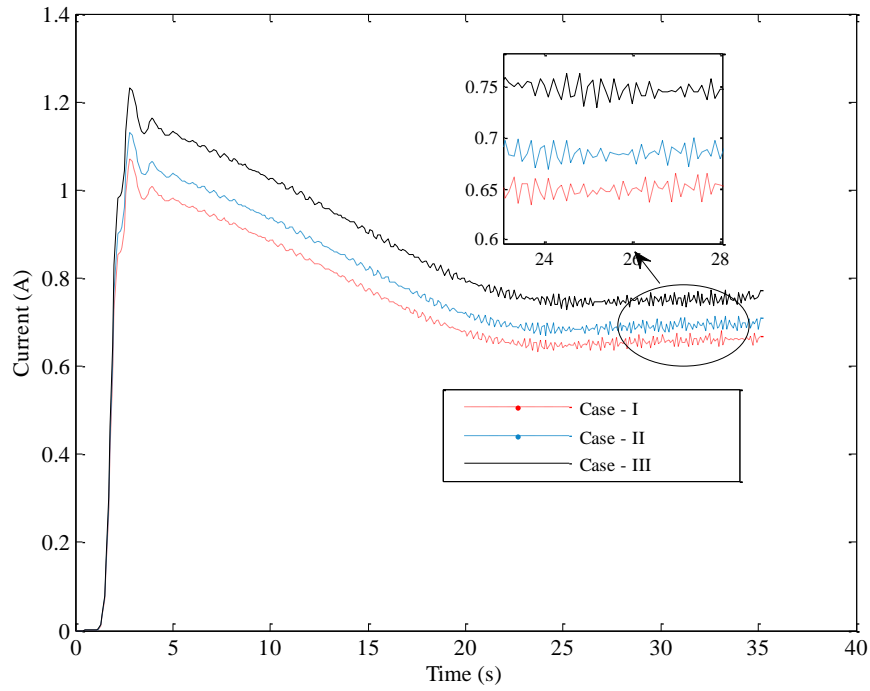


Figure 6.52 Current response of LBC2 at different loads

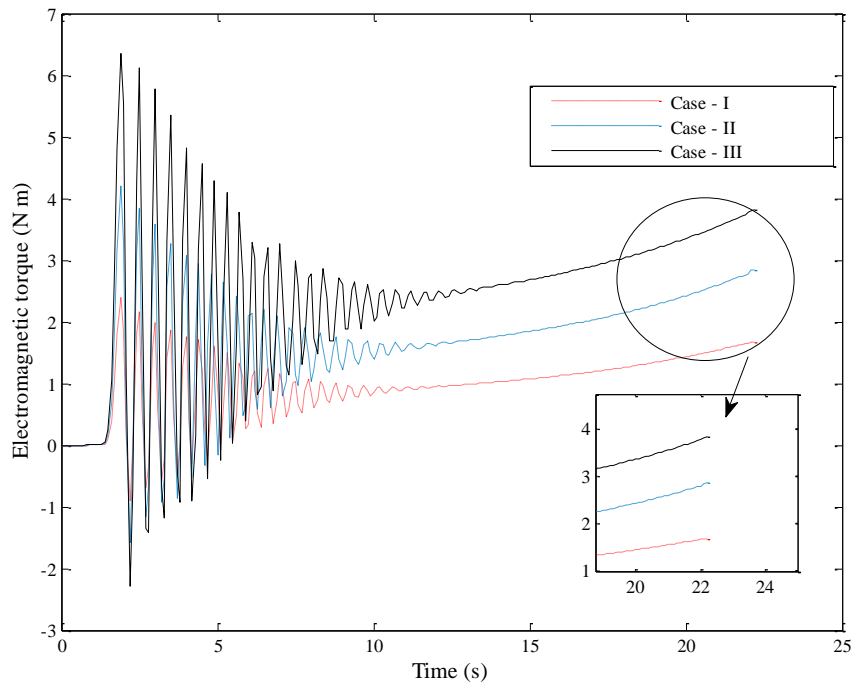


Figure 6.53 Electromagnetic torque response of LBC3 at different loads

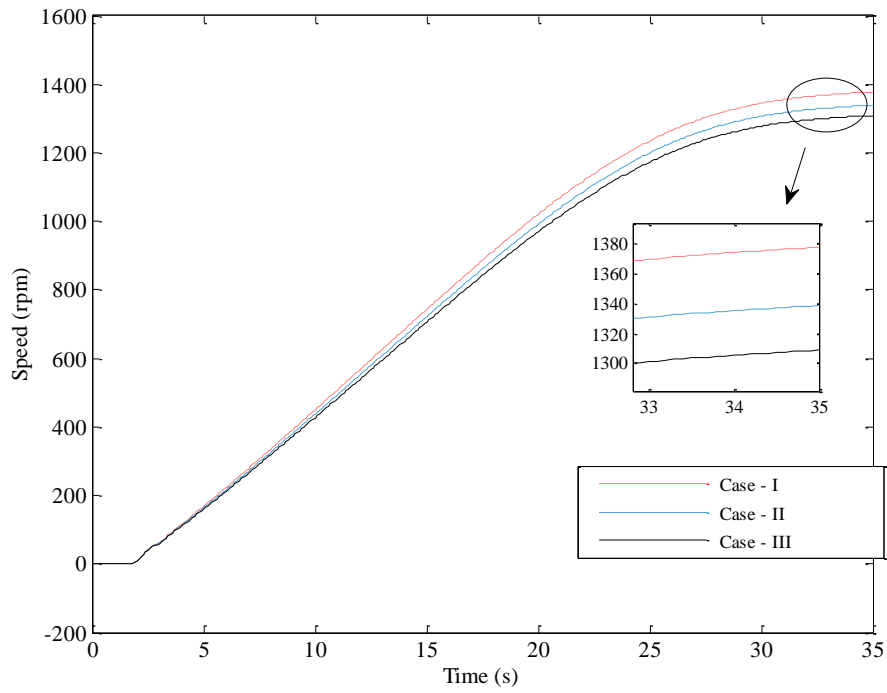


Figure 6.54 Speed response of LBC3 at different loads

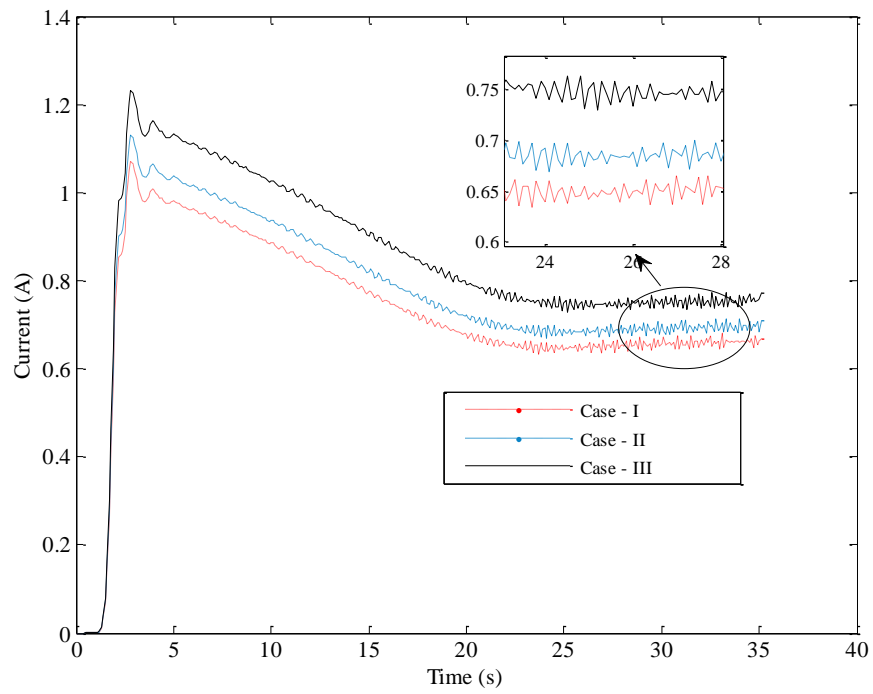


Figure 6.55 Current response of LBC3 at different loads

From the above analysis it is concluded that, the electromagnetic torque developed in the motor at a steady state is 1.66 N m when it is not connected to the belt conveyor. The nature of electromagnetic is pulsating decay. The no-load torque of the LBC1, LBC2, and LBC3 are 2.62 N m, 2.78 N m and 2.85 N m, respectively. The full load torque of the LBC1, LBC2, and LBC3 are 3.19 N m, 3.49 N m and 3.86 N m, respectively. The no-load and full load torques were found to be in the order $LBC1 < LBC2 < LBC3$. This is due to the varying height to which the material has to be delivered; which is also found to be in the order $LBC1 < LBC2 < LBC3$. The startup time of the all three LBCs is 24 s. The electromagnetic torque is pulsating in magnitude in between 0 to 10 s interval; after that, the magnitude of torque is slightly increasing between the interval 10 to 24 s. The electromagnetic torque has its peak values of 2.5 N m, 4.5 N m, and 6.5 N m at Case I, Case II, and Case III, respectively for all the three LBCs. The startup time of LBCs is greater when compared to FBCs. This is due to the speed of FBC drive motor is greater than the speed of LBC drive motor.

6.4.4 Comparison of non-VFD and VFD based FBCs and LBCs based on current

Comparative simulation analysis was done at full load condition with and without VFD for FBCs and LBCs to analyze the response of current drawn by the motor. The results obtained were in the form of scope and display. The scope represents the variation of dynamic response with varying time. The display represents magnitude of the current with varying time. By analyzing scope and display results, the performance of FBCs and LBCs were evaluated, with and without VFDs. Based on these results an optimum FBC and LBC system can be designed, fabricated and it can be implemented in the field for optimum power consumption.

6.4.4.1 Dynamic response of current for non-VFD and VFD based FBCs- An analysis

Figure 6.56 show simulation analysis for motor current at full load condition for non-VFD and VFD based FBC1 system. As observed in Figure 6.56, the settling time of the non-VFD based FBC1 is 8 s whereas in case of VFD based FBC1 it is 2 s. This indicates that, at the full load condition the settling time required for non-VFD is more than the VFD, because the non-VFD model has low dynamic response when compared to VFD model. From Figure 6.56, it is also

observed that the intensity of current for non-VFD is high oscillatory and having a peak value of 470 A. But in case of VFD the intensity of current is smooth and non-oscillatory. The intensity current peaks shows that VFD based FBC1 will settle faster than the non-VFD based FBC1. Also, the magnitude of current, at steady state for a non-VFD based FBC1 is 60 A, whereas in case of VFD based FBC1 it is 30 A i.e. 50 % variation in current was observed between non-VFD and VFD based FBC1 models. The simulation results shows that VFD model consumes less current compared to non-VFD FBC1 model, which ultimately reduces power consumption of the FBC1 model.

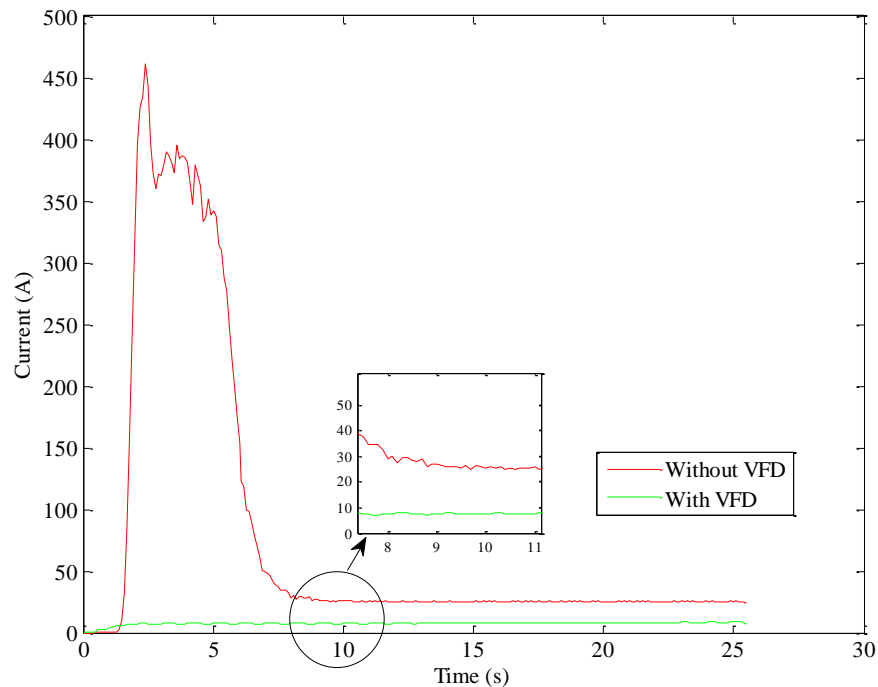


Figure 6.56 Current response for FBC1 model

Similarly, from Figure 6.57 it can be observed that the settling time of the non-VFD based FBC2 is 12.5 s whereas it is 2 s for VFD based model. This reduced settling time improves the dynamic behavior of the system and makes the system stable. The full load current at steady state, for a non-VFD based FBC2 is 91 A whereas 83 A for VFD based FBC2 model. The percentage variation between non-VFD and VFD based models is 9.78. The current is oscillatory and having a peak value of 470 A for a non-VFD based FBC2, whereas smooth non-oscillatory current response in case of VFD based FBC2. However, the current response

of VFD based FBC2 have little harmonics, compared to current response of VFD based FBC1. This is due to the load torque FBC2 is high when compared to FBC1.

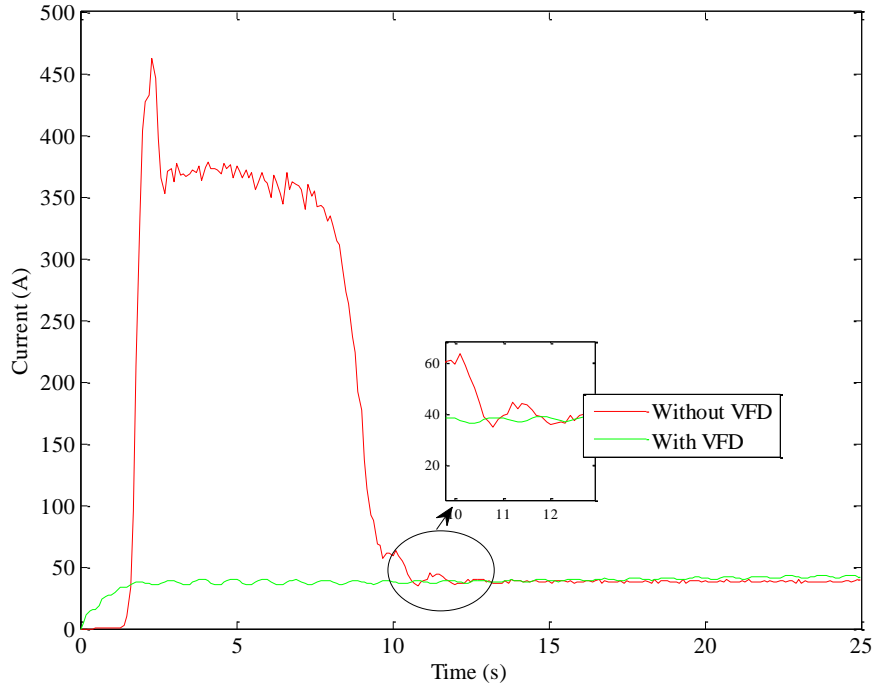


Figure 6.57 Current response for FBC2 model

As shown in Figure 6.58, the settling time of the non-VFD based FBC3 is 11.5 s, whereas it is 2 s for VFD based model. The full load current at steady state, for a non-VFD based FBC3 is 86 A, whereas it is 72 A for VFD based FBC3 model. The percentage variation between non-VFD and VFD based models is 16.27. The current is oscillatory and having a peak value of 470 A for a non-VFD based FBC3 whereas smooth non-oscillatory current response in case of VFD based FBC3. However, the current response of VFD based FBC3 have little harmonics, compared to current response of VFD based FBC1. This is due to the load torque of FBC3 is high when compared to FBC1.

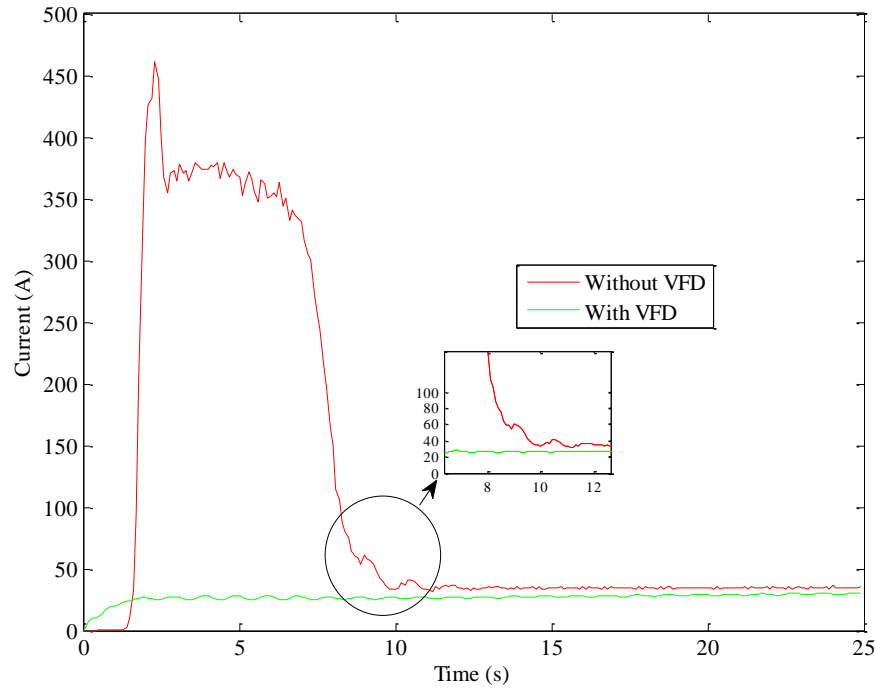


Figure 6.58 Current response for FBC3 model

From the above analysis, it is concluded that, when the conveyors (i.e. FBC1, FBC2 and FBC3) are not interfaced with VFD the motor's starting current is very high (4.75 times the full load value), the current waveform has a high magnitude of oscillations in between 0 to 10 s interval, thereafter it reaches to steady-state and the current reaches its peak value at 3 s. The high magnitude oscillations in the current waveform are removed when the motor is interfaced with the VFD. The variation of full load current with respect to VFD interfacing for all the three conveyors was tabulated and given in Table 6.22. Table 6.22 indicate that the variation of full load current is high in case of FBC1 system when compared to FBC2 and FBC3. The percentage variations in current with and without connecting VFD are 50, 9.78 and 16.27 for FBC1, FBC2 and FBC3, respectively.

Table 6.22 Variation of full load motor current for non-VFD and VFD based FBC

Conveyor	Full load current for Non-VFD (in A)	Full load current for VFD (in A)	Percentage variation in current
FBC1	60	30	50
FBC2	92	83	9.78
FBC3	86	72	16.27

6.4.4.2 Dynamic response of current for non-VFD and VFD based LBCs- An analysis

The analysis with respect to dynamic response of current for both VFD and non-VFD LBC system was done similar to FBC system.

Figure 6.59 show simulation analysis for motor current at full load condition for non-VFD and VFD based LBC1 system. As observed in Figure 6.59, the settling time of the non-VFD based LBC1 is 25 s whereas in case of VFD based LBC1 it is 2 s. This indicates that, at the full load condition the settling time required for non-VFD is more than the VFD, because the non-VFD model has low dynamic response when compared to VFD model. From Figure 6.59, it is also observed that the intensity of current for non-VFD is high oscillatory and having a peak value of 1.25 A. But in case of VFD the intensity of current is smooth and non-oscillatory. The intensity current peaks shows that VFD based LBC1 will settles faster than the non-VFD based LBC1. Also, the magnitude of current, at steady state for a non-VFD based LBC1 is 0.77 A, whereas in case of VFD based LBC1 it is 0.65 A, i.e. 14.2% variation in current was observed between non-VFD and VFD based LBC1 models. The simulation results shows that VFD model consumes less current compared to non-VFD FBC1 model, which ultimately reduces power consumption of the LBC1 model.

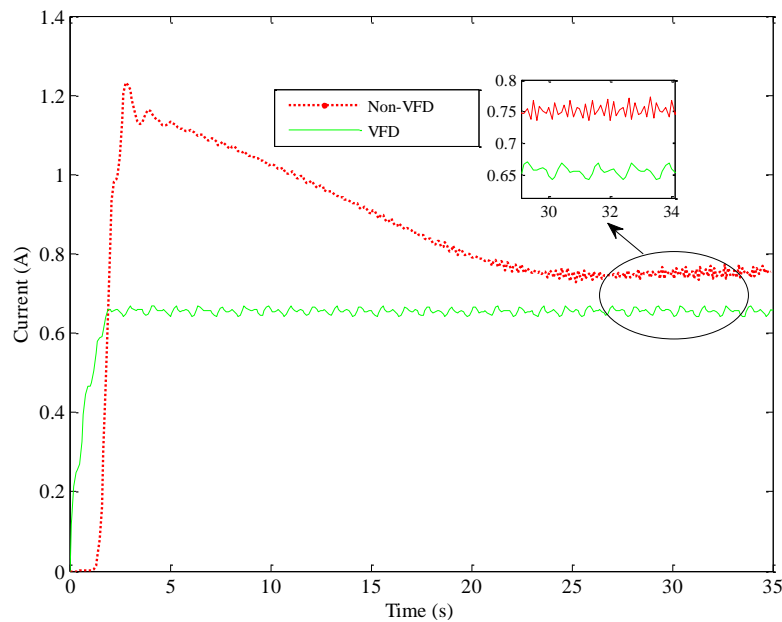


Figure 6.59 Current response of LBC1 system

Similarly, from Figure 6.60 it can be observed that the settling time of the non-VFD based LBC2 is 26 s whereas it is 2 s for VFD based model. This reduced settling time improves the dynamic behavior of the system and makes the system stable. The full load current at steady state, for a non-VFD based FBC2 is 0.78 A, whereas 0.69 A for VFD based LBC2 model. The percentage variation between non-VFD and VFD based models is 11.5. The current is oscillatory and having a peak value of 1.25 A for a non-VFD based LBC2, whereas smooth non-oscillatory current response in case of VFD based LBC2.

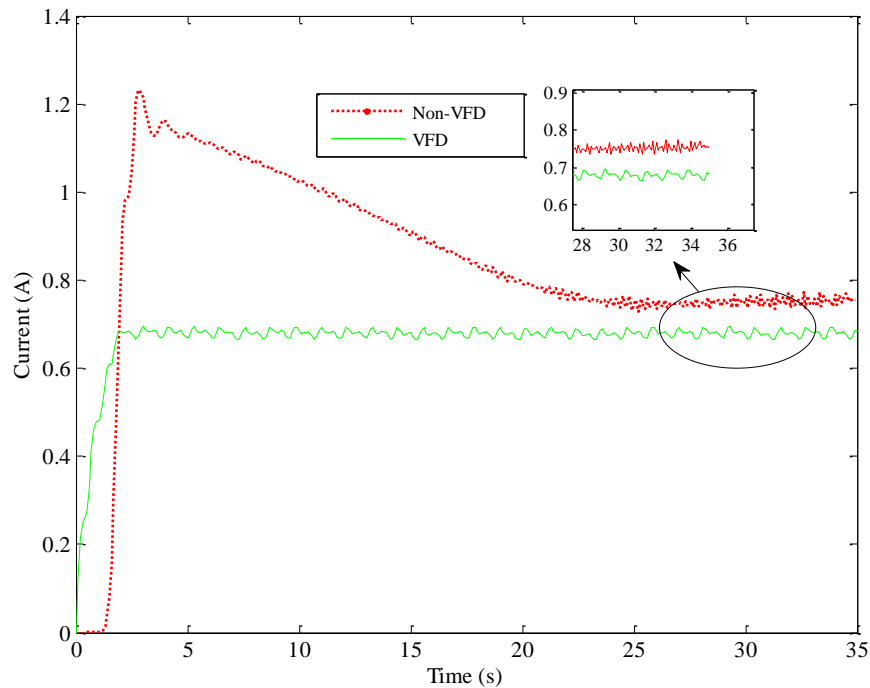


Figure 6.60 Current response of LBC2 system

As shown in Figure 6.61, the settling time of the non-VFD based LBC3 is 26 s, whereas it is 2 s for VFD based model. The full load current at steady state, for a non-VFD based LBC3 is 0.79 A, whereas it is 0.72 A for VFD based FBC3 model. The percentage variation between non-VFD and VFD based models is 8.86. The current is oscillatory and having a peak value of 1.25 A for a non-VFD based LBC3 whereas smooth non-oscillatory current response in case of VFD based FBC3.

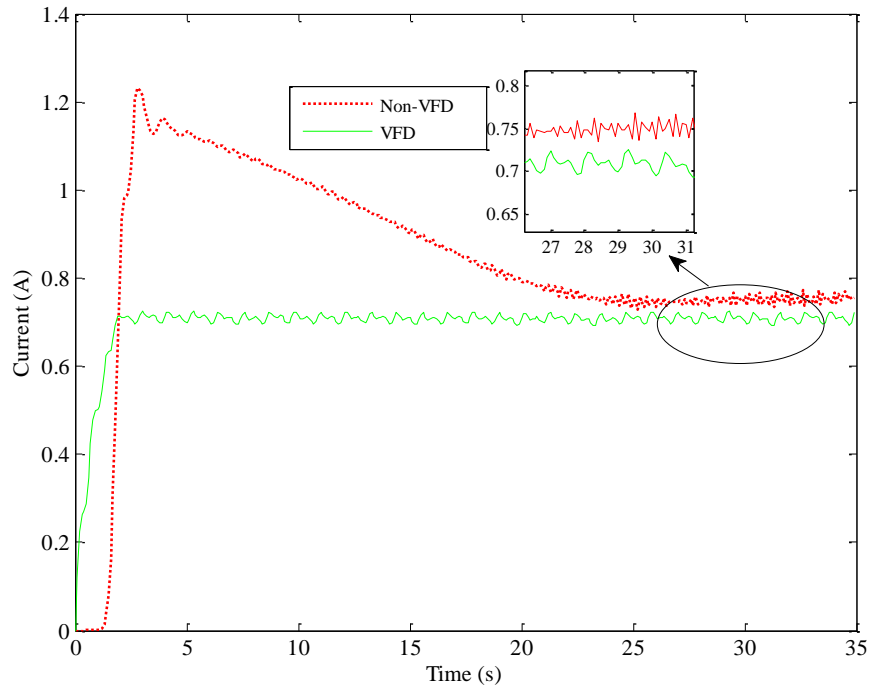


Figure 6.61 Current response of LBC3 system

From the above analysis, it is concluded that, when the conveyors (i.e. LBC1, LBC2 and LBC3) are not interfaced with VFD the motor's starting current is very high (1.56 times the full load value), the current waveform has a high magnitude of oscillations in between 0 to 26 s interval, thereafter it reaches to steady-state and the current reaches its peak value at 3 s. The high magnitude oscillations in the current waveform are removed when the motor is interfaced with the VFD. The variation of full load current with respect to VFD interfacing for all the three conveyors was tabulated and given in Table 6.23. Table 6.23 indicate that the variation of full load current is high in case of LBC1 system when compared to LBC2 and LBC3. The percentage variations in current with and without connecting VFD are 14.2, 11.5 and 8.86 for LBC1, LBC2 and LBC3, respectively.

Table 6.23 Variation of full load motor current for non-VFD and VFD based LBC

Conveyor	Full load current for Non-VFD ,A	Full load current for VFD, A	Percentage variation in current
LBC1	0.77	0.65	14.2
LBC2	0.78	0.69	11.5
LBC3	0.79	0.72	8.86

6.5 Overall Discussion and Findings of Simulation Studies

A simulation study was carried out using MATLAB-Simulink to optimize the performance of FBCs by mounting a VFD. Six different models considering all three FBCs were developed considering both non-VFD and VFD incorporations. Parameters of FBCs namely, belt speed, energy consumption, efficiency and specific energy were studied. Scatter graphs of individual conveyor parameters against varying feed rate (40 t/h to 200 t/h) were plotted for all three FBCs. Observations reveal that;

- Belt speed of a FBC system can be optimized by incorporating a VFD to a belt conveyor systems. The highest variation in speed achieved was found during the initial stage of material loading; which was found to be 50%, 47.36% and 50% for FBC1, FBC2 and FBC3, respectively.
- Minimization in annual energy consumption was achieved by interfacing VFD to belt conveyor systems; which was found to be 9.4%, 2.31% and 7.3% with respect to FBC1, FBC2 and FBC3.
- Efficiency of a FBC system can be improved by incorporating VFD to belt conveyor systems. The highest improvement in efficiency achieved is found during the initial stage of material loading which was found to be 16.76%, 1.01% and 11.51% for FBC1, FBC2 and FBC3, respectively.
- Specific energy is indirectly proportional to material feed rate. Specific energy can be reduced with implementation of VFD to belt conveyor systems. The amount of reduction in specific energy was found highest at the initial stage of feed rate which was found to be 10.4%, 2.55% and 5.93% for FBC1, FBC2 and FBC3, respectively.

Simulation study considering both non-VFD and VFD for LBCs were developed to estimate belt speed, energy consumption, efficiency and specific energy. A comparison study in the form of scatter plot for both non-VFD and VFD based LBC models were drawn. Observations reveal that;

- Belt speed of a LBC system can be optimized by incorporating a VFD to a belt conveyor system. The highest variation in speed achieved was found during the initial stage of material loading which was found to be 21.34%, 26.55% and 31.42% for LBC1, LBC2 and LBC3, respectively.

- Minimization in annual energy consumption was achieved on interfacing VFD to belt conveyor systems; which was found to be 20.24%, 16.69% and 15.52% with respect to LBC1, LBC2 and LBC3.
- Efficiency of a LBC system can be improved by incorporating a VFD to a belt conveyor systems. The highest improvement in efficiency achieved was found during the initial stage of material loading which was found 22.24%, 17.58% and 15.59% for LBC1, LBC2, and LBC3, respectively.
- Specific energy is indirectly proportional to material loading. Specific energy can be reduced with implementation of VFD to belt conveyor systems. The amount of reduction in specific energy was found highest at the initial stage of material loading which is 20.24%, 16.69% and 15.52% for LBC1, LBC2 and LBC3, respectively.

CHAPTER 7

LABORATORY STUDIES

7.1 Experimentation and Methodology

This study investigates the performance parameters of the belt conveyor drive system, in the laboratory, under different loading and gradient conditions. A belt conveyor system was fabricated, which consists of - a control circuit board, voltage source inverter, three-phase induction motor, current sensors, voltage sensors, speed sensor, multi-functional meter and a belt conveyor as load. Table 7.1 gives the details of the equipment's used. The block diagram of belt conveyor system is given in Figure 7.1 and Figure 7.2 shows its pictorial view. The load on the conveyor was varied from 3 kg/m to 15 kg/m, in steps of 3 kg (i.e. 3 kg/m, 6 kg/m, 9 kg/m, 12 kg/m and 15 kg/m) and the study was carried out for 10°, 15° and 20° inclinations. Figure 7.3 shows the fabricated laboratory belt conveyor system and Figure 7.4 shows the detailed description of it.

Table 7.1 Details of the equipment used

Sl. No.	Name	Description
1	Control circuit board	A DSP controller board is used to control the speed and analog to digital conversions.
2	Rectifier bridge	A 1200V, 25A Converter Bridge is used for AC-DC conversion.
3	DC link	A capacitor is used as a dc link for harmonic reduction.
4	Voltage source inverter	An IGBT inverter is used to convert DC into an AC supply.
5	AC motor	A 0.5HP three-phase squirrel cage induction motor is used as a drive motor.
6	Current and voltage sensors	Four number of Hall effect current sensors are used to sense the dc-link current & 3 output current of the inverter bridge, 3 number of Hall effect voltage sensor to sense motor output voltages.
7	Speed sensor	A rotary type sensor (512PPR) is used for speed feedback

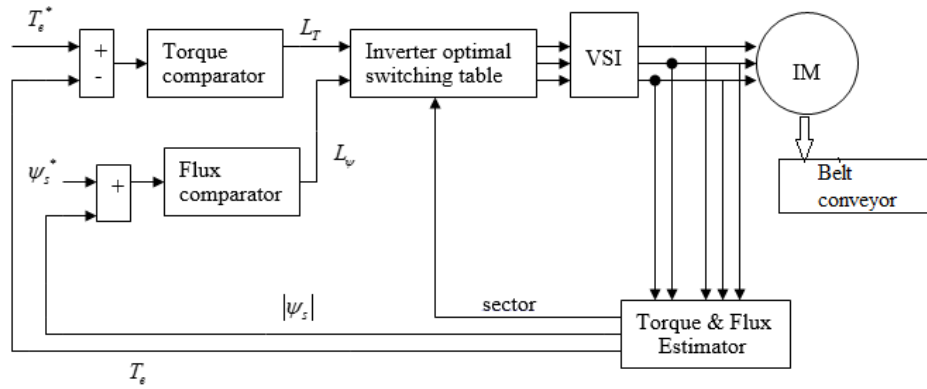


Figure 7.1 Block diagram representation of belt conveyor drive system

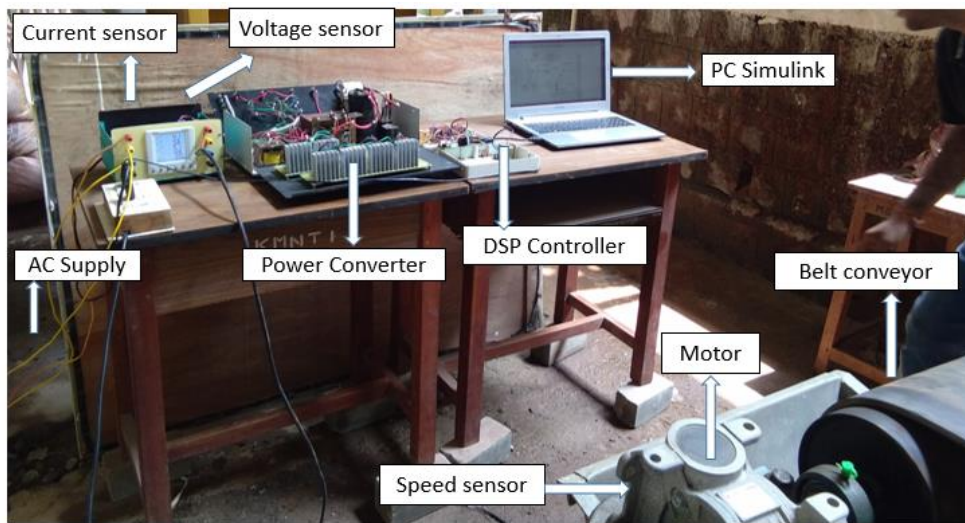
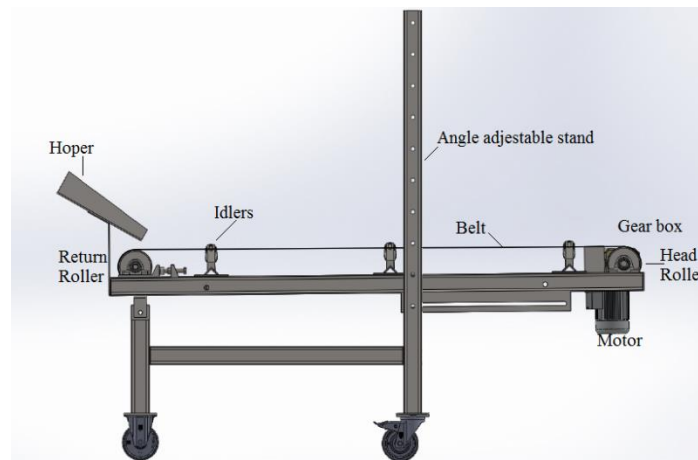


Figure 7.2 Pictorial view of belt conveyor drive system



7.3 Fabricated belt conveyor system

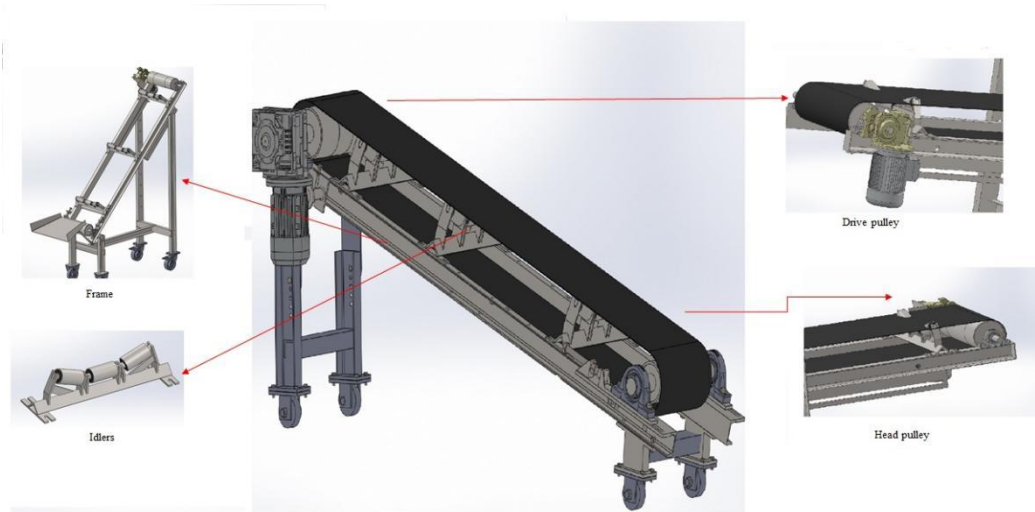


Figure 7.4 Description of laboratory belt conveyor system

The following methodology was adopted for conducting experiments on the belt conveyor drive system:

1. The belt conveyor was operated with two operational conditions i.e. on non-VFD and VFD configured LBC system.
2. In the first operational condition, a non-VFD configured LBC system was connected to the multifunctional meter, which is used to measure current, line voltage, active power, reactive power and apparent power during no-load and loading condition.
3. The material load was applied on the conveyor belt from feed hoper and the load was varied from 3 kg/ m to 15 kg/m in the steps of 3kg/m.
4. The conveyor belt system was operated at different inclination positions i.e. 10° , 15° and 20° to evaluate the belt conveyor performance w.r.t. the inclination of belt conveyor.
5. For each varied load and inclination, the speed of the conveyor system was measured using tachometer.
6. The performance parameters, such as current, line voltage, active power, reactive power and apparent power were measured using multifunctional meter, for varied load on the conveyor.

7. Similarly, the above procedure (i.e. step 2 to step 6) was repeated for VFD configuration system.

7.2 Specifications and Fabrication Details of LBCs

The specifications of the LBCs are given in Table 7.2 and Table 7.3.

Table 7.2 Specifications of belt and rollers of LBCs

Nominal parameters	Symbol	Value	Unit
Maximum conveying capacity	Q_m	10	t / h
Belt speed	v	0.18	m / s
Belt width	B	300	mm
Loaded material weight	M_l	15	kg / m
Conveying length	L	2	m
Conveying height	H	0.35/ 0.53/ 0.72	m
Inclination angle	β	10/ 15/ 20	$^\circ$
Belt length	L_b	4.2	m
Belt thickness	T_b	12	mm
Belt weight	M_b	3	kg / m
idler weight	M_r	12	kg / m
Radius of drive pulley	R_d	7	cm
Friction coefficient	C_f	0.1	-
Made	PVC	Type2	-

Table 7.3 Specifications of drive of LBCs

Nominal parameters	Symbol	Value	Unit
Power	P	0.5/ 0.375	hp / kW
Line Voltage	V	415	$Volt$
Frequency	f	50	Hz
Stator resistance	R_s	25.5	Ω
Stator inductance	L_s	0.168	H
Rotor resistance	R_r	18.54	Ω
Rotor inductance	L_r	0.168	H
Mutual inductance	L_m	2.02	H
Moment of inertia of the rotor	J	0.018	$kg - m^2$
Friction factor	...	0	---
Pole pairs	p	2	---
Current	I	1.1	Amp
Power factor	$\cos \phi$	0.74	-

Efficiency	η	65	%
Torque at full load	T_{fl}	3.856	$N-m$
breakdown torque	T_b	2.6×3.856	$N-m$
Approximate motor weight	M_m	17.5	kg
Rated motor speed	N	1385	rpm
Gear reduction ratio	K	1:60	-
Reduction gear speed	N_{gr}	23	rpm
Slip	s	6	%
Rotor frequency	f_r	3	Hz
Rotational losses	w_1	72	W
Stay load losses	w_2	9	W
Stator copper loss	w_3	36	W
Rotor copper losses	w_4	18	W
Constant losses	$w_1 + w_2$	81	W
Variable losses	$w_3 + w_4$	45	W
Total power losses at Full load	w_t	126	W

7.3 Results and Discussions

Laboratory studies were conducted on LBC systems, considering non-VFD and VFD systems, and the results of the study are presented in Table 7.4 and Table 7.5. The performance parameters, such as belt speed was measured and the annual energy consumption, efficiency, specific energy and motion resistance were estimated for each of the LBC system. A graph of each parameter against mass of the material was plotted.

Table 7.4 Laboratory results of a non-VFD configured LBC system

LBC	M_i	F	v	V	I	$\cos\phi$	P_i	P_o	η	E_m	E_y	W_s
LBC1	3	129	0.178	386	0.72	0.21	101	23	22.75	20.22	242.61	2.53
	6	455	0.178	385	0.73	0.33	161	81	50.42	32.13	385.54	2.01
	9	750	0.176	385	0.74	0.43	212	132	62.21	42.44	509.25	1.77
	12	955	0.176	384	0.75	0.52	259	168	64.77	51.88	622.54	1.62
	15	1029	0.175	385	0.77	0.54	277	180	64.92	55.45	665.45	1.39
LBC2	3	152.5	0.177	386	0.73	0.24	117	27	23.05	23.43	281.12	2.93
	6	576.3	0.177	389	0.73	0.37	182	102	56.05	36.40	436.76	2.27
	9	817.1	0.175	387	0.74	0.45	223	143	64.06	44.64	535.71	1.86
	12	1023	0.175	387	0.76	0.54	275	179	65.07	55.02	660.22	1.72
	15	1138	0.174	386	0.78	0.58	302	198	65.46	60.49	725.91	1.51
LBC3	3	274.3	0.175	387	0.74	0.26	129	48	37.22	25.79	309.52	3.22
	6	651.4	0.175	388	0.74	0.39	194	114	58.78	38.79	465.48	2.42
	9	885.1	0.174	389	0.76	0.48	246	154	62.65	49.16	589.90	2.05
	12	1069	0.174	385	0.76	0.56	284	186	65.54	56.76	681.14	1.77

	15	1207	0.174	387	0.79	0.6	318	210	66.1	63.54	762.54	1.59
Note: M_1 = Mass of material (in kg/m), F = Total driving force (in N m), v = Belt speed (m/s), V = Voltage (in V), I = Current (in A), $\cos\phi$ = Power factor, P_i = Input/ electrical power (in W), P_o = Output/ mechanical power (in W), η = Efficiency (in %), E_m = Energy consumption/month (in kWh), E_y = Energy consumption/year (in kWh) and W_s = Specific energy (in kWh).												

Table 7.5 Laboratory results of a VFD configured LBC system

LBC	M_1	F	v	V	I	$\cos\phi$	P_i	P_o	η	E_m	E_y	W_s
LBC1	3	129	0.14	392	0.5	0.24	81	30	36.82	16.30	196	2.037
	6	455	0.15	391	0.55	0.35	130	68	52.16	26.07	313	1.630
	9	750	0.16	391	0.6	0.45	183	118	64.53	36.57	439	1.524
	12	955	0.17	390	0.62	0.58	243	160	65.87	48.58	583	1.518
	15	1029	0.18	389	0.65	0.6	263	174	66.22	52.55	631	1.314
LBC2	3	152	0.13	390	0.52	0.28	98	27	27.45	19.67	236	2.459
	6	576	0.14	389	0.58	0.4	156	95	60.78	31.26	375	1.954
	9	817	0.15	389	0.62	0.47	196	138	70.29	39.27	471	1.636
	12	1023	0.16	388	0.68	0.569	260	178	68.46	52.00	624	1.625
	15	1138	0.17	388	0.69	0.621	288	197	68.41	57.59	691	1.440
LBC3	3	274	0.12	388	0.54	0.3	109	40	36.74	21.77	261	2.722
	6	651	0.13	388	0.6	0.43	173	108	62.29	34.68	416	2.167
	9	885	0.14	389	0.64	0.52	224	146	65.11	44.85	538	1.869
	12	1069	0.15	387	0.7	0.58	272	180	66.14	54.43	653	1.701
	15	1207	0.16	387	0.72	0.63	304	201	66.11	60.81	730	1.520
Note: M_1 = Mass of material (in kg/m), F = Total driving force (in N m), v = Belt speed (m/s), V = Voltage (in V), I = Current (in A), $\cos\phi$ = Power factor, P_i = Input/ electrical power (in W), P_o = Output/ mechanical power (in W), η = Efficiency (in %), E_m = Energy consumption/month (in kWh), E_y = Energy consumption/year (in kWh) and W_s = Specific energy (in kWh).												

7.3.1 Influence of mass of the material on belt speed for non-VFD and VFD LBC systems

Figure 7.5, Figure 7.6 and Figure 7.7 depict the influence of mass of material on conveyor's speed for a non-VFD and VFD configured LBC1, LBC2 and LBC3 systems, respectively. As shown in Figure 7.5, Figure 7.6 and Figure 7.7, the speed of the LBC with implementation of VFD can optimize the power losses at initial stage. The variations in speed, for maximum and minimum load, was found to be 2.21% to 31.2%.

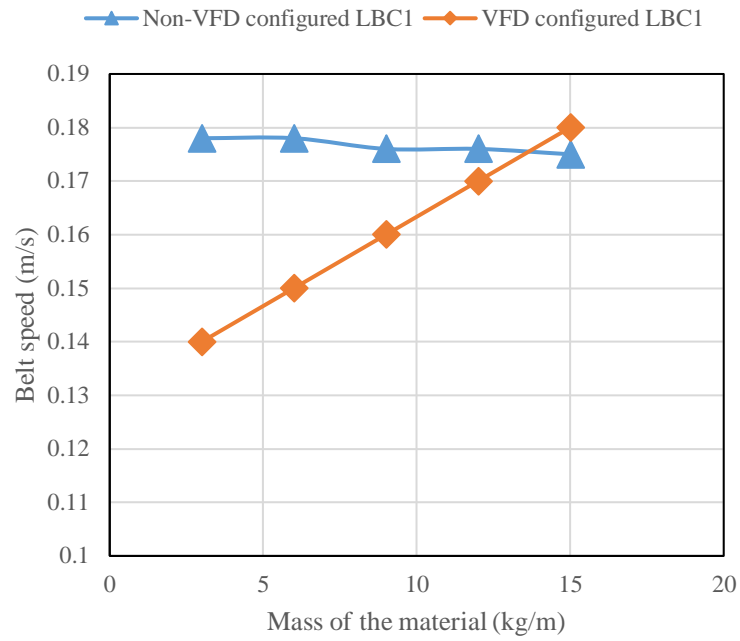


Figure 7.5 Influence of mass of the material on belt speed for LBC1 system

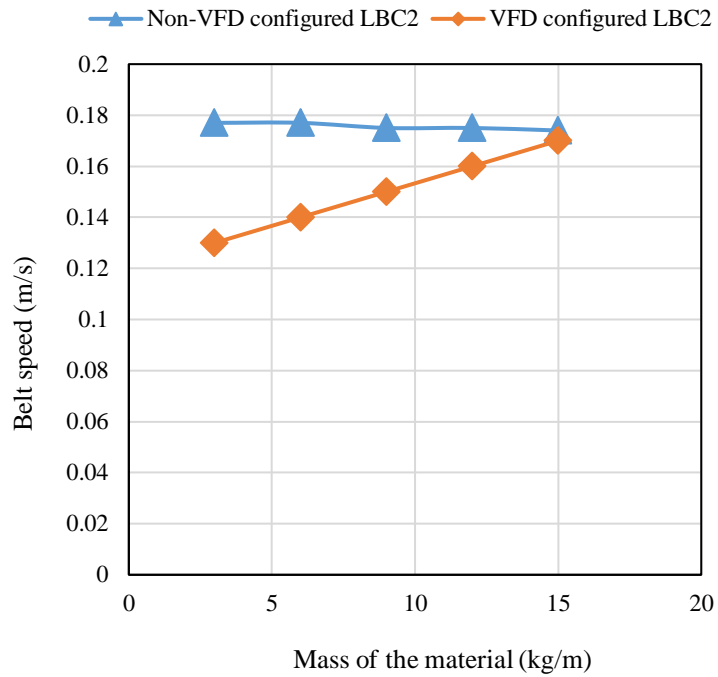


Figure 7.6 Influence of mass of the material on belt speed for LBC2 system

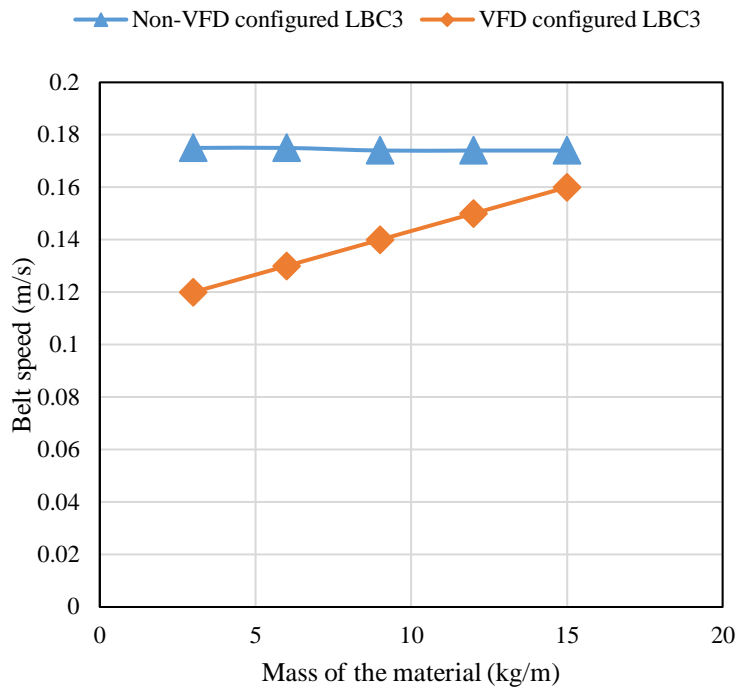


Figure 7.7 Influence of mass of the material on belt speed for LBC3 system

7.3.2 Influence of mass of the material on annual energy consumption of non-VFD and VFD LBC systems

Figures 7.8, Figure 7.9 and Figure 7.10 depicts influence of mass of material on annual energy consumption for a non-VFD and VFD configured LBC1, LBC2 and LBC3 systems, respectively. From Figures 7.8, Figure 7.9 and Figure 7.10 it is observed that the minimization in annual energy consumption is achieved on interfacing VFD to belt conveyor system, which is 19.26%, 15.02% and 14.42%, with respect to LBC1, LBC2 and LBC3, as shown in Figure 7.11.

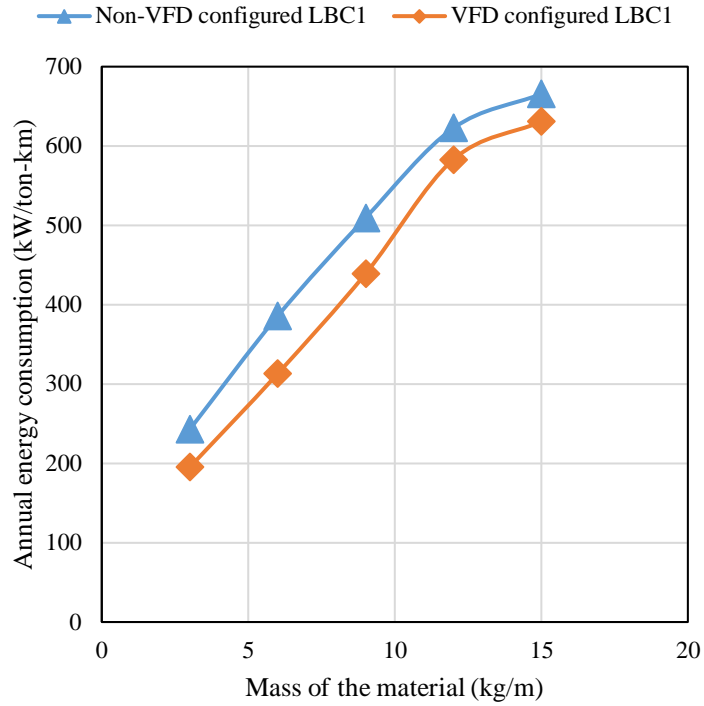


Figure 7.8 Influence of mass of the material on annual energy consumption for LBC1 system

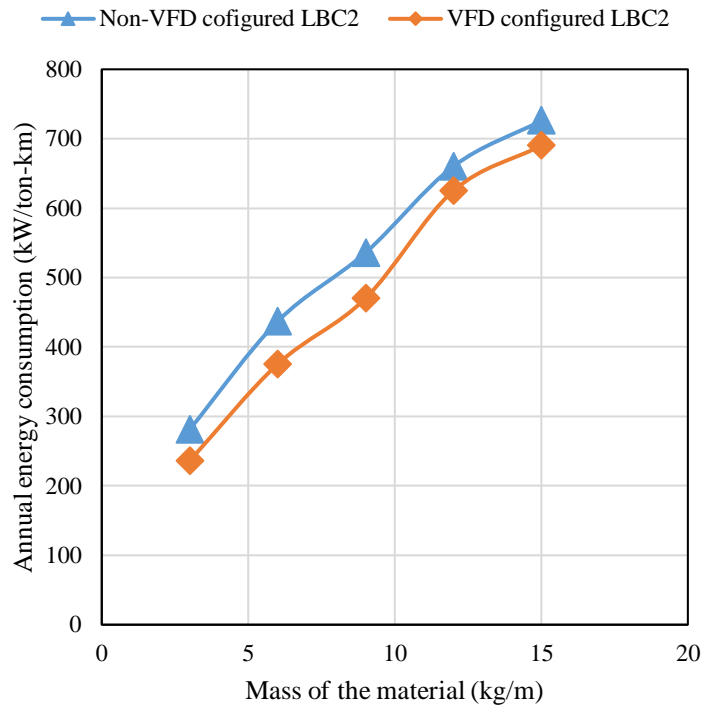


Figure 7.9 Influence of mass of the material on annual energy cons. for LBC2 system

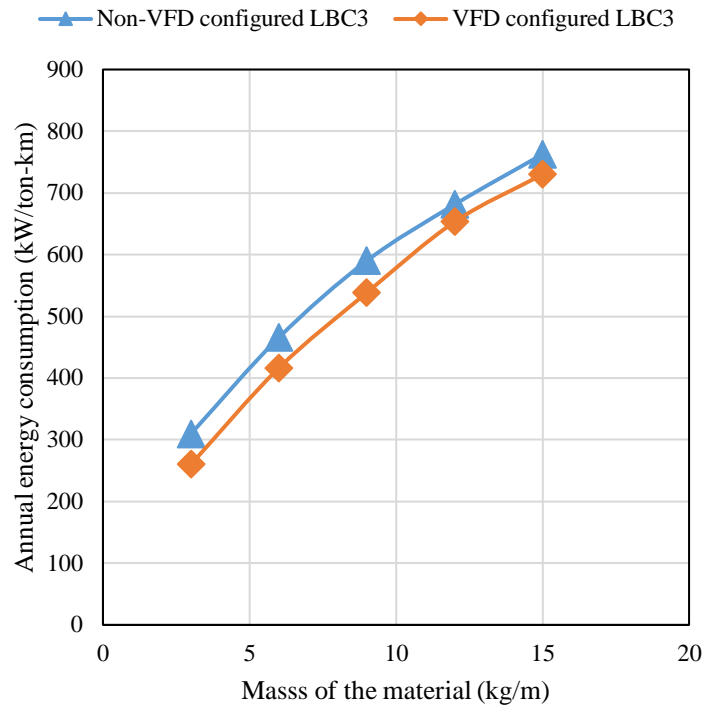


Figure 7.10 Influence of mass of the material on annual energy consumption for LBC3 system

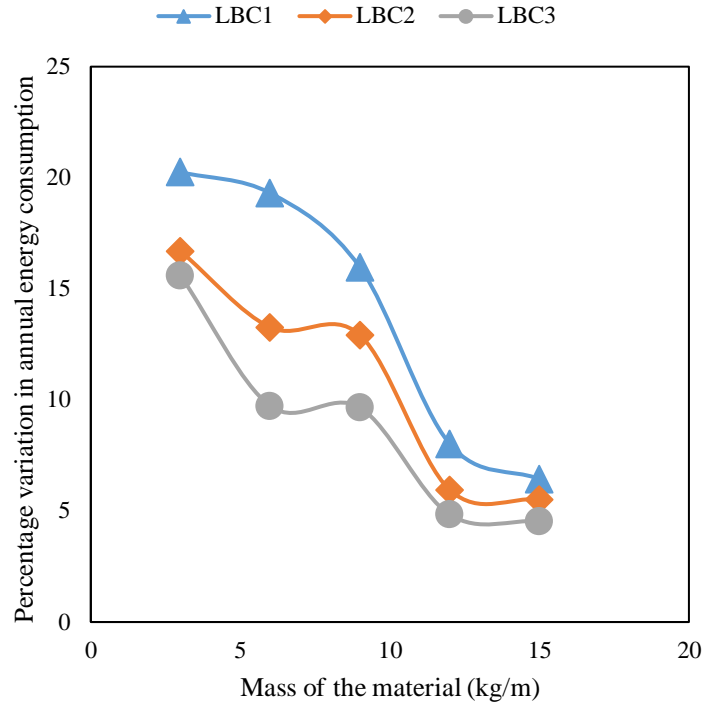


Figure 7.11 Influence of feed rate on percentage variation in annual energy consumption between non-VFD and VFD configured LB1, LBC2 and LBC3

7.3.3 Influence of mass of the material on efficiency for non-VFD and VFD configured LBC systems

Figure 7.12 shows the influence of mass of material on efficiency of LBC1, LBC2, and LBC3 systems. From Figure 7.12, it is observed that the efficiency of conveyor system increases with the increase in load.

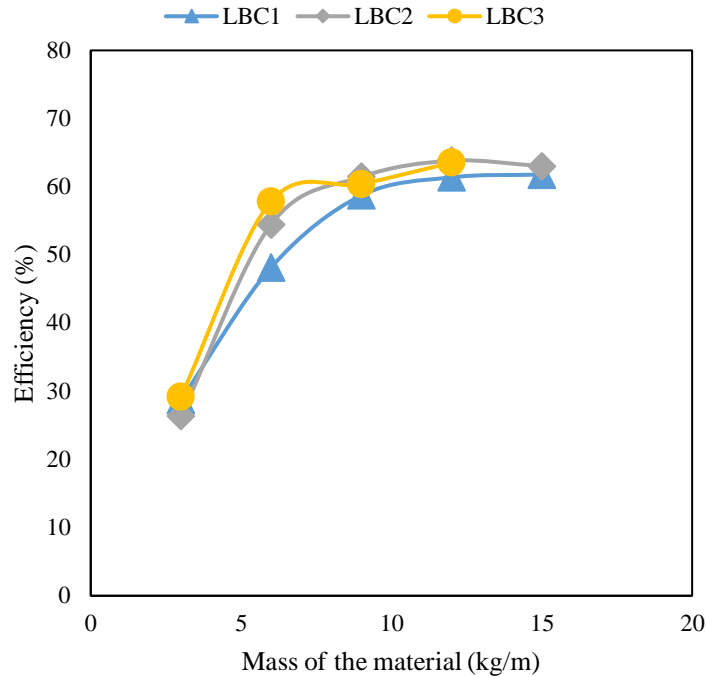


Figure 7.12 Efficiency of LBC system with respect to material mass

The efficiency of the LBC1 is less than the efficiency of the LBC2 and LBC3, which is due to the low inclination of LBC1 compared to that of LBC2 and LBC3. The maximum efficiency of all the three conveyors (i.e. LBC1, LBC2 and LBC3) is 66% at 70-80% of the rated load condition; thereafter, the efficiency of the conveyors is decreased slightly, i.e., from 66% to 65%. From Figure 7.12 it is also observed that the efficiency of the motor highly depends on the load when compared to inclination of the conveyor. Under lightly loaded condition, the power factor of the motor is very less; therefore, the efficiency is poor at light loads. The subjective assessment of efficiency of the motor is given by the IEEE Standard 112. According to Figure 7.12, the efficiency of the motor is poor for loads in between 2 kg/m to 5 kg/m (i.e., 20% to 40% only). Between 5 kg/m to 6 kg/m, the efficiency is very low, and between 6 kg/m to 12 kg/m, the efficiency is normal. At 12kg/m load, the efficiency of the motor is maximum and thereafter, the efficiency of the motor decreases slightly due to high copper losses. The variation of efficiency of LBC system is given in Table 7.6.

Table 7.6 Load versus Efficiency of LBC (IEEE Standard 112)

LBC	Load (in kg/m)	Efficiency
<i>LBC1</i>	2-5	Poor
<i>LBC2 & LBC3</i>	2-5	Very Low
<i>LBC1, LBC2 & LBC3</i>	5-9	Normal
<i>LBC1, LBC2 & LBC3</i>	9-15	Good

Figure 7.13, Figure 7.14 and Figure 7.15 Figure depicts influence of mass of material on efficiency for a non-VFD and VFD configured LBC1, LBC2 and LBC3 systems respectively. From Figure 7.13, Figure 7.14 and Figure 7.15 it is observed that the efficiency of a LBC system can be improved by incorporating a VFD. The highest improvement in efficiency was found during the initial stage of material loading, which is 27%, 16% and 12.5% for LBC1, LBC2 and LBC3, respectively as shown in Figure 7.16.

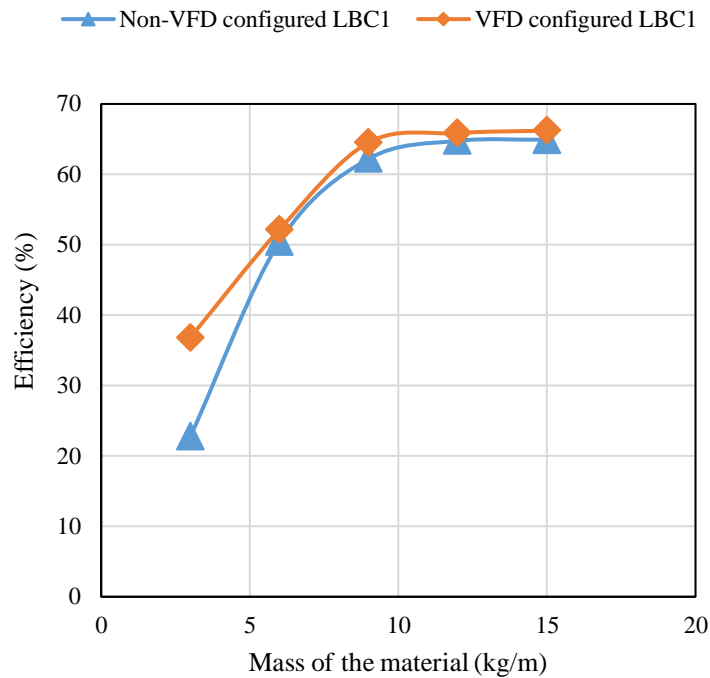


Figure 7.13 Influence of mass of the material on efficiency for LBC1 system

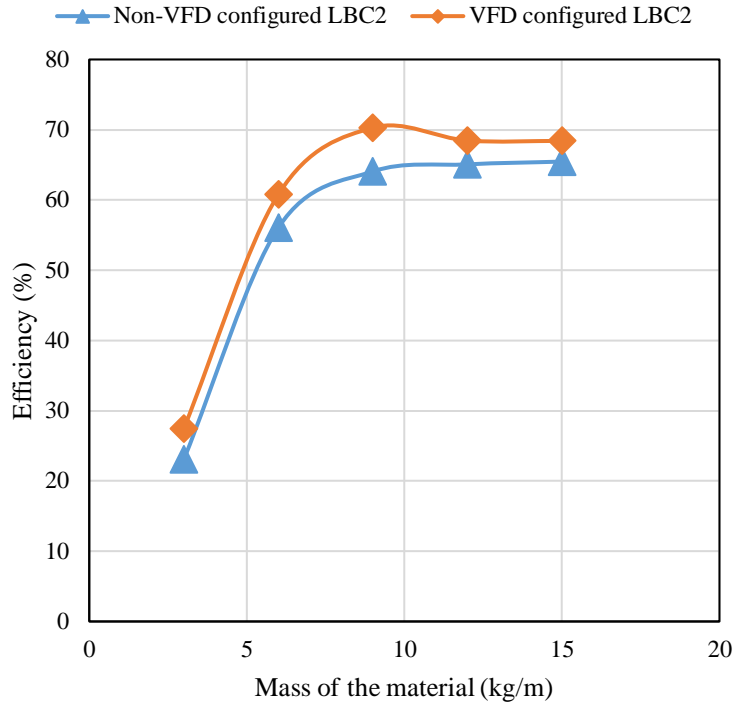


Figure 7.14 Influence of mass of the material on efficiency for LBC2 system

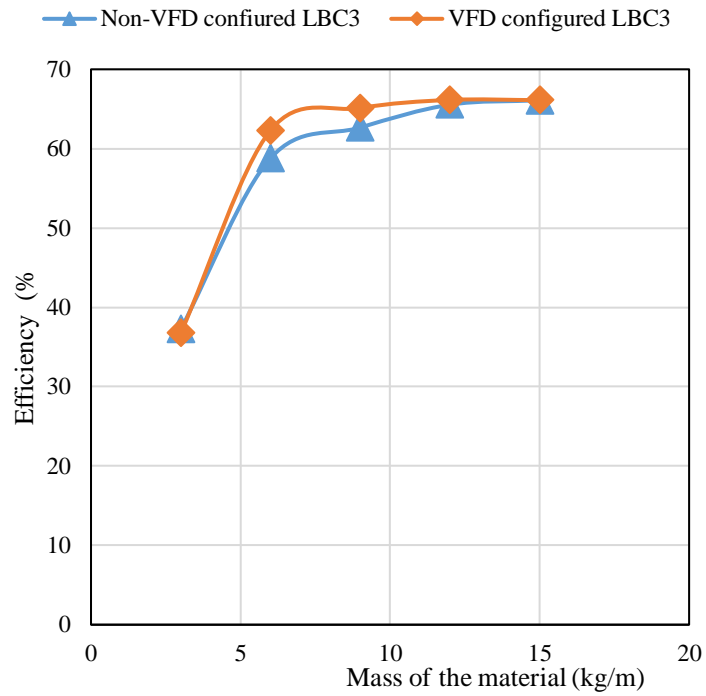


Figure 7.15 Influence of mass of the material on efficiency for LBC3 system

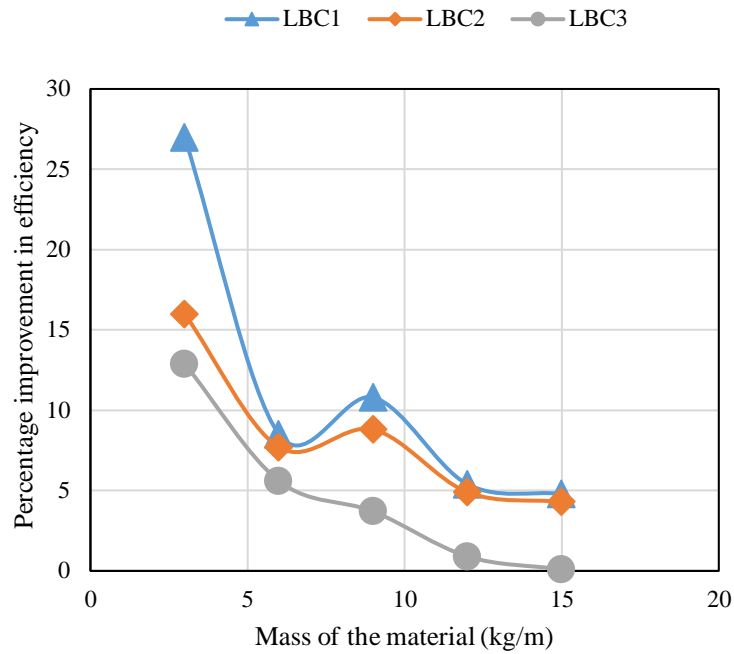


Figure 7.16 Influence of feed rate on percentage improvement in efficiency between Non-VFD and VFD configured LB1, LBC2 and LBC3

7.3.4 Influence of mass of the material on specific energy of non-VFD and VFD based models

Figure 7.17, Figure 7.18 and Figure 7.19 depicts the influence of mass of material on specific energy for a non-VFD and VFD configured LBC1, LBC2 and LBC3 systems, respectively. From the Figure 7.17, Figure 7.18 and Figure 7.19, it is observed that the specific energy is indirectly proportional to material loading and specific energy can be reduced with implementation of VFD. The amount of reduction in specific energy is found to be the highest at the initial stage of material loading, which is 19.5%, 15.5% and 15% for LBC1, LBC2 and LBC3, respectively as shown in Figure 7.20. As shown in Figure 7.20, the specific energy is reducing with the increase in angle of inclination of conveyor. However, this study is confined with a maximum angle of 20°.

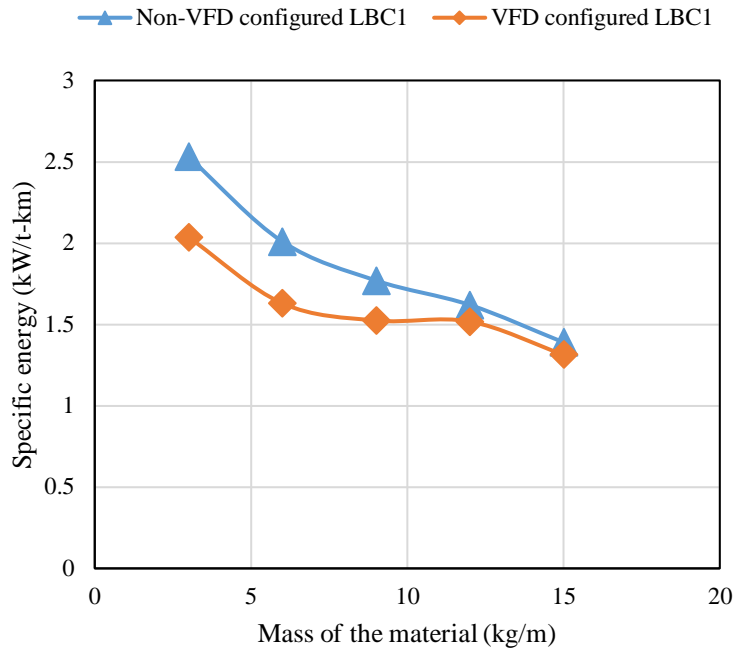


Figure 7.17 Influence of mass of the material on specific energy for LBC1 system

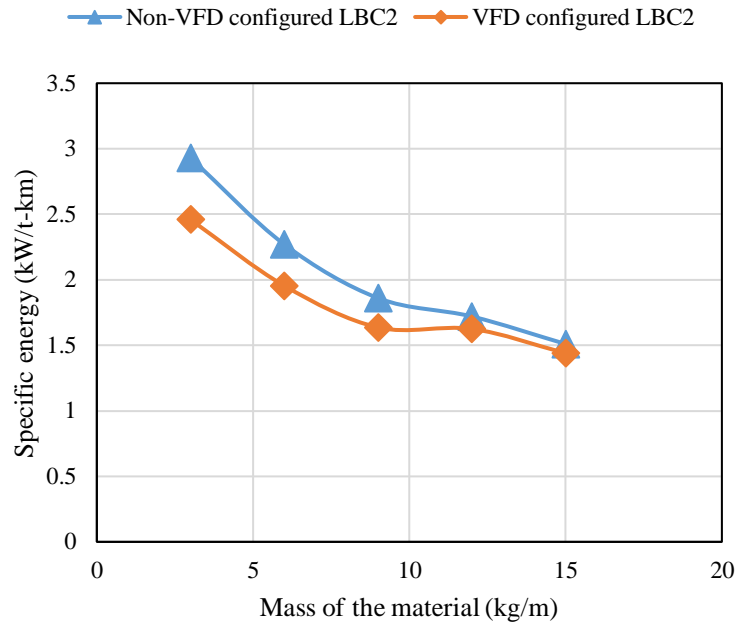


Figure 7.18 Influence of mass of the material on specific energy for LBC2 system

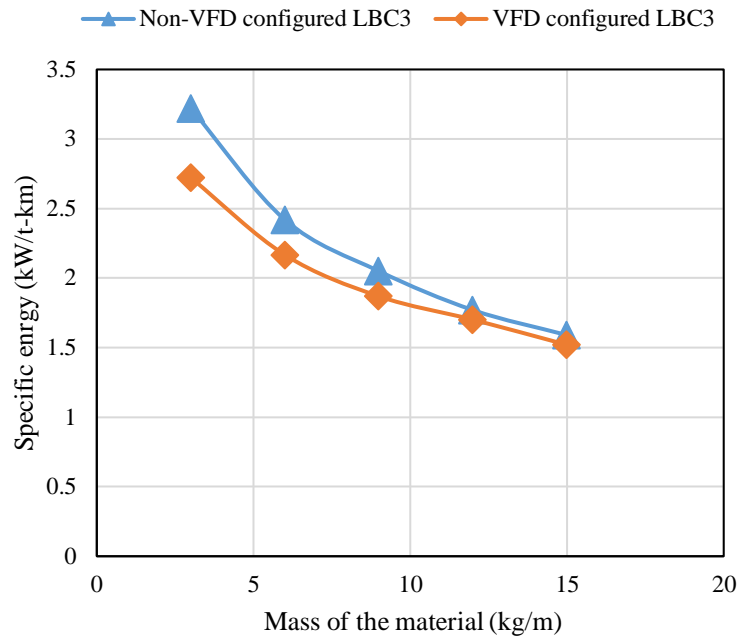


Figure 7.19 Influence of mass of the material on specific energy for LBC3 system

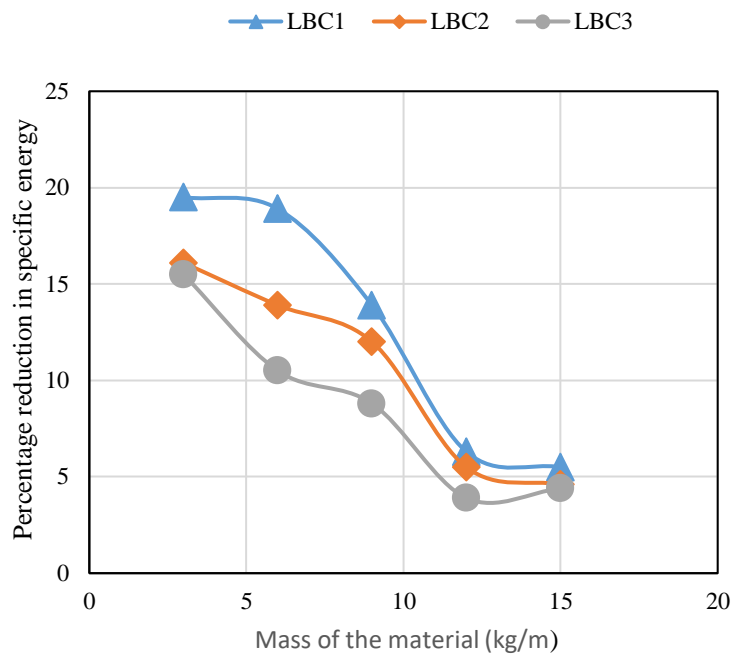


Figure 7.20 Influence of feed rate on percentage reduction in specific energy between

Non-VFD and VFD configured LB1, LBC2 and LBC3

7.3.5 Influence of mass of material on total resistive force

Figure 7.21 shows the influence of mass of material on total resistive force acting on the conveyor for all three conveyors, i.e. LBC1, LBC2, and LBC3. As given by equation (2.1), the conveyor's motion resistance (known as total resistive force) is depends on various mass elements, like drums, idlers, belt, the material on the belt etc. Figure 7.21 illustrates that the total resistive force starts at a non-zero value of around 200 N, even at zero loading condition (i.e., unit mass of the material is zero), due to the other inertias present in the system. This is the force required to run the empty conveyor. As the material load increases on the belt from 3 kg/m to 15 kg/m, the conveyor's total resistive force was changed from 200 N to around 1200 N for all three conveyors.

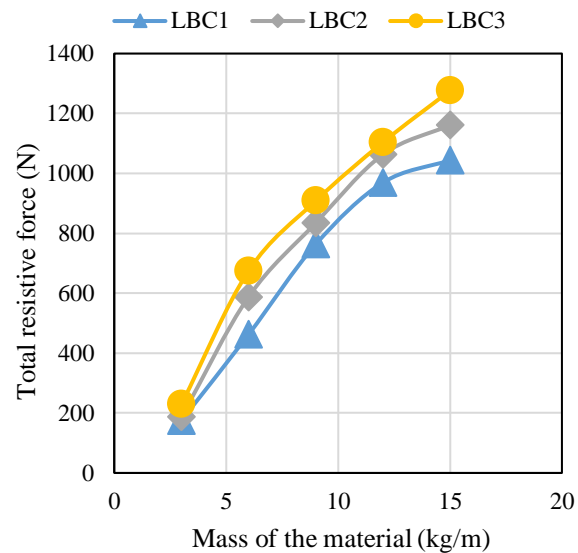


Figure 7.21 Total resistive force with respect to material mass

7.4 Comparison of results - Field, laboratory and simulation

The results obtained from the field investigation, simulation studies and laboratory studies were discussed and presented in Chapters 5, Chapters 6 and Chapters 7. To know the accuracy of the results obtained from the field and laboratory studies, they are compared with the simulation results. The comparative study results are tabulated and presented in Annexure - A. The comparative study reveals that the field and laboratory results are well validated with the simulation results with an accuracy of 95%.

7.5 Summarized Findings

To validate the simulation study an experimental investigation was carried out for a laboratory conveyor (LBCs). In order to arrive at the categories of models simulation, three different inclinations were chosen. Parameters of LBCs namely, belt speed, energy consumption, efficiency and specific energy were studied. Observations reveal that;

- The belt speed of the LBC with implementation of VFD can optimize at the power losses at initial stage. The variations in speed is found to be 2.21% to 31.2%.
- Minimization in annual energy consumption was achieved on interfacing VFD to belt conveyor systems; which was found to be 20.24%, 16.69% and 15.52% with respect to LBC1, LBC2 and LBC3.
- The efficiency of a LBC system can be improved by incorporating a VFD. The highest improvement in efficiency achieved was found during the initial stage of material loading which was found to be 20%, 16% and 14.5% for LBC1, LBC2, and LBC3, respectively.
- Specific energy can be reduced with implementation of VFD. The amount of reduction in specific energy is found to highest at the initial stage of material loading which is 19.5%, 15.5% and 15% for LBC1, LBC2 and LBC3, respectively.

CHAPTER 8

STATISTICAL ANALYSIS

Statistical analysis, namely ANOVA (Analysis of variance) analysis and multiple linear regression modelling was carried out using Minitab V17. This was done for both non-VFD and VFD configured LBC systems. The models were developed to predict the specific energy of the belt conveyor systems. The significance of input parameters are tested using ANOVA.

8.1 Non-VFD Configured LBC System

8.1.1 ANOVA analysis for non-VFD configured LBC system

The results of ANOVA analysis for specific energy of a non-VFD configured LBC system were presented in Table 8.1. According to Table 8.1, inclination, applied force, belt speed, power factor and power output were found statistically significant on specific energy as their P-values are less than 0.05. Table 8.1 and Figure 8.1 shows that the most influencing parameters on specific energy of a non-VFD configured LBC system is the applied force with contribution of 89% followed by inclination, power output, belt speed and power factor with 7.65%, 1.44%, 0.85% and 0.34%, respectively.

Table 8.1 Results of ANOVA for non-VFD configured LBC system

Source	DF	Seq. SS	Adj. MS	F-Value	P-Value	Contribution
Regression	5	3.94903	0.789805	147.56	0.000	98.79%
Inclination ($^{\circ}$)	1	0.30561	0.167947	31.38	0.000	7.65%
Applied force (N)	1	3.53830	0.069510	12.99	0.006	88.52%
Belt speed (m/s)	1	0.03399	0.086741	16.21	0.003	0.85%
Power factor	1	0.01369	0.034115	6.37	0.033	0.34%
Power output (kW)	1	0.05743	0.057435	10.73	0.010	1.44%
Error	9	0.04817	0.005352			1.21%
Total	14	3.99720				100.00%

Note: DF=Degree of freedom; Seq SS=Sequential sum of squares; Adj MS=Adjusted mean square; F-value=Fisher value (Variance ratio); P-value=Probability value

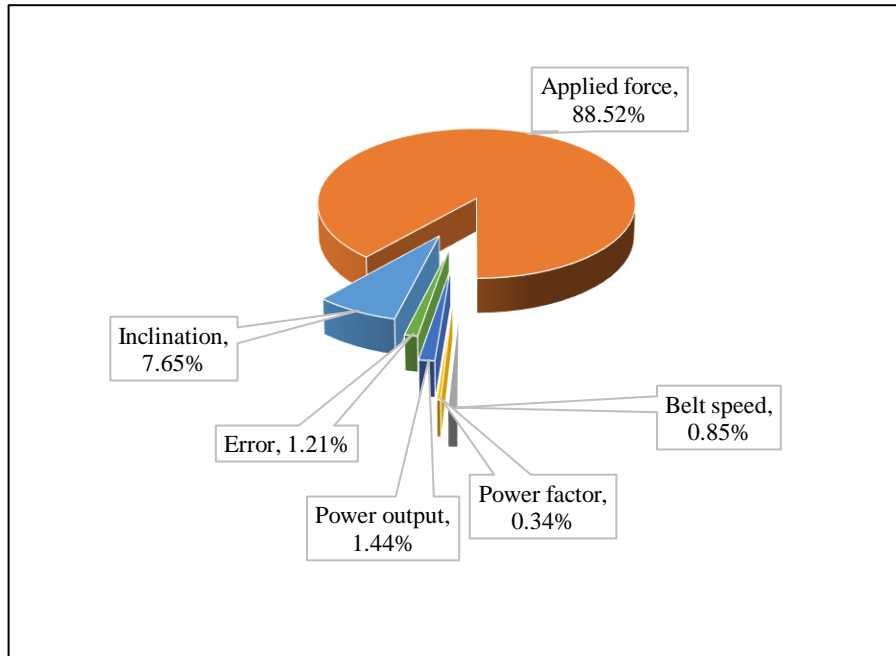


Figure 8.1 Percentage contribution of input parameters on specific energy of non-VFD configured LBC system

8.1.2 Development of regression model for prediction of the specific energy of a non-VFD configured LBC system

The regression model was developed for prediction of specific energy of a non-VFD based LBC system and is given by equation (8.1).

$$W_s = 33.00 + 0.004619 \beta - 0.03255 F - 179.1 v + 6.51 \cos \phi + 0.1626 P_o \quad (8.1)$$

where, W_s is the specific energy (in kWh/ t-km), β is the inclination (in degrees), F is the total applied force (in N), v is the speed of the belt (in m/s), $\cos \phi$ is the power factor and P_o is the power output (in kW) The obtained equation (8.1) represents the specific energy of a non-VFD configured LBC system in terms of conveyor inclination, total applied force, belt speed, power factor and power output. Figure 8.2 show that the predicted and experimental specific energy with the variance of 98.79% can be explained by the variables, such as inclination, total applied force, belt speed, power factor and power output. The coefficient of

determination (R^2) of the model was found 0.9879 and it is shown in Table 8.2. Table 8.3 show that the P-value of the input variables is less than 0.05, which means that the derived model is statistically significant. Figure 8.3 display the error between the predicted and experimental specific energy and the error was found to be 1.21%, which is within the permissible limit.

Table 8.2 Model summary of non-VFD configured LBC system

R^2	Predicted R^2	Adjusted R^2	Standard error
98.79%	95.24%	98.13%	0.073

Table 8.3 Regression analysis results of a non-VFD based LBC system

Model	Variable	Coefficient	T-value	P-value
Equation 8.1	Constant	33.00	4.20	0.002
	Inclination	0.04619	5.60	0.000
	Applied force	-0.03255	-3.60	0.006
	Belt speed	-179.1	-4.03	0.003
	Power factor	6.51	2.52	0.033
	Power output	0.1626	3.28	0.010

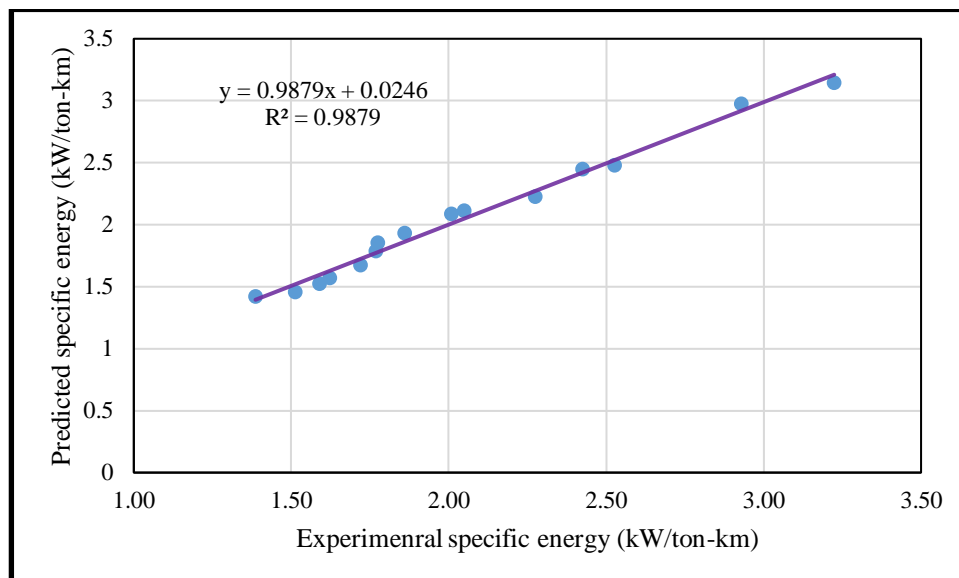


Figure 8.2 Relation between predicted and experimental values of specific energy of a non-VFD configured LBC system.

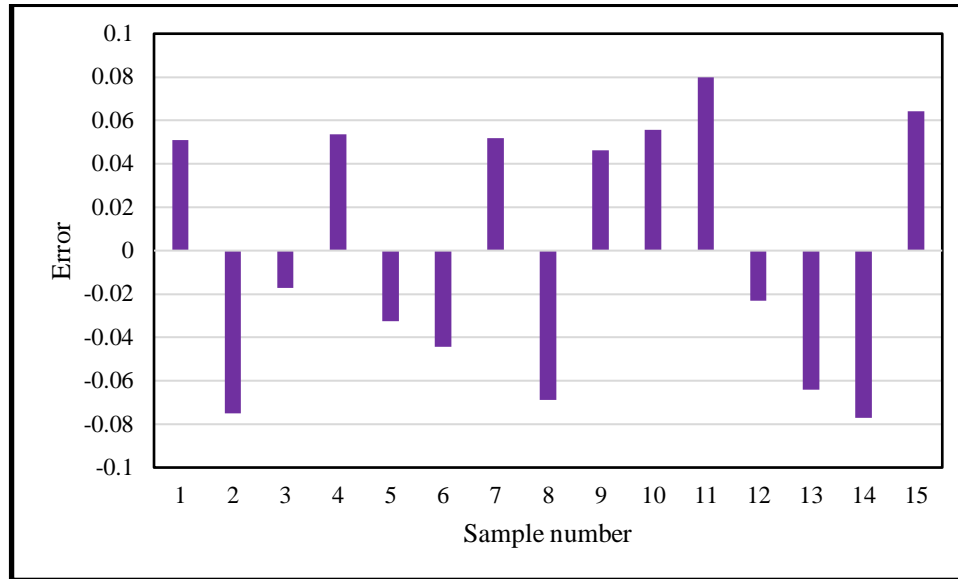


Figure 8.3 Error plot for specific energy for a non-VFD configured LBC system

8.2 VFD Configured LBC System

8.2.1 ANOVA analysis for VFD configured LBC system

The results of ANOVA analysis for specific energy of a VFD configured LBC system were presented in Table 8.4. According to Table 8.4, inclination, applied force, and power factor were found statistically significant on specific energy as their P-values are less than 0.05. Table 8.4 and Figure 8.4 shows the most influencing parameters on specific energy of a VFD configured LBC system, i.e. applied force with contribution of 75.21% followed by inclination and power factor with 17.41%, and 3.46%, respectively.

Table 8.4 Results of ANOVA for non-VFD configured LBC system

Source	DF	Seq. SS	Adj. MS	F-Value	P-Value	Contribution
Regression	3	2.11252	2.11252	90.02	0.000	96.09%
Inclination (\circ)	1	0.38279	0.77629	99.24	0.000	17.41%
Applied force (N)	1	1.65362	0.19538	24.98	0.000	75.21%
Power factor	1	0.07611	0.07611	9.73	0.001	3.46%
Error	11	0.08605	0.08605			3.91%
Total	14	2.19857				100.00%

Note: DF=Degree of freedom; Seq SS=Sequential sum of squares; Adj MS=Adjusted mean square; F-value=Fisher value (Variance ratio); P-value=Probability value

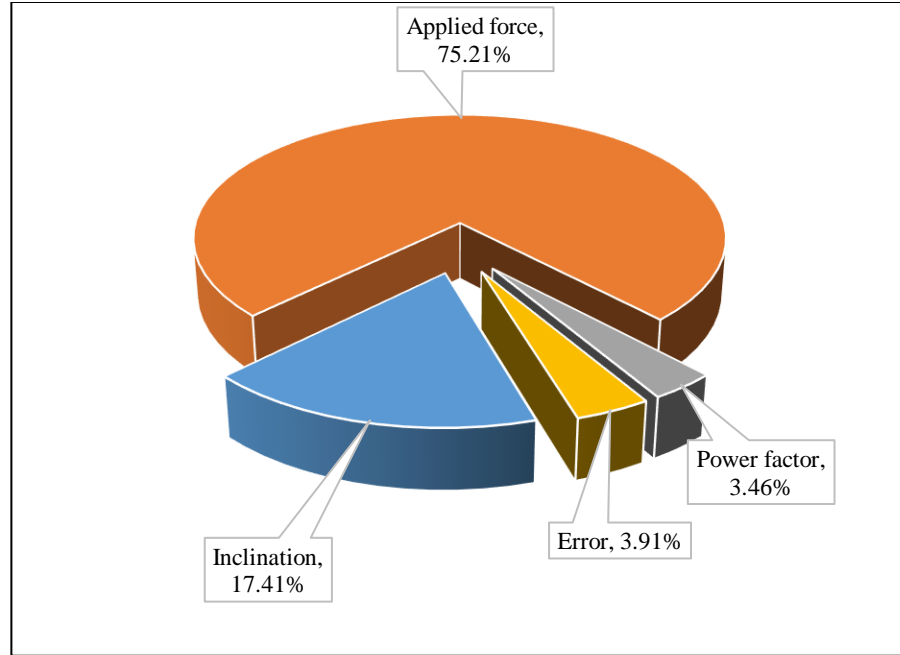


Figure 8.4 Percentage contribution of input parameters on specific energy of VFD configured LBC system

8.2.2 Development of regression model for prediction of the specific energy of a VFD configured LBC system

The regression model was developed for prediction of specific energy of a VFD based LBC system and is given by equation (8.2).

$$W_s = 0.816 + 0.05786 \beta - 0.002576 F + 4.34 \cos \phi \quad (8.2)$$

where, W_s is the specific energy ($kWh/t-km$), β is the inclination, F is the total applied force (N) and $\cos \phi$ is the power factor. The obtained equation (8.2) represents the specific energy of a VFD configured LBC system in terms of conveyor inclination, total applied force and power factor. Figure 8.5 show that the predicted and experimental specific energy with the variance of 96.09% can be explained by the variables inclination, total applied force, belt speed, power factor and power output, which means that the coefficient of determination (R^2) of the model was found 0.9609 and it is shown in Table 8.5. Table 8.6 show that, the P-value of the input variables is less than 0.05. This means that the derived model is statistically

significant. Figure 8.6 show the error between the predicted and experimental specific energy and the error was found to be 4 %, which is within the permissible range.

Table 8.5 Model summary of VFD configured LBC system

R²	Predicted R²	Adjusted R²	Standard error
96.09%	91.88%	95.02%	0.088

Table 8.6 Regression analysis results of a VFD based LBC system

Model	Variable	Coefficient	T-value	P-value
Equation 8.2	Constant	0.816	2.67	0.022
	Inclination	0.05786	9.96	0.000
	Applied force	-0.002576	-5.00	0.000
	Power factor	4.34	3.12	0.010

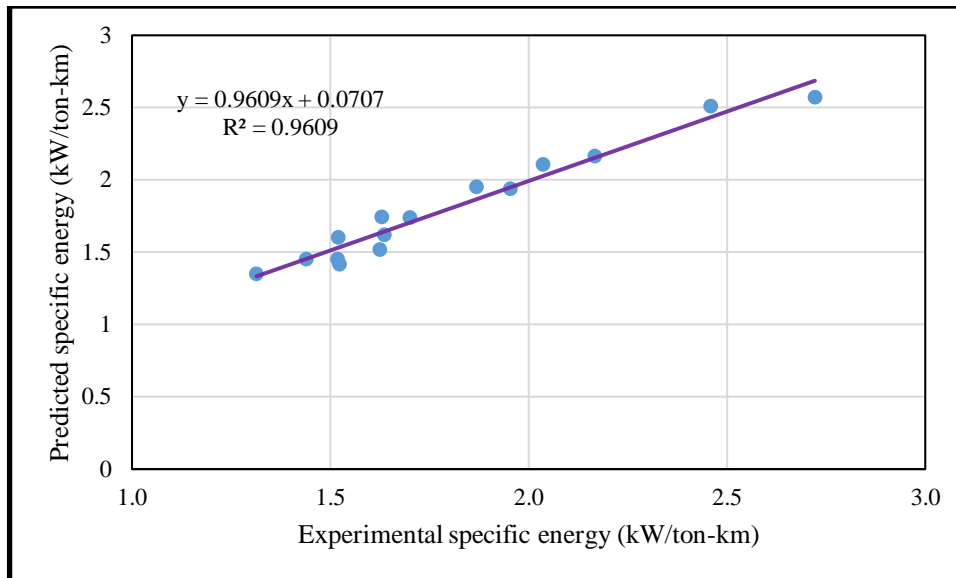


Figure 8.5 Relation between predicted and experimental values of specific energy of a VFD configured LBC system

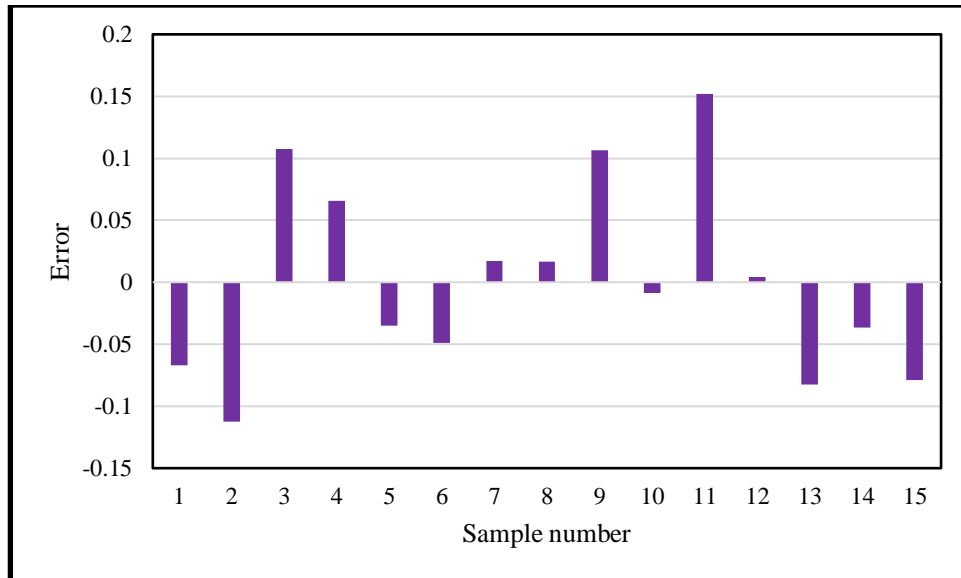


Figure 8.6 Error plot for specific energy for a VFD configured LBC system

8.3 Summarized Findings

A regression analysis was carried using Minitab V 18 to predict specific energy of laboratory belt conveyor system, considering experimental data. Models were developed individually for both VFD and non-VFD incorporations. The specific energy of the belt conveyor system depends on various factors; the speed of the belt, inclination, applied force, power factor and power output. However, its significance on the specific energy of the belt conveyor system has been varied for non-VFD and VFD configured LBC system. The most influencing parameters on specific energy of a non-VFD configured LBC system were the applied force with contribution of 89%, followed by inclination, power output, belt speed, and power factor which was 7.65%, 1.44%, 0.85% and 0.34%, respectively. The most influencing parameters on specific energy of a VFD configured LBC system were the applied force with contribution of 75.21% followed by inclination and power factor which was 17.41%, and 3.46%, respectively. And the error between the predicted and experimental specific energy was found to be 1.21% and 4% for non-VFD and VFD configured LBCs which were within the permissible limits.

CHAPTER 9

CONCLUSIONS AND SCOPE FOR FUTURE WORK

9.1 Conclusions

In this study, the field belt conveyor performance in terms of speed, energy consumption, efficiency and specific energy were analysed. The study concludes that with varying feed rate (40 t/h to 200 t/h) the speed remain mere closer irrespective of length and inclination of the conveyor. However, the energy consumption and efficiency were lower for FBC1 (Lower length belt conveyor). The specific energy consumption was higher for lower length belts. And it was observed that

- The amount of variation in speed w.r.t. feed rate were found to be 10%, 10% and 5.2% for FBC1, FBC2 and FBC3, respectively.
- The amount of variation of energy consumption w.r.t. feed rate were found to be 66.66%, 47.96% and 62.29% for FBC1, FBC3 and FBC3, respectively.
- The amount of variation of conveyor efficiency w.r.t. feed rate were found to be 23.92%, 3.14% and 18.75% for FBC1, FBC2 and FBC3, respectively.
- The amount of variation of specific energy w.r.t. feed rate was found that 41.69%, 59.4% and 46.44% for FBC1, FBC2 and FBC3, respectively.

Simulation model was developed for field belt conveyors using Simulink and the performance of simulated model was studied. The performance study was carried out by introducing a variable frequency drive. The study concluded that VFD drive are capable of optimising and improving the speed, energy consumption, efficiency and specific energy of the belt conveyor systems.

- Belt speed of a FBC system can be optimized by incorporating a VFD to a belt conveyor systems. The highest variation in speed achieved was found during the initial stage of material loading; which was found to be 50%, 47.36% and 50% for FBC1, FBC2 and FBC3, respectively.

- Minimization in annual energy consumption was achieved by interfacing VFD to belt conveyor systems; which was found to be 9.4%, 2.31% and 7.3% with respect to FBC1, FBC2 and FBC3.
- The highest improvement in efficiency achieved is found during the initial stage of material loading which was found to be 16.76%, 1.01% and 11.51% for FBC1, FBC2 and FBC3, respectively.
- The amount of reduction in specific energy was found highest at the initial stage of feed rate which was found to be 10.4%, 2.55% and 5.93% for FBC1, FBC2 and FBC3, respectively.

Simulation study considering both non-VFD and VFD for LBCs were developed to estimate belt speed, energy consumption, efficiency and specific energy. A comparison study in the form of scatter plot for both non-VFD and VFD based LBC models were drawn. Observations reveal that;

- The highest variation in speed achieved was found during the initial stage of material loading which was found to be 21.34%, 26.55% and 31.42% for LBC1, LBC2 and LBC3, respectively.
- Minimization in annual energy consumption was achieved on interfacing VFD to belt conveyor systems; which was found to be 20.24%, 16.69% and 15.52% with respect to LBC1, LBC2 and LBC3.
- The highest improvement in efficiency achieved during the initial stage of material loading which was found 22.24%, 17.58% and 15.59% for LBC1, LBC2, and LBC3, respectively.
- The amount of reduction in specific energy was found highest at the initial stage of material loading which was 20.24%, 16.69% and 15.52% for LBC1, LBC2 and LBC3, respectively.

A laboratory belt conveyor was simulated and a prototype of the same was developed to validate the performance of VFD incorporations to belt conveyors. The results of the laboratory study reveals that the incorporation of VFD optimized and improved the performance of belt conveyor compared to a non VFD belt conveyor.

- The belt speed of the LBC with implementation of VFD can optimize at the power losses at initial stage. The variations in speed is found to be 2.21% to 31.2%.
- Minimization in annual energy consumption was achieved on interfacing VFD to belt conveyor systems; which was found to be 20.24%, 16.69% and 15.52% with respect to LBC1, LBC2 and LBC3.
- The efficiency of a LBC system can be improved by incorporating a VFD. The highest improvement in efficiency achieved was found during the initial stage of material loading which was found to be 20%, 16% and 14.5% for LBC1, LBC2, and LBC3, respectively.
- Specific energy can be reduced with implementation of VFD. The amount of reduction in specific energy is found to highest at the initial stage of material loading which is 19.5%, 15.5% and 15% for LBC1, LBC2 and LBC3, respectively.

A regression model was also developed to predict the specific energy of non-VFD and VFD configured LBC systems. The models were found significant as per their R-square values. The most influencing parameters on specific energy of a non-VFD configured LBC system were the applied force with contribution of 89%, followed by inclination, power output, belt speed, and power factor which was 7.65%, 1.44%, 0.85% and 0.34%, respectively. The most influencing parameters on specific energy of a VFD configured LBC system were the applied force with contribution of 75.21% followed by inclination and power factor which was 17.41%, and 3.46%, respectively. And the error between the predicted and experimental specific energy was found to be 1.21% and 4% for non-VFD and VFD configured LBCs which were within the permissible limits.

9.2 Scope for Future Work

1. Optimization studies on specific energy for different varied length and height field belt conveyors.
2. Model-Prototype based simulation study for assessing specific energy of belt conveyor systems.

REFERENCES

- ABB. (2000). "Variable-speed drives for belt-conveyor systems A project report of the revamp of a lignite conveyor line." *ABB Process Industries - Open Pit Mining & Materials Handling, Cottbus/Germany*. www.abb.com/mining, 1–7.
- Akparibo, A. R., and Normanyo, E. (2020). "Application of resistance energy model to optimising electric power consumption of a belt conveyor system." *International Journal of Electrical and Computer Engineering*, 10(3), 2861–2873.
- Alsofyani, I. M., and Idris, N. R. N. (2013). "A review on sensorless techniques for sustainable reliability and efficient variable frequency drives of induction motors." *Renewable and Sustainable Energy Reviews*, 24, 111–121.
- Arias, A., Jayne, M. G., Witting, P. A., and Romeral, J. L. (2005). "New DTC control scheme for induction motors fed with a three-level inverter." *AUTOMATIKA*, 46(1), 73–81.
- Astrom, K. J., and Hugglund, T. (2001). "The future of PID control." *Control Engineering Practice*, 9(11), 1163–1175.
- Bansal, H. O., Sharma, R., and Shreeraman, P. R. (2012). "PID controller tuning techniques: a review." *Journal of Control Engineering and Technology*, 2(4), 168–176.
- Belhaouchet, N., Hamla, H., and Rahmani, L. (2018). "A modified direct torque control for induction motor drives." *Revue Roumaine des Sciences Techniques Serie Electrotechnique et Energetique*, 63(1), 38–45.
- Bose, B. K. (1987). "Modern power electronics and AC drives." *Prentice Hall*.
- Buja, G. S., and Kazmierkowski, M. P. (2004). "Direct torque control of PWM inverter-fed AC motors - A survey." *IEEE Transactions on Industrial Electronics*, 51(4), 744–757.
- Casadei, D., Serra, G., and Tani, A. (2001). "The use of matrix converters in direct torque control of induction machines." *IEEE Transactions on Industrial Electronics*, 48(6), 1057–1064.

Chan, Y., and Kantamaneni, R. (2015). “Study on energy efficiency and energy saving potential in industry and on possible policy mechanisms.” *ICF International*, 1(1), 2–6.

Deepa, M. (2015). “Design of VFD drive for a 3-phase induction motor.” *International Journal of Innovative Research in Science, Engineering and Technology*, 4(1), 18755–18762.

Depenbrock, M. (1988). “Direct self control (DSC) of inverter-fed induction machine.” *IEEE Power Electronics Specialists Conference*, 3(4), 420–429.

Dharmaprakash, R., and Henry, J. (2015). “Comparison of direct torque control of induction motor using two-level and three level inverter.” *Middle-East Journal of Scientific Research*, 23, 89–96.

DIN22101. (2011). *DIN22101- Continuous conveyors – Belt conveyors for loose bulk materials – Basis for calculation and dimensioning*.

DJL, M., and Calmeyer, J. . (2004). “An integrated conveyor model methodology.” *The Transactions of the SA Institute of Electrical Engineers*, 3, 256–264.

G, B., and R, R. (2004). “An optimized algorithm for torque oscillation reduction in DTC-induction motor drives using 3-level NPC inverter.” *IEEE International Symposium on Industrial Electronics. IEEE.*, 2, 1215–1220.

G, H. T., Francesco, P., Michele, P., and M, T. L. (1992). “Direct torque control of induction machines using space vector modulation.” *IEEE Transactions on Industry Applications*, 28(5), 1045–1053.

Geetha, R., T, T., Vedam, S., and Shimila, R. (2009). “Torque ripple minimization in double fed induction machine used in wind mills with artificial neural network.” *Journal of Theoretical and Applied Information Technology*, 7(1), 53–57.

Gierse, G. (1992). “Direct self control (DSC) of inverter-fed induction machine: A basis for speed control without speed measurement.” *IEEE Transactions on Industry Applications*, 28(3), 581–588.

Goriparti, N. V. S., Murthy, C. S. N., and Aruna, M. (2020). "Prediction of energy efficiency of main transportation system used in underground coal mines – A statistical approach." *A Statistical Approach. In International Conference on Emerging Trends in Engineering (ICETE), Springer, Cham., 2, 337-344* https://doi.org/10.1007/978-3-030-24314-2_.

Gupta, Y. B. S. S., and Rao, S. S. (2020). "A modified inverter topology for fault-tolerant direct torque control induction motor drive." *International Journal of Electronics*, 107(12), 1985–2005.

Hassankhan, E., Khaburi, D. A., and Scheme, A. C. D. T. C. (2008). "DTC-SVM scheme for induction motors fed with a three-level inverter." *Proceedings of World Academy of Science , Engineering and Technology*, 34, 168–172.

He, D., Pang, Y., and Lodewijks, G. (2016a). "Speed control of belt conveyors during transient operation." *Powder Technology*, 301, 622–631.

He, D., Pang, Y., and Lodewijks, G. (2016b). "Determination of acceleration for belt conveyor speed control in transient operation." *International Journal of Engineering and Technology*, 8(3), 206–211.

He, D., Pang, Y., and Lodewijks, G. (2017). "Green operations of belt conveyors by means of speed control." *Applied Energy*, 188, 330–341.

Hiltermann, J., Lodewijks, G., Schott, D. L., Rijsenbrij, J. C., Dekkers, J. A. J. M., and Pang, Y. (2011). "A methodology to predict power savings of troughed belt conveyors by speed control." *Particulate Science and Technology*, 29(1), 14–27.

Ioannides, M. G., Papazis, S. A., and Ioannidou, F. G. (2003). "Implementation of scalar control scheme for variable frequency induction motor actuator system." *Sensors and Actuators A: Physical*, 106((1-3)), 306–309.

ISO-5048. (1989). "Continuous mechanical handling equipment - belt conveyors with carrying idlers - calculation of operating power and tensile forces."

Jefteni, B., Risti, L., Bebi, M., and Štatki, S. (2009). “Controlled induction motor drives supplied by frequency converters on belt conveyors – modeling and commissioning.” *35th Annual Conference of IEEE Industrial Electronics*, 1063–1068.

Ji, J., Miao, C., and Li, X. (2020). “Research on the energy-saving control strategy of a belt conveyor with variable belt speed based on the material flow rate.” *PLoS ONE*, 15(1), 1–14.

Johannes, D., and Marx, L. (2005). “Energy audit methodology for belt conveyors.” *Doctorial Dissertation, University of Pretoria*.

Kawalec, W., Suchorab, N., Konieczna-Fuławka, M., and Król, R. (2020). “Specific energy consumption of a belt conveyor system in a continuous surface mine.” *Energies*, 13(19).

Khurram, A., Rehman, H., Mukhopadhyay, S., and Ali, D. (2018). “Comparative analysis of integer-order and fractional-order proportional integral speed controllers for induction motor drive systems.” *Journal of Power Electronics*, 18(3), 723–735.

Krishnan, R. (2001). “Electric motor drives: modeling, analysis and control.” *Prentice Hall*.

Krol, R., Kawalec, W., and Gladysiewicz, L. (2017). “An effective belt conveyor for underground ore transportation systems.” *IOP Conference Series: Earth and Environmental Science*, 95(4), 1–9.

Lascu, C., and Trzynadlowski, A. M. (2004). “Combining the principles of sliding mode, direct torque control, and space-vector modulation in a high-performance sensorless AC drive.” *IEEE Transactions on Industry Applications*, 40(1), 170–177.

Lauhoff, H. (2006). “Speed control on belt conveyors - Does it really save energy?” *Glueckauf*, 142, 10–18.

Lech, G., Witold, K., and Robert, K. (2016). “Selection of carry idlers spacing of belt conveyor taking into account random stream of transported bulk material.” *Eksploatacja i Niezawodność – Maintenance and Reliability*, 18(1), 32-37.
<http://dx.doi.org/10.17531/ein.2016.1.5>.

- Lin, B., Wu, Y., and Zhang, L. (2011). “Estimates of the potential for energy conservation in the Chinese steel industry.” *Energy Policy*, 39(6), 3680–3689.
- Luo, J., Huang, W., and Zhang, S. (2015). “Energy cost optimal operation of belt conveyors using model predictive control methodology.” *Journal of Cleaner Production*, 105, 196–205.
- Manuel, A., and Francis, J. (2013). “Simulation of direct torque controlled induction motor drive by using space vector pulse width modulation for torque ripple reduction.” *International Journal of Advanced Research in Electrical, Electronics and Instrumentation Engineering*, 2(9), 4471–4478.
- Marino, P., D’Incecco, M., and Visciano, N. (2001). “A comparison of direct torque control methodologies for induction motor.” *2001 IEEE Porto Power Tech Proceedings*, 2, 91–96.
- Mathaba, T., and Xia, X. (2017). “Optimal and energy efficient operation of conveyor belt systems with downhill conveyors.” *Energy Efficiency*, 10(2), 405–417.
- Motor, I. I., Drive, S., Zhang, Y., Zhu, J., Member, S., Zhao, Z., Member, S., Xu, W., Dorrell, D. G., Member, S., and Abstract, A. (2012). “An improved direct torque control for three-level inverter-fed induction motor sensorless drive.” *IEEE Transactions on Power Electronics*, 27(3), 1502–1513.
- Overlin, M. R., Member, S., Kirtley, J. L., and Fellow, L. (2019). “A geometric interpretation of reference frames and transformations: dq0, Clarke, and Park.” *IEEE Transactions on Energy Conversion*, 34(4), 2070–2083.
- Ozkop, E., and Okumus, H. I. (2008). “Direct torque control of induction motor using space vector modulation (SVM-DTC).” *2008 12th International Middle-East Power System Conference*, 368–372.
- Pang, Y., and Lodewijks, G. (2011). “Improving energy efficiency in material transport systems by fuzzy speed control.” *3rd IEEE International Symposium on Logistics and Industrial Informatics*, 159–164.

Pimkumwong, N., Onkrong, A., and Sapaklom, T. (2012). “Modeling and simulation of direct torque control induction motor drives via constant Volt/Hertz technique.” *Procedia Engineering*, 31, 1211–1216.

Popescu, N., Dinu, R. C., and Mircea, I. (2013). “Conveyor energy efficiency parameters determination using MATLAB – Simulink.” *Journal of Sustainable Energy*, 4(3), 4–7.

Rawlinson, R. (1978). “Underground transport in coal mines.” *Information Symposium*, 1(1), 9–12.

Reza, C. M. F. S., Islam, M. D., and Mekhilef, S. (2014). “A review of reliable and energy efficient direct torque controlled induction motor drives.” *Renewable and Sustainable Energy Reviews*, 37, 919–932.

Ristić, L. B., and Jeftenić, B. I. (2012). “Implementation of fuzzy control to improve energy efficiency of variable speed bulk material transportation.” *IEEE Transactions on Industrial Electronics*, 59(7), 2959–2969.

Sarathbabu Goriparti, N. V., Murthy, C. S. N., and Aruna, M. (2019). “Minimization of specific energy of a belt conveyor drive system using space vector modulated direct torque control.” *International Journal of Innovative Technology and Exploring Engineering*, 8(4), 505–511.

Suchorab, N. (2019). “Specific energy consumption - The comparison of belt conveyors.” *Mining Science*, 26, 263–274.

Swarupa, M. L., Das, G. T. R., and Gopal, P. V. R. (2009). “Simulation and analysis of SVPWM based 2-level and 3-level inverters for direct torque of induction motor.” *International Journal of Electronic Engineering Research*, 1(3), 169–184.

Takahashi, I., and Noguchi, T. (1986). “A new quick-response and high-efficiency control strategy of an induction motor.” *IEEE Transactions on Industry Applications*, 22(5), 820–827.

Tan, Z., Li, Y., and Li, M. (2001). “A direct torque control of induction motor based on three-

level NPC inverter.” *32nd Annual Power Electronics Specialists Conference , IEEE*, 3, 1435–1439.

Tazerart, F., Mokrani, Z., Rekioua, D., and Rekioua, T. (2015). “Direct torque control implementation with losses minimization of induction motor for electric vehicle applications with high operating life of the battery.” *International Journal of Hydrogen Energy*, 40(39), 13827–13838.

TI. (2013). “Scalar (V / f) control of 3-phase induction motors.” *Application Report SPRABQ8*, 1–25.

Vas, P. (1998). “Sensorless vector and direct torque control.” *Oxford University Press, USA*.

Wankhade, S. D., and Salodkar, M. R. (2016). “Review on comparison of 2-L & 3-L inverter fed induction motor DTC drives.” *International Journal of Innovative and Emerging Research in Engineering*, 3(10), 1–5.

Yongchang, Z., Zhenming, Z., Jianguo, Z., Wei, X., and D.G, D. (2009). “Speed sensorless direct torque control of 3-level inverter-fed induction motor drive based on optimized switching table.” *35th Annual Conference of IEEE Industrial Electronics, IEEE.*, (1), 1316–1321.

Zhang, S., and Xia, X. (2009). “A new energy calculation model of belt conveyor.” *AFRICON 2009 IEEE*, 1–6.

Zhang, S., and Xia, X. (2010). “Optimal control of operation efficiency of belt conveyor systems.” *Applied Energy*, 87(6), 1929–1937.

Zhang, S., and Xia, X. (2011). “Modeling and energy efficiency optimization of belt conveyors.” *Applied Energy*, 88(9), 3061–3071.

Zhang, Y., Zhu, J., and Guo, Y. (2009). “A sensorless DTC strategy of induction motor fed by three-level inverter based on discrete space vector modulation.” *Australasian Universities Power Engineering Conference IEEE*, 1–6.

Zhang, Y., Zhu, J., and Member, S. (2011). "Direct torque control of permanent magnet synchronous motor with reduced torque ripple and commutation frequency." *IEEE Transactions on Power Electronics*, 26(1), 235–248.

ANNEXTURE-A

A.1 Comparative Study Results of Field and Simulation

The results obtained from the three belt conveyors used in the field are compared with the results obtained from the simulation studies and error values are given in Tables A.1 to A.12.

A.1.1 Comparative study results of FBC1

Table A.1 Error in speed

Load (N)	Speed (Field) (m/s)	Speed (Simulation) (m/s)	Error in Speed (%)
2250	2	2.08	3.8
4420	1.9	1.97	3.6
6279	1.9	1.96	3.1
7561	1.9	1.94	2.1
9724	1.8	1.83	1.6

Table A.2 Error in output power

Load (N)	Output Power (Field) (W)	Output Power (Simulation) (W)	Error in Output power (%)
2250	4500	4594	2.0
4420	8398	8500	1.2
6279	11930	12031	0.8
7561	14365	14466	0.7
9724	17504	17604	0.6

Table A.3 Error in Efficiency

Load (N)	Efficiency (Field) (%)	Efficiency (Simulation) (%)	Error in Efficiency (%)
2250	66.27	67.62	2.0
4420	79.23	79.44	0.3
6279	84.43	84.54	0.1
7561	86.75	86.8	0.1
9724	88.84	88.89	0.1

Table A.4 Error in Specific energy

Load (N)	Specific Energy (Field) (kWh/t.km)	Specific Energy (Simulation) (kWh/t.km)	Error in Specific Energy (%)
2250	2.8292	2.8307	0.1

4420	2.2083	2.2292	0.9
6279	1.9625	1.9765	0.7
7561	1.725	1.7361	0.6
9724	1.6418	1.6503	0.5

A.1.2 Comparative study results of FBC2

Table A.5 Error in speed

Load (N)	Speed (Field) (m/s)	Speed (Simulation) (m/s)	Error in Speed (%)
12107	2	2.05	2.4
13293	2	2.04	2.0
17537	1.9	1.98	4.0
23044	1.8	1.86	3.2
26961	1.8	1.84	2.2

Table A.6 Error in output power

Load (N)	Output Power (Field) (W)	Output Power (Simulation) (W)	Error in Output power (%)
12107	24214	24315	0.4
13293	26486	26588	0.4
17537	33320	33426	0.3
23044	41480	41587	0.3
26961	48530	48632	0.2

Table A.7 Error in efficiency

Load (N)	Efficiency (Field) (%)	Efficiency (Simulation) (%)	Error in Efficiency (%)
12107	91.68	91.7	0.02
13293	91.79	91.83	0.04
17537	93.79	93.82	0.03
23044	94.95	94.97	0.02
26961	94.66	94.67	0.01

Table A.8 Error in specific energy

Load (N)	Specific Energy (Field) (kWh/t.km)	Specific Energy (Simulation) (kWh/t.km)	Error in Specific Energy (%)
12107	1.572	1.5782	0.4
13293	0.8588	0.8617	0.3
17537	0.7049	0.7069	0.3
23044	0.6501	0.6516	0.2
26961	0.6103	0.6116	0.2

A.1.3 Comparative study results of FBC3

Table A.9 Error in speed

Load (N)	Speed (Field) (m/s)	Speed (Simulation) (m/s)	Error in Speed (%)
7263	2	2.06	2.9
12016	2	2.04	2.0
14827	1.9	1.96	3.1
21848	1.8	1.86	3.2
26739	1.8	1.83	1.6

Table A.10 Error in output power

Load (N)	Output Power (Field) (W)	Output Power (Simulation) (W)	Error in Output power (%)
7263	14525	14626	0.7
12016	24032	24134	0.4
14827	28171	28274	0.4
21848	39326	39424	0.2
26739	48130	48235	0.2

Table A.11 Error in Efficiency

Load (N)	Efficiency (Field) (%)	Efficiency (Simulation) (%)	Error in Efficiency (%)
7263	76.76	76.87	0.14
12016	86.2	86.24	0.05
14827	89.52	89.55	0.03
21848	94.72	94.74	0.02
26739	94.59	94.61	0.02

Table A.12 Error in Specific energy

Load (N)	Specific Energy (Field) (kWh/t.km)	Specific Energy (Simulation) (kWh/t.km)	Error in Specific Energy (%)
7263	1.8195	1.8294	0.5
12016	1.3404	1.3454	0.4
14827	1.0087	1.012	0.3
21848	0.9981	1.0006	0.2
26739	0.9785	0.9805	0.2

A.2 Comparative Study Results of Laboratory and Simulation

The results obtained from the belt conveyor used in the laboratory study are compared with the results obtained from the simulation studies in both the conditions with and without connecting the VFD, and error values are given in Tables A.13 to A.20.

A.2.1 Comparative study results of laboratory and simulation without VFD

Table A.13 Error in speed

Inclination (deg)	Load (kg)	Speed (Laboratory) (m/s)	Speed (Simulation) (m/s)	Error in Speed (%)
10°	3	0.178	0.186	4.301
	6	0.178	0.184	3.261
	9	0.176	0.182	3.297
	12	0.176	0.18	2.222
	15	0.175	0.178	1.685
15°	3	0.177	0.184	3.804
	6	0.177	0.182	2.747
	9	0.175	0.18	2.778
	12	0.175	0.178	1.685
	15	0.174	0.176	1.136
20°	3	0.175	0.182	3.846
	6	0.175	0.18	2.778
	9	0.174	0.178	2.247
	12	0.174	0.176	1.136
	15	0.174	0.175	0.571

Table A.14 Error in output power

Inclination (deg)	Load (kg)	Output Power (Laboratory) (m/s)	Output Power (Simulation) (m/s)	Error in Output Power (%)
10°	3	23	28	17.857
	6	81	82	1.220
	9	132	134	1.493
	12	168	170	1.176
	15	180	182	1.099
15°	3	27	32	15.625
	6	102	104	1.923
	9	143	146	2.055
	12	179	186	3.763
	15	198	202	1.980
20°	3	48	50	4.000
	6	114	118	3.390
	9	154	158	2.532
	12	186	192	3.125

	15	210	222	5.405
--	----	-----	-----	-------

Table A.15 Error in efficiency

Inclination (deg)	Load (kg)	Efficiency (Laboratory) (%)	Efficiency (Simulation) (%)	Error in Efficiency (%)
10°	3	22.75	25	9.000
	6	50.42	48.2	4.606
	9	62.21	58.7	5.980
	12	64.77	61.4	5.489
	15	64.92	61.8	5.049
15°	3	23.05	26.3	12.357
	6	56.05	54.5	2.844
	9	64.06	61.4	4.332
	12	65.07	63.8	1.991
	15	65.46	63	3.905
20°	3	37.22	36.3	2.534
	6	58.78	57.9	1.520
	9	62.65	60.4	3.725
	12	65.54	63.5	3.213
	15	66.1	66.19	0.136

Table A.16 Error in specific energy

Inclination (deg)	Load (kg)	Specific Energy (Laboratory) (kWh/t.km)	Specific Energy (Simulation) (kWh/t.km)	Error in Specific energy (%)
10°	3	2.53	2.7	6.296
	6	2.01	2.13	5.634
	9	1.77	1.9	6.842
	12	1.62	1.73	6.358
	15	1.39	1.47	5.442
15°	3	2.93	3.13	6.390
	6	2.27	2.39	5.021
	9	1.86	1.98	6.061
	12	1.72	1.82	5.495
	15	1.51	1.6	5.625
20°	3	3.22	3.44	6.395
	6	2.42	2.55	5.098
	9	2.05	2.18	5.963
	12	1.77	1.89	6.349
	15	1.59	1.68	5.357

A.2.2 Comparative study results of laboratory and simulation with VFD

Table A.17 Error in speed

Inclination (deg)	Load (kg)	Speed (Laboratory) (m/s)	Speed (Simulation) (m/s)	Error in Speed (%)
10°	3	0.14	0.145	3.448
	6	0.15	0.152	1.316
	9	0.16	0.163	1.840
	12	0.17	0.171	0.585
	15	0.18	0.189	4.762
15°	3	0.13	0.135	3.704
	6	0.14	0.144	2.778
	9	0.15	0.153	1.961
	12	0.16	0.162	1.235
	15	0.17	0.172	1.163
20°	3	0.12	0.126	4.762
	6	0.13	0.136	4.412
	9	0.14	0.144	2.778
	12	0.15	0.153	1.961
	15	0.16	0.161	0.621

Table A.18 Error in output power

Inclination (deg)	Load (kg)	Output Power (Laboratory) (m/s)	Output Power(Simulation) (m/s)	Error in Output Power (%)
10°	3	30	33.3	9.910
	6	68	70.5	3.546
	9	118	120.6	2.156
	12	160	161.1	0.683
	15	174	176.2	1.249
15°	3	33	34.2	3.509
	6	95	96.3	1.350
	9	138	141.8	2.680
	12	178	182.7	2.573
	15	197	200.7	1.844
20°	3	40	42.3	5.437
	6	108	110.6	2.351
	9	146	150.4	2.926
	12	180	182.5	1.370
	15	201	204.5	1.711

Table A.19 Error in efficiency

Inclination (deg)	Load (kg)	Efficiency (Laboratory) (%)	Efficiency (Simulation) (%)	Error in Efficiency (%)
10°	3	36.82	38.7	4.858
	6	52.16	51.3	1.676
	9	64.53	62.9	2.591
	12	65.87	63.2	4.225
	15	66.22	63.9	3.631
15°	3	27.45	32.8	16.311
	6	60.78	58.2	4.433
	9	70.29	68.5	2.613
	12	68.46	66.7	2.639
	15	68.41	66.3	3.183
20°	3	36.74	36.4	0.934
	6	62.29	60.1	3.644
	9	65.11	63.6	2.374
	12	66.14	63.5	4.157
	15	66.11	63.8	3.621

Table A.20 Error in specific energy

Inclination (deg)	Load (kg)	Specific Energy (Laboratory) (kWh/t.km)	Specific Energy (Simulation) (kWh/t.km)	Error in Specific energy (%)
10°	3	2.037	2.15	5.256
	6	1.63	1.72	5.233
	9	1.524	1.6	4.750
	12	1.518	1.59	4.528
	15	1.314	1.38	4.783
15°	3	2.459	2.61	5.785
	6	1.954	2.07	5.604
	9	1.636	1.72	4.884
	12	1.625	1.71	4.971
	15	1.44	1.51	4.636
20°	3	2.722	2.9	6.138
	6	2.167	2.3	5.783
	9	1.869	1.97	5.127
	12	1.701	1.8	5.500
	15	1.52	1.6	5.000

ANNEXURE-B

B.1 Belt Conveyor Calculations

Maximum conveying capacity = 200 t/h

Belt speed = 2 m/s

Belt width = 900 mm

Conveying length = 60 m

Conveying height = 10 m

$$\text{Inclination of the conveyor} = \tan^{-1}\left(\frac{\text{height of the conveyor}}{\text{length of the conveyor}}\right) = \tan^{-1}\left(\frac{63}{260}\right) = 9.46^\circ$$

Let, the material feed rate = 40 t/h .

$$\text{Loading factor} = \frac{\text{Actual feeding rate}}{\text{Maximum capacity}} = \frac{40}{200} = 0.2$$

$$\text{Mass of the bulk material on the belt conveyor} = \frac{\text{Actual feeding rate}}{3.6 \times \text{Belt speed}} = \frac{200}{3.6 \times 1.8} = 30.86 \quad \text{kg/m}$$

Mass of the belt = 15 kg/m

Mass of the idlers = 54 kg/m

Friction coefficient = 0.11

Belt cross section = 0.1607 m^2

Radius of the pulley = 35.1 cm

The total resistive force (motional resistance) required by the belt conveyor for its run is calculated by using Equation (2.1)

$$F = fLg[m_{idler} + (2m_{belt} + m_{load}) \cos \beta] + Hm_{load}g$$

$$F = 0.11 \times 260 \times 9.81[54 + (2 \times 15 + 30.46) \cos(9.46)] + 10 \times 30.46 \times 9.81 = 10346 \text{ N}$$

The mechanical (output) power required by the motor to oppose the resistive force =

$$\text{Total resistive force} \times \text{belt speed} = 10346 \times 1.8 = 18622 \text{ W}$$

The electrical (input) power consumed by the conveyor = mechanical (output) power

$$+ \text{Total power losses in the motor} = 18622 + 4398 = 23020 \text{ W}$$

$$\text{The efficiency of the drive system} = \frac{\text{output}}{\text{input}} = \frac{18622}{23020} = 80.89\%$$

$$\text{Time for one revolution} = \frac{\text{Central distance between the two pulley}}{\text{Belt speed}} = \frac{260}{2} = 130 \text{ s}$$

Energy required for one revolution = power required \times time for one revolution

$$= \frac{18622}{1000} \times \frac{130}{3600} = 0.672 \text{ kWh}$$

Energy required for one day = power required \times working hours of the conveyor in a day

$$= \frac{18622}{1000} \times 8 \times 1 = 149 \text{ kWh}$$

Energy required for one month = power required \times working hours of the conveyor in a

$$\text{month} = \frac{18622}{1000} \times (8 \times 25) = 3724.4 \text{ kWh}$$

Energy required for one year = power required \times working hours of the conveyor in a

$$\text{month} = \frac{18622}{1000} \times (8 \times 300) = 44692 \text{ kWh}$$

The daily, monthly and annual energy consumptions were calculated for 8, 200 and 2400 working hours respectively.

$$\text{The specific energy required} = \frac{\text{power required to run the conveyor}}{\text{material discharge rate} \times \text{conveying distance}}$$

$$= \frac{\left(\frac{18622}{1000}\right)}{200 \times \left(\frac{200}{1000}\right)} = 0.4655$$

$$\text{Power} = 55 \text{ kW} / 75 \text{ hp}$$

$$\text{Rated voltage} = 415 \text{ V}$$

$$\text{Rated current} = 90 \text{ A}$$

$$\text{Rated frequency} = 50 \text{ Hz}$$

$$\text{Rated motor speed} = 1482 \text{ rpm}$$

$$\text{Gear reduction ratio} = 30:1$$

$$\text{The speed after gear reduction} = N_2 = \frac{60 \times \text{belt speed}}{2\pi \times \text{Radius of the pulley}} = 50 \text{ rpm}$$

NATIONAL INSTITUTE OF TECHNOLOGY KARNATAKA, SURATHKAL

List of Publications based on Ph.D. Research Work

Sl. No.	Title of the paper	Authors (In the same order as in the paper. Underline the Research Scholar's name)	Name of the Journal/ Conference/ Symposium, Vol., No., Pages	Month & Year of Publications	Category *
1	Minimization of Specific Energy of a Belt Conveyor Drive System using Space Vector Modulated Direct Torque Control	<u>N V Sarathbabu Goriparti</u> , Ch. S. N. Murthy, M. Aruna	International Journal of Innovative Technology and Exploring Engineering, Vol. 8 (4), 505-511 (Scopus)	February 2019	1
2	Prediction of Energy Efficiency of Main Transportation System Used in Underground Coal Mines – A Statistical Approach.	<u>N V Sarathbabu Goriparti</u> , Ch. S. N. Murthy, M. Aruna	Springer Book Chapter, Learning and Analytics in Intelligent Systems, Vol.2, 337-344 (Scopus)	22 nd & 23 rd March 2019	3
3	Simulation and Experimental Studies on Belt Conveyor Drive System	<u>N V Sarathbabu Goriparti</u> , Ch. S. N. Murthy, M. Aruna	Journal of Mines Metals & Fuels	Communicated	1
4	SVM-DTC for energy efficiency of belt conveyor system: Simulation study and experimental validation	<u>N V Sarathbabu Goriparti</u> , Ch. S. N. Murthy, M. Aruna	4th International Conference on Communication and Computational Technologies (ICCCCT 2022)	Communicated	3

*Category: 1: Journal paper, full paper reviewed 2: Journal paper, Abstract reviews 3: Conference/Symposium paper, full paper reviewed
4: Conference/Symposium paper, abstract reviewed 5: Others (including papers in Workshops, NITK Research Bulletins, Short notes etc.)
(If the paper has been accepted for publication but yet to be published, the supporting documents must be attached.)



N V Sarathbabu Goriparti
Research Scholar





Prof. Ch. S.N. Murthy & Dr. M. Aruna
Research Guides

BIODATA

- 1. Name** : N V Sarathbabu Goriparti
2. Father's Name : Ravisekhar Goriparti
3. Mather's Name : Maha Lakshmi Goriparti
3. Date of Birth : 09-08-1984
4. Nationality : Indian
5. Marital Status : Married
6. Present Position : Research Scholar, NITK, Surathkal
7. Address for Communication : # 6B-8-16, Southern street, Eluru,
West Godavari (D), AP, India -534001
8. Mobile : (+91)-8096765403
9. E-mail : sarathyadav225@gmail.com
10. Academic Qualifications:

Degree	Specialization	Year	College	University	%
M. Tech (Full Time)	Control Systems	2009- 2012	Malla Reddy Engineering College (MREC) Pochampally, Secunderabad.	Jawaharla Nehru Technological University Hyderabad, Hyderabad, Andhra Pradesh, India-500085	78.31%
B. E (Full Time)	Electrical & Electronics Engineering	2002- 2006	Swarnandhra College of Engineering and Technology (SCET), Narasapur	Jawaharla Nehru Technological University, Hyderabad, Andhra Pradesh, India-500072	64.33%

11. Work Experience: (7 Years)

From	To	Designation	Organization
June 2013	Dec 2015	Assistant Professor (Electrical and Electronics Engg.)	Sri Vasavi Engineering College- Pedatadepally, Tadepalligudem
May 2012	April 2013	Assistant Professor (Electrical and Electronics Engg.)	St.Peter's Engineering College- Dhulapally, Hyderabad
May 2006	June 2009	Assistant Professor (Electrical and Electronics Engg.)	Malla Reddy Institute of Eng.& Tech. Dhulapally, Hyderabad

